No. 112

September 1971

FREE-SURFACE EFFECTS IN HULL PROPELLER INTERACTION

by

Horst Nowacki and Som D. Sharma

This research was carried out
in part under the
Naval Ship Systems Command
General Hydromechanics Research Program
Subproject SR 009 01 01, administered by the
Naval Ship Research and Development Center.
Contract No. N00014-67-A-0181-0028

Department of Naval Architecture
and Marine Engineering
College of Engineering
The University of Michigan
Ann Arbor, Michigan 48104

CONTENTS

CONTENTS (Contd.)

LIST OF FIGURES

LIST OF SYMBOLS

Note:- The standard symbols recommended by the ITTC Presentation Committee have been used wherever possible. See also Section B.1 for the special notation used in Appendix B.

B	Beam of hull
C_B	Block coefficient of hull form
C_D	Drag coefficient of propeller blade section
C_{DD}	Value of C_D at design point J_D
C_F	Coefficient of friction, Equation (7)
C_{FD}	Coefficient of residual towing force = $2F_D/\rho SV^2$
C_{FM}	Value of C_F at model Reynolds number
C_{FS}	Value of C_F at ship Reynolds number
C_L	Lift coefficient of propeller blade section
C_{LD}	Value of C_L at design point J_D
C_M	Midship section area coefficient
C_P	Longitudinal prismatic coefficient
C_T	Coefficient of total resistance = $2R_T/\rho SV^2$
C_{Th}	Thrust loading coefficient, Equation (B15)
C_V	Coefficient of viscous resistance = $2R_V/\rho SV^2$
C_{VM}	Value of C_V at model Reynolds number
C_{VS}	Value of C_V at ship Reynolds number
C_W	Coefficient of wave resistance = $2R_W/\rho SV^2$
C_{WP}	Waterplane area coefficient
C, S	Fourier cosine, sine transforms, Equation (B50)

C^*, S^*	Modified Fourier cosine, sine transforms, Eqn. (B70)
D	Diameter of propeller
E(u)	Free-wave amplitude spectrum
$E_H(u)$	E(u) of hull alone
$E_P(u)$	E(u) of propeller alone
$E_T(u)$	E(u) of total system hull and propeller
$E_{i,j}$	Special function, Equation (B39)
F(u)	Sine component of free-wave spectrum
	Subscripts H, P, T apply as to E(u)
F_D	Residual towing force in self-propulsion test
F_n	Froude number $= V/\sqrt{gL}$
F_{nh}	Submergence Froude number $= V/\sqrt{gh}$
$F^{(N)}$	N = 1,2,3; Special functions, Equation (B24)
$\tilde{F}_P$, $\tilde{G}_P$	Free-wave spectrum of propeller in a coordinate system with origin in the propeller plane, Eqn. (B73)
G	Nondimensional bound circulation $= \Gamma/\pi DV$
G	Green's function of point source, Equation (B33),(B57)
G_x	Partial derivative of G, Equation (B58)
G(u)	Cosine component of free-wave spectrum
	Subscripts H, P, T apply as to E(u)
$G^{(N)}$	N = 1,2,3; Special functions, Equation (B47)
Im	Imaginary part of
I_o	Modified Bessel function of zero order
J	Advance coefficient of propeller
	$= V/nD$ for free-running propeller
	$= V_A/nD$ for propeller operating behind hull
J_D	Value of J at the design (optimum) point

J_f	Virtual advance coefficient of propeller operating near the free surface, Equation (14)
J_H	Advance coefficient of propeller based on hull speed = V/nD
J_M	Mean of J_Q and J_T
J_Q	Value of J at torque identity $K_Q = K_{QH}$
J_T	Value of J at thrust identity $K_T = K_{TH}$
K_Q	Torque coefficient of free-running propeller = $Q/\rho n^2 D^5$
K_{QH}	Torque coefficient of propeller behind hull = $Q_H/\rho n^2 D^5$
K_T	Thrust coefficient of free-running propeller = $T/\rho n^2 D^4$
K_{TH}	Thrust coefficient of propeller behind hull = $T_H/\rho n^2 D^4$
L	Length of hull
Oxyz	Coordinate system, see Figure 1
P	Pitch of propeller
Q	Propeller torque in open water
Q_H	Propeller torque behind hull
Re	Real part of
R_H	Propeller hub radius
R_n	Reynolds number of hull = VL/ν
R_P	Propeller tip radius
R_T	Total resistance of hull
R_V	Viscous resistance of hull
R_W	Wavemaking resistance
R_{WH}	R_W of hull alone
R_{WP}	R_W of propeller alone
R_{WT}	R_W of total system hull and propeller
R, θ	Polar coordinates in propeller plane, Equation (B9)

R', θ'	Coordinates of source point in propeller plane
S	Wetted surface area
T	Draft of hull
T	Propeller thrust in open water
T_H	Propeller thrust behind hull
V	Speed of advance of hull
V	Speed of advance of free-running propeller
V_A	Speed of advance of propeller relative to wake in the behind hull condition
V_m	Speed of model
Z	Number of blades of propeller
a_1, a_2	Empirical constants defining propeller foil characteristics, Equation (C13)
b	Half beam of hull = B/2
c	Chord length of propeller blade section
c_w	Empirical constant, Equation (10)
dD	Drag generated by blade element, Equation (C10)
dL	Lift generated by blade element, Equation (C8)
f(x,z)	Function defining hull surface, Equation (B4)
g	Acceleration due to gravity
h	Submergence measured to propeller axis
i	Imaginary number = $\sqrt{-1}$
i_A	Induction factor for axial velocity, Equation (C5)
i_E	Angle of entrance of hull
i_R	Angle of run of hull
i_T	Induction factor for tangential velocity, Eqn. (C6)

k	Empirical factor defining propeller foil characteristics, Equation (C12)
k	Circular wave number (Appendix B)
k_w	Empirical wake corrector, Appendix C.3
$k+1$	Viscous form factor, Equation (8)
l	Half length of hull = L/2
m	Hull form parameter, Equation (3)
n	Hull form parameter, Equation (3)
n	Rate of revolutions of propeller
r_1	Distance between field point and source point, Equation (B33)
r_2	Distance between field point and mirror image of source point, Equation (B33)
s	Function of u, $s = \sqrt{(1+v)/2}$
t	Thrust deduction fraction
t_p	Potential component of t
t_v	Viscous component of t
t_w	Wave component of t
u	Transverse wave number
u_A	Axial velocity induced at the lifting line by the vortex trail of the propeller
u_T	Tangential velocity induced at the lifting line by the vortex trail of the propeller
v	Function of u, $v = \sqrt{1+4u^2}$
w	Longitudinal wave number (only in Appendix B)
w	Wake fraction (Unless otherwise specified, the disk average of the nominal, axial wake is implied.)

w_f	Self-induced free-surface wake of propeller
w_p	Potential component of wake w
w_v	Viscous component of wake w
w_w	Wave component of wake w
w(R)	Circumferentially averaged value of $w(R,\theta)$
	Subscripts f, p, v, w apply as to w
$w(R,\theta)$	Local nominal wake fraction at point (R,θ)
	Subscripts f, p, v, w apply as to w
w_E	Effective wake fraction
w_M	Mean of w_Q and w_T
w_Q	Effective wake fraction from torque identity
w_T	Effective wake fraction from thrust identity
$\tilde{w}_T$	Simulated effective wake fraction, Equation (C18)
w_1, w_2	Weights in iteration formula, Equation (C11)
x	Longitudinal coordinate, positive forward
x_P	Longitudinal coordinate of center of propeller
x,y,z	Coordinates of field point
x',y',z'	Coordinates of hull source point
y	Transverse coordinate, positive to port
y_o	Transverse position of longitudinal wave profile
y_P	Transverse coordinate of center of propeller
z	Vertical coordinate, positive upward
z_P	Vertical coordinate of center of propeller
$\Gamma(R)$	Bound circulation along propeller blade
Φ	Geometric pitch angle, Equation (C3)

Δt	Step size in time t
Δu	Step size in wave number u
Δx	Step size in distance x
α	Angle of attack of blade section, Equation (C2)
α_D	Value of α at design point J_D
β_i	Hydrodynamic pitch angle, Equation (C4)
β_{iD}	Hydrodynamic pitch angle at design point J_D
γ_o	Nondimensional spped-length parameter $= gL/2V^2$
$\delta_H R_{WP}$	Increase in propeller wave resistance due to presence of hull
$\delta_P R_{WH}$	Increase in hull wave resistance due to presence of propeller = force of thrust deduction
ϵ	Hull form parameter in Appendix B, Equation (B5)
ϵ	Drag/lift ratio in Appendix C, Equation (C18)
$\zeta(x,y)$	Free-surface elevation at point (x,y)
η_D	Propulsive efficiency, Equation (15)
η_H	Hull efficiency, Equation (16)
	Additional subscripts M, Q, T defined in Eqn. (22)
η_O	Open water propeller efficiency $= K_T J/2\pi K_Q$
	Additional subscripts M, Q, T apply as to J
η_R	Relative rotative efficiency, Equation (15)
	Additional subscripts M, Q, T defined in Eqn. (23)
θ	Direction of wave propagation in Appendix B
θ, R	Polar coordinates in propeller plane, Equation (B9)
θ',R'	Polar coordinates of propeller source point
λ	Scale ratio

ν	Kinematic viscosity of water
ν	Summation index, Equation (B50)
ξ,η,ζ	Relative field point coordinates, Equation (B36)
ξ',ζ'	Relative source point coordinates, Equation (B36)
ρ	Density of water
σ	Source strength = Source output / 4π
$\sigma(x,z)$	Density of hull source distribution
$\sigma(R,\theta)$	Density of propeller source distribution
$\sigma(R)$	Circumferentially averaged value of $\sigma(R,\theta)$
τ	Draft/half-length ratio, Equation (B36)
φ	Velocity potential of perturbation flow
$\varphi_x,\varphi_y,\varphi_z$	Partial derivatives of φ
φ_x^H	Longitudinal flow induced by hull
φ_x^P	Axial flow induced by propeller
$\varphi_x^{(N)}$	N = 1,2,3,4; Components of φ_x, Equation (B34)
ω	Angular velocity of propeller = $2\pi n$
∇	Displacement volume of hull

1 - INTRODUCTION

The purpose of this research was to clarify by analysis, computation and experiment the quantitative role of wavemaking at the free surface in the phenomenon of hull propeller interaction and consequently its contribution to the hydrodynamic propulsive efficiency of the system hull and propeller.

Following Froude (1883), hull propeller interaction is conveniently studied in terms of three propulsion factors: wake, thrust deduction and relative rotative efficiency. The wake is caused by the presence of the hull and the free surface and is a simple measure of the change in propeller inflow as compared to an equivalent open-water condition (free running propeller in an infinite parallel stream). The thrust deduction is really an indirect expression of the fact that the force of resistance acting on the hull is modified (usually augmented as compared to the towed condition) as a result of propeller action. With the present state of our knowledge, only wake and thrust deduction are amenable to rational analysis, the relative rotative efficiency being an empirical catch-all for various unclarified effects of relatively insignificant magnitude.

Since the fundamental work of Dickmann (1938, 39), it has been customary to study hull propeller interaction as a superposition of three basic effects: "potential" effects due to an ideal displacement flow about a deeply submerged double body (the zero Froude number approximation), viscous effects due to

the boundary layer and viscous wake, and wave effects due to the presence of the free surface. Using standard symbols w and t for wake and thrust deduction fractions respectively, one may write formally

$$w = w_p + w_v + w_w \tag{1}$$

$$t = t_p + t_v + t_w \tag{2}$$

where the subscripts p, v and w denote potential, viscous and wave respectively. By comprehensive theoretical analysis and careful experiments Dickmann demonstrated that the most significant components were w_p, t_p and w_v.

Among Dickmann's most impressive achievements were 1) a theoretical relation between potential wake and thrust deduction involving the thrust loading coefficient, and 2) a reasonable explanation of the effect of the free surface on propulsive efficiency. His main analytical tools were a simple actuator disk model of the propeller (momentum theory), the method of singularities (Lagally's theorem) for calculating forces on the hull and Havelock's method of images for a linearized treatment of the free surface.

In recent years considerable effort has been put into the investigation of potential and viscous effects in hull propeller interaction (see Bibliography). Especially in this country, Beveridge in a series of papers (1962, 63, 66, 68) has refined the technique of calculating the potential thrust deduction to a state of near perfection. At the same time, Hucho (1965, 68)

in Germany has made significant contributions to our understanding of viscous effects. The wave effects, however, were persistently ignored for nearly thirty years since Dickmann (1939), until the fundamental treatise of Yamazaki (1967) revived interest in this subject and inspired the recent work of Nakatake (1967, 68) in Japan.

Still far from resolving the complex issues at stake, Nakatake's papers are just added evidence of the same conviction that underlies the present study (which, incidentally, was initiated without knowledge of the Japanese effort), namely that the time is now ripe to make a fresh attempt at the further clarification of this admittedly difficult problem. This is due mainly to the following reasons:

1) Major advances in the vortex theory of propellers now allow the use of a far more refined mathematical model of the propeller.

2) The recently developed technique of wave profile measurement and analysis enables us to verify by (almost) direct measurement the wave effects predicted by analytical theory.

3) The general availability of large electronic computers allows the use of more realistic singularity distributions for representing the hull, the propeller and their images in the free surface.

Besides the intrinsic interest of a fundamental problem in ship hydrodynamics, a recommendation by the Performance Committee of the International Towing Tank Conference 1966 for specific research in the basic problem area of hull propeller

interaction - of which free surface effects are certainly the most intriguing aspect - as well as the prospect of practical application to modern high speed craft with propellers operating at shallow or even partial submergence were further motivations for undertaking this research.

2 - GENERAL APPROACH

The originality of the present study lies not in the development of a novel method but in the concerted application of miscellaneous existing analytical, computational and experimental techniques to our specific purpose. Since these numerous tools have to be applied in a rather intricate sequence to get the information desired, it seems necessary in the interest of clarity to precede the account of work done by a brief schematic description of our general approach. The internal details of the individual techniques are only of indirect interest in the present context and will therefore be banished to appropriate appendices.

The basic aim is to determine for a given hull-propeller system the propulsion factors and their potential, viscous and wave components by all feasible analytical and experimental means. This dictates roughly the following set of operations.

First, a considerable amount of basic information can be gathered by a number of independent experiments and theoretical calculations which may be executed in any convenient sequence. On the experimental side we may deploy the following more or less routine model tests in the towing tank:

E1) Hull resistance test,

E2) Propeller open water test (at deep and shallow submergence),

E3) Self-propulsion test with hull and propeller,

E4) Nominal wake measurements behind the hull in forward and reverse motion, and

E5) Wave profile measurements (e.g.longitudinal cuts) for the hull with and without propeller.

On the theoretical side only few calculations can be performed without resort to some empirical data; these are

T1) Wavemaking resistance of the hull,

T2) Wave wake induced by the hull in the propeller plane (both in forward and reverse motion), and

T3) Potential wake induced by the hull in the propeller plane.

From here on the further analysis is of a semi-empirical nature and must be conducted in an essentially predetermined sequence because at each new step certain information from previous steps is required. It is helpful to list separately the pure hull analysis, the pure propeller analysis, and the interaction analysis.

The purpose of the hull analysis is to verify the mathematical representation of the hull as a source distribution and to establish the degree and range of validity of the linearized wave theory.

H1) The total resistance measured in step E1 can be subjected to a simple form-factor analysis (based on a suitable plane friction formula) so as to yield the viscous and wavemaking components.

H2) An alternative estimate of wavemaking resistance can be obtained from a Fourier analysis of the wave profiles

measured in step E5.

H3) The experimental estimates of wavemaking resistance derived in the two preceding steps may now be compared with the theoretical calculations of step T1.

H4) For a more exacting test of the theory the experimental and theoretical free-wave spectra can be compared at each speed.

H5) An additional test of the theory lies in comparing the sum of the calculated wave wake and potential wake from steps T2 and T3 to the measured wake in reverse motion from step E4 since the latter is essentially free of viscous effects.

H6) If the mathematical model of the hull flow can be verified in the preceding steps then the calculated wave wake and potential wake may be subtracted from the measured total wake in forward motion to yield the important viscous wake component.

The purpose of the propeller analysis is to determine a vortex model of the propeller and to verify the validity of its alternative representation as a source distribution which is to serve as the basis for calculating thrust deduction and wave effects.

P1) A computer program based on lifting line theory in conjunction with the Lerbs (1952) induction factor method may be used to calculate for any given propeller geometry and assumed foil characteristics the equivalent distribution of bound circulation over the radius and hence by Kutta-Joukowsky's

theorem the thrust and torque coefficients as functions of the advance ratio.

P2) The thrust and torque predictions of the previous step are compared with the actual performance as measured in step E2 and the agreement is improved iteratively by adjusting the assumed foil characteristics. Again the crucial link in the algorithm is the circulation distribution.

P3) Using the Hough and Ordway (1965) approximation, the circulation distribution is now translated into an equivalent source distribution over the propeller disk.

P4) This source distribution is the basis for calculating the wavemaking due to the propeller by Havelock's (1932) theory. In particular, the axial velocities induced by the operation of the propeller near the free surface, in other words the self-induced free-surface wake of the propeller, can be calculated.

P5) This self-induced wake is fed back into the propeller performance program based on lifting line theory to obtain predictions of thrust and torque with the propeller operating at shallow submergence.

P6) A comparison of propeller performance predicted in step P5 with actual measurements at the same submergence then provides a check on the correct accounting of free surface effects in the theoretical model.

After the mathematical representations of hull and propeller have been verified the actual <u>interaction analysis</u> can be executed as follows.

I1) The Froude propulsion factors (mean effective wake, thrust deduction, relative rotative efficiency and propeller efficiency in the equivalent open water condition) are first determined from the results of tests E1, E2 and E3 in the usual manner.

I2) The radial distribution of nominal wake from step E4 is adjusted to match the mean effective wake from step I1 and fed into the propeller performance program. The output is the circulation distribution of the propeller in the behind ship condition at each Froude number.

I3) Again the Hough and Ordway relation is used to translate the circulation distribution into a source representation of the propeller in the behind-ship self-propulsion condition.

I4) From the now known source representations of the hull and propeller free-wave spectrum and wavemaking resistance are calculated and compared with the corresponding results of the Fourier analysis of the wave profiles measured in step E5. This provides a check on the principle of linear superposition of hull and propeller waves.

I5) The mutual flow patterns of hull and propeller can now be calculated and thence by Lagally's theorem the potential and wave thrust deduction.

I6) Finally the viscous component of thrust deduction can be estimated indirectly by subtracting the potential and wave components from the total thrust deduction of step I1.

3 - DISCUSSION OF RESULTS

3.1 - Choice of Hull and Propeller

Since our work was to consist essentially of a single concrete example of the actual application of the sequence of operations outlined in the previous section it was rather important to choose as instructive and useful an example as possible. After considering various alternatives we finally selected the somewhat idealized hull propeller configuration of Fig. 1 that has a sufficiently simple geometry for the ease of theoretical calculations and yet quite realistic proportions for the results to be of practical value. The arguments leading to this choice can be summarized as follows.

In order to keep the wavemaking calculations manageable it was decided to use a symmetric hull form with parabolic waterlines and frames. The wetted surface is then defined by the equation

$$y = \frac{B}{2} \{1 - (2x/L)^{2m}\}\{1 - (-z/T)^{n}\} \qquad (3)$$

The hull above water is a simple continuation of the underwater form with vertical sidewalls. The integer powers m,n and the form ratios L/B, B/T were chosen to satisfy the following requirements: 1) sufficiently thin hull for linearized theory to be valid, 2) sufficiently large angle of run to get measurable interaction with the propeller, and 3) realistic value of block coefficient.

This led to the following set of parameters:

$$m = 2, \quad n = 4$$

$$L/B = 10, \quad B/T = 1.5$$

$$C_M = C_P = C_{WP} = 0.8$$

$$C_B = 0.64$$

$$i_E = i_R = \arctan 0.4 \approx 21.8^o \qquad (4)$$

The absolute size of the model for the towing experiments was dictated by the size of the tank and equipment available:

$$L = 4.500 \text{ m} = 14.764 \text{ ft}$$

$$B = 0.450 \text{ m} = 1.476 \text{ ft}$$

$$T = 0.300 \text{ m} = 0.984 \text{ ft}$$

$$\nabla = 0.3888 \text{ m}^3 = 13.731 \text{ ft}^3$$

$$S = 3.4962 \text{ m}^2 = 37.633 \text{ ft}^2$$

The choice of propeller was governed mainly by considerations of availability and simplicity. Fortunately, it was possible to borrow a very suitable propeller from the Hamburg Ship Model Basin (HSVA), namely a 200 mm diameter model of the Standard Propeller recommended by the ITTC Cavitation Committee in 1960 for comparative testing, see Burrill (1960). It has a simple geometry (constant pitch, no rake, no skew) with accurately defined offsets (Fig. 2), and performance characteristics were already available from previous tests at the Hamburg and other tanks. Its two-dimensional foil characteristics, however, were not known. The center of the propeller was positioned at

$$x_P = -0.51 \; L$$

$$y_P = \; 0$$

$$z_P = -0.50 \; T \qquad (6)$$

in the coordinate system of Fig. 1. This arrangement relative to hull ensured complete submergence (0.75 D at rest) at all speeds and a low axial clearance (0.225 D) with accordingly accentuated interaction effects.

3.2 - Summary of Model Tests

In accordance with the scheme outlined in Section 2 the following model experiments were conducted:

E1) Measurement of bare hull resistance over the entire feasible speed range of $0.1 \leq F_n \leq 0.45$.

E2) Measurement of propeller performance in open water (thrust and torque as functions of speed of advance and rate of revolutions) over the range of advance coefficient $0 \leq J \leq 1.2$ at four depths of submergence: $h/R_p = 3.47$, 2.00, 1.50 and 1.00.

E3) Propulsion tests with the propeller operating behind the hull (measurement of thrust, torque and residual towing force as functions of model speed and propeller rate of revolutions) at fourteen discrete speeds corresponding to $\gamma_o =$ 3.5 step 0.5 until 8.0 step 1.0 until 11.0, and 12.5. At each speed the propeller revolutions were varied to obtain a sufficient range of loading usually covering both the model and the ship self-propulsion points (for an arbitrarily assumed model scale of 1:80).

E4) Measurement of nominal wake in the propeller plane behind the hull ($x_p = -0.51$ L) in both forward and reverse motion at three selected speeds corresponding to $\gamma_o = 4.0$, 7.0

and 12.5. At each speed the circumferential average of the axial wake velocity was measured by means of calibrated wake wheels at ten different radii R/R_P = 0.2 step 0.1 until 1.1.

E5) Measurement of longitudinal wave profiles at a fixed transverse distance (y_o = 0.134L) from the model center plane in two conditions; 1) model with propeller running at ship self propulsion point and 2) model with propeller replaced by a dummy hub, each at two selected speeds corresponding to γ_o = 4.0 and 7.0

Revelant details of the test procedure are given in Appendix A.

3.3. - Hull Analysis

Fig. 3 shows the measured total resistance of the bare hull as a function of speed in the usual nondimensional coefficient form: C_T versus F_n (or R_n). Also shown in the figure are the ITTC 1957 model-ship correlation line

$$C_F = 0.075 \; / \; (\log_{10} R_n - 2)^2 \qquad (7)$$

and the curve of estimated viscous resistance coefficient

$$C_V = (1+k)\, C_F \qquad (8)$$

The latter is based on the Hughes form factor concept and determined from the measured total resistance at low Froude numbers by the graphical method of Prohaska (1966), Assume

$$C_T = C_V + C_W \qquad (9)$$

and further for $F_n \to 0$:

$$C_W = c_w F_n^4 \tag{10}$$

Then $$C_T/C_F = (1+k) + c_w(F_n^4/C_F) \tag{11}$$

so the constants $(1+k)$ and c_w may be determined from a linear fit to the plot of C_T/C_F versus F_n^4/C_F for low Froude numbers. Fig. 4 shows that the linear relation implied by Equation (11) applies reasonably well to our model up to Froude numbers up to 0.2. The numerical values of the viscous from factor $(1+k)$ and the coefficient c_w were found to be

$$(1+k) = 1.025 \qquad c_w = 0.73 \tag{12}$$

The coefficient of wavemaking resistance thus indirectly derived

$$C_W = C_T - (1+k)\, C_F \tag{13}$$

has been plotted in Fig. 5 against the appropriate speed-length parameter γ_o and compared with the corresponding calculations based on linearized thin ship theory (see Appendix B, especially Equation (B28)). Although there is a remarkable semblance between theory and experiment (e.g. the second, third and fourth humps can be clearly identified in the measured curve), it is disappointing to observe that even for our relatively thin ship $(L/B = 10)$ reasonable quantitative agreement between theoretical predictions and experimental reality could be established only over a limited speed range of $2.5 \leq \gamma_o \leq 4.5$. At higher γ_o (i.e. lower Froude num-

bers) the experimental curve exhibits much less pronounced humps and hollows and its general level is only half as high as the theoretical curve. This suggests that the viscous boundary layer and separation probably made the stern quite ineffective in wavemaking.

In any case, the two speeds corresponding to $\gamma_o = 4$ ($F_n = 0.354$) and $\gamma_o = 7$ ($F_n = 0.267$) were singled out from Fig. 5 as the most promising for further investigation. At these speeds the wavemaking resistance was evaluated directly from measured wave profiles by the longitudinal cut method described in Appendix B.8. The result, as indicated by the two isolated spots in Fig. 5, showed that the wavemaking resistance associated with the wave pattern actually generated by the model was about 30 to 40 percent less than the theoretical prediction or the empirical estimate of Equation (13). Further discussion of the results of wave profile analysis will follow in Section 3.5.

The next step in hull analysis was the evaluation of nominal wake, i.e. the flow perturbation created by the hull in the propeller plane in the absence of the propeller. In order to avoid the complications invariably caused by viscous effects behind the hull, we first compared the calculated and measured wake in reverse* motion, see Fig. 6. The measured values were

*Incidentally, by virtue of the longitudinal symmetry of our hull the "stern" wake in the propeller plane $x = x_p$ in reverse motion is equivalent to the "bow" wake in the reflected propeller plane $x = -x_p$ in forward motion.

obtained from calibrated wake wheels directly as circumferential averages at ten discrete radii. The calculated values based on thin ship theory (see Appendix B.5, especially Equation (B56)) were available pointwise in the propeller plane and were numerically averaged along the circumference at various radii for the ease of comparison with measurements. It is encouraging to observe in Fig. 6 the fair agreement between theory and experiment, the discrepancy being nowhere larger than 0.03. In particular, both the mean effect of Froude number and the general variation with radius are correctly predicted by theory. However, the measured wake shows some erratic oscillations of unclarified origin at the outer radii.

Fig. 7 shows an analogous comparison of calculated and measured wake in forward motion. Here we cannot expect direct agreement between experiment and theory since the former contains a substantial viscous component not included in the latter. However, if we subtract the calculated from the measured wake, we notice that the remainder is relatively insensitive to Froude number (see Fig. 7) as we would expect of the true viscous component. This may be interpreted as indirect evidence that wave effects actually present in the measured total wake are of the same order of magnitude as predicted by thin ship theory. This is quite encouraging, especially in view of the relatively poor agreement between calculated and measured values of wavemaking resistance.

For the sake of completeness the conventional "potential" or zero Froude number component of wake as calculated by theory

(Appendix B.5, Equation (B54)) is also plotted in Fig. 7. It is by definition independent of Froude number. In view of the foregoing, the trichotomy of nominal wake in potential, wave and viscous components as displayed in Fig. 7 can be regarded as quite meaningful. Evidently, the wave effects are by no means negligible as commonly assumed.

3.4. - Propeller Analysis

Measured propeller performance characteristics for three depths of submergence are plotted in Fig. 8 in the usual non-dimensional coefficient form. The largest depth ($h/R_p = 3.47$) was the maximum attainable with the propeller boat available for open water tests, and the smallest ($h/R_p = 1,50$) corresponds exactly to the immersion selected for self-propulsion tests ($z_p = -0.5T$) described later. Apart from verifying the measurements conducted previously at an even lager depth ($h/R_p = 4.0$) in the Hamburg Ship Model Basin (HSVA), the principal conclusion from these tests was that free-surface effects are negligibly small for depths $h/R_p \geq 1.50$.

At the shallowest depth investigated, however, with the propeller disk just touching the static water level ($h/R_p=1.0$), pronounced free-surface effects were measured, see Fig. 9. The observed loss of thrust and torque as compared to the deeply submerged condition, the steady accentuation of the effect with increasing loading (i.e. decreasing advance coefficient), and a slight drop in efficiency are to be naturally expected from the combined effects of ventilation and wavemaking at the free

surface. It is not intuitively obvious, however, why the thrust and torque should suddenly break down at some "critical" advance coefficient, here $J \approx 0.41$. Similar discontinuities have been measured by others, notably by Shiba (1953). Flow observations reveal that the discontinuity is accompanied by a sudden transition from partly ventilated to fully ventilated condition. A satisfactory theoretical explanation of this phenomenon would certainly require an intricate analysis of the stability of partly ventilated flow. It is also intriguing to note that the drop in thrust and torque is nearly proportionate so that the discontinuity is hardly perceptible in the curve of efficiency. This lends some credibility to Dickmann's (1939) simplified treatment of propeller ventilation as a mere reduction in the density of the medium due to a mixture of air with water!

For the sake of completeness it should be reported that ventilation also occurred to some extent at two of the deeper immersions, namely $h/R_p = 1.5$ and 2.0, especially in the bollard condition and at the lowest advance coefficients. It was distinctly audible and often visible as a vortex from the free surface to the propeller tip, but its effect on thrust and torque was obviously too small to be measurable (see Fig.8).

The measured thrust and torque characteristics (in the deeply submerged condition) were transformed into an equivalent vortex model of the propeller by means of a computer program based on lifting line theory and using assumed (or adjusted) two-dimensional foil characteristics as the connecting link

between propeller geometry and forces after taking account of the velocity perturbation induced by the trailing vortices. Without going into details, which are given in Appendix C, Fig. 10 is presented as evidence for the close fit finally achieved between calculations and measurement. Note that the results of two different calculations are displayed. The four sets of crosses mark the calculated performance of a series of hypothetical propellers individually designed at each respective advance coefficient so as to produce the known measured thrust with a minimum loss of energy (i.e. optimum distribution). The exact agreement with the measured K_T values is therefore trivial, while the good agreement with the measured K_Q values proves that hydrodynamic losses were reasonably estimated in the calculation and that the actual performance of the propeller is nearly optimum over the range $0.6 \leq J \leq 0.9$. On the other hand, the four sets of squares in Fig. 10 mark at each respective advance coefficient the calculated performance of the given propeller with predetermined geometry. Hence, the perfect agreement with measured K_T and K_Q values is trivial only at the design point, assumed to be at $J = 0.8$, whereas at the three other points it demonstrates the usefulness of the scheme devised to calculate the off-design performance with the aid of assumed (or empirically adjusted) foil characteristics. In particular, it may be anticipated from the trend visible in Fig. 10 that a more elaborate off-design analysis (as compared to the simpler design point analysis) would probably pay off at higher loadings (lower J values) by

producing a more accurate simulation of actual propeller performance.

The heart of the vortex model of the propeller used above is the calculated distribution of bound circulation along the blade. This is shown in a suitable nondimensional form in Fig. 11 for each of the four advance coefficients marked in Fig.10. It serves to illustrate the effect of loading and variation with radius, and is the basis of all further analysis. In passing we note that the two different calculations just discussed produced practically identical (within one percent) circulation distributions in the four cases considered here.

The vortex model of the propeller was in turn transformed into a sink disk model by means of the Hough and Ordway (1965) relation, and linearized wavemaking theory was applied to calculate its self-induced wake when operating near the free surface, see Appendix B, especially Equations (B13) and (B61). The final results of four such calculations for a relatively shallow submergence of $h/R_p = 1.0$ are shown in Fig. 12. It is a rather remarkable coincidence that although the calculated self-induced wake varied strongly over the disk, its circumferential averages came out almost independent of the radius. The disk average $|w_f|$ increases steadily with loading (i.e. decreasing J) as one would naturally expect.

The next and final step in our propeller analysis was aimed at an indirect verification of the entire theoretical model by comparing the calculated performance at shallow submergence (based only on theory and the known performance at

deep submergence) with actual measurements. For this purpose the calculated self-induced free-surface wake $w_f(R)$ was used in two ways. First, following Dickmann (1939), its disk average value w_f was used simply to define a virtual advance coefficient

$$J_f = (1-w_f)\ J \tag{14}$$

at which the thrust and torque values were read off from the known deep submergence characteristics (Fig. 8) and replotted against J (see squares in Fig. 13) as the predicted characteristics at shallow submergence. Second, the radial distribution $w_f(R)$ was fed into the computer program for off-design performance which then calculated the thrust and torque by vortex theory (see crosses in Fig. 13). Since this program matched perfectly with the deep submergence characteristics (see Fig. 10) and since $w_f(R)$ was practically constant over the radius (see Fig. 12), the net effect was the same as in the first method, namely a loss of thrust and torque owing to the negative value of self-induced wake and increasing steadily with loading. The actually measured characteristics, replotted from Fig. 9 as the dashed curves in Fig. 13, indeed confirm that the calculated effect is in the right direction and of the right magnitude.

Encouraged by this success of the theory, we repeated the above calculation for the entire range of advance coefficients $J = 0.10$ step 0.05 until 1.10. However, for the sake of simplicity, we now estimated the source strength directly from the thrust coefficient by Dickmann's relation (i.e. substituting

Equation (B10) instead of (B13) into (B61)) and applied only the simple method of virtual advance coefficient J_f explained above. The result is represented by the continuous curves in Fig. 13. Although not as accurate as the previous calculations, which made use of vortex theory, even this simple approach leads to fairly reasonable predictions of the effect of wavemaking on propeller performance. Of course, at very high loadings, especially for advance coefficients below the "critical" value of 0.41, ventilation rather than wavemaking is the decisive factor, and hence wavemaking theory alone fails to predict the behavior found in the experiment.

As explained in Appendix B.6, the wavemaking resistance of the propeller follows directly from its self-induced wake, see Equation (B62). Hence, opportunity was taken to compare the three different source representations of the propeller, defined by Equations (B10), (B11) and (B13), by plotting for each the ratio of calculated wavemaking resistance to measured thrust as a function of advance coefficient, see Fig. 14. Since the source disk is not a valid model for calculating <u>forces</u> acting on the propeller, the wavemaking resistance R_{WP} is not necessarily equal to the loss of thrust experienced by a propeller operating near the free-surface as compared to an equivalent deeply submerged condition. More appropriately, the ratio R_{WP}/T should be regarded as a measure of the loss of propeller efficiency due to the expenditure of energy for maintaining its steady wave pattern.

3.5 - Wave Analysis

It has already been stated that longitudinal wave profiles were measured at a fixed transverse distance (y_o = 0.134 L) from the model center plane in two conditions: 1) model with propeller running at the ship self-propulsion point (for an arbitrarily assumed model scale of 1:80), and 2) model with propeller replaced by a dummy hub, each at two selected speeds corresponding to the two values of speed-length parameter γ_o = 7.0 (F_n = 0.267) and γ_o = 4.0 (F_n = 0.354). Two pairs of corresponding profiles are reproduced in suitable nondimensional form in Fig. 15 and 16 respectively with the vertical scale magnified 100 times for the sake of clarity.

Evidently, the propeller exercised a measurable influence on the wave pattern of the model, the transverse wave amplitude behind the stern being higher with the propeller running in the cases shown. Even within the linearized wave theory two significantly different explanations can be offered for this effect. First, it might be a purely linear effect due to a superposition of the propeller wave on the hull wave. Second, it might be a pseudo-nonlinear effect due to a modification of the wavemaking properties of the hull itself as a result of propeller suction.

Another point of interest to note is the slight breaking of the bow wave clearly visible at the leading peaks in Fig. 16. It shows that the wave pattern was in places steep enough to introduce truly nonlinear effects, at least locally. This should be kept in mind when making comparisons with the calculations based on strictly linearized theory.

The measured wave profiles were analysed by the Fourier transform method as explained in Appendix B.8 and the results compared with the corresponding theoretical calculations based on explicit source representations of the hull and the propeller. The measured and calculated nondimensional free-wave amplitude spectrum E, and its sine, cosine components F, G are plotted as functions of nondimensional transverse wave number u in Fig. 17 to 19 for $\gamma_0 = 7.0$ and in Fig. 20 to 22 for $\gamma_0 = 4.0$. The following remarks are added to avoid any ambiguities of interpretation. The bare hull calculations are based on Equation (B23), the propeller calculations on Equation (B27) in conjunction with (B16), and the total system hull-propeller on Equation (B30). The free-wave spectra of the propeller alone in Fig. 19 and 22 are referred to a coordinate system with its origin in the propeller plane, see Equation (B73), whereas all others refer to a coordinate system with its origin in the midship section of the hull (see Fig. 1).

Some obvious conclusions are in order here. First, the agreement between calculations and measurement is only qualitative at the lower speed, but quite good at the higher speed. Second, the discrepancy between theory and experiment for the bare hull is mostly in phase and not so much in the amplitude of the free-wave spectrum. This is consistent with previous results of similar comparisons, see Sharma (1969). Third, the fair agreement between the "measured" free-wave spectrum of the propeller - it was actually derivedfrom the principle of linear superposition, see Equation (B72) - and the calculated spectrum

shows that our theoretical model of propeller wavemaking is reasonable and that the pseudo-nonlinear effect of the propeller on the hull waves referred to above is at least not the predominant phenomenon.

Finally, the calculated and measured wavemaking resistance according to Equations (B28, 29) and (B74) respectively are compared in the following table.

Nondimensional coefficient $R_W g^2/\rho V^6$ as calculated (measured)

Speed-length parameter	γ_o=7 or F_n=0.267	γ_o=4 or F_n=0.354
Hull alone	0.0650 (0.0380)	0.0354 (0.0245)
Propeller alone	0.0037 (0.0039)	0.0013 (0.0037)
Interaction term	0.0017 (0.0001)	0.0058 (0.0025)
System hull and propeller	0.0704 (0.0420)	0.0425 (0.0307)

As already noted in Section 3.3 (see Fig. 5), the measured values fall considerably short of the calculated ones, presumably due to viscous effects at the stern which reduce the wavemaking effectiveness of the afterbody. An interesting point to observe is that in one case the hull-propeller interaction term is found to be several times larger than the wave resistance of the propeller itself. This can be understood by reference to Equation (B32) which shows that the order of magnitude of the interaction term is intermediate between that of hull wave resistance R_{WH} and propeller wave resistance R_{WP}. Since the wave resistance associated with the propeller is an indirect measure of the loss

of efficiency, it follows that the effect of propeller waves on the propulsive efficiency of the system hull and propeller can be significantly larger than one would expect from the observed loss of open water propeller efficiency at the same submergence and loading.

3.6 - Interaction Analysis

3.6.1 - Propulsive Efficiencies

The first step in hull-propeller interaction analysis was the empirical determination of the conventional Froude propulsion factors by an analysis of the self-propulsion tests in conjunction with the results of the hull resistance and propeller performance (open water) tests. Using standard definitions and symbols, the factors in question are: the hull efficiency η_H, the equivalent open water efficiency η_O, and the relative rotative efficiency η_R, which combine to yield the propulsive efficiency η_D.

$$\eta_D = R_T V / 2\pi n Q_H$$
$$= \eta_H \eta_O \eta_R \qquad (15)$$

In the present context, the factor of primary interest is the hull efficiency η_H, which combines the effect of thrust deduction fraction t and the effective wake fraction w_E.

$$\eta_H = (1 - t)/(1 - w_E) \qquad (16)$$

Unfortunately, the breakdown of propulsive efficiency into

various factors is not unique (except for the fraction t), but depends on the somewhat arbitrary definition of an "equivalent" open water propeller condition. The common alternatives are the thrust identity and the torque identity methods. In order not to prejudice our results by the arbitrary choice of any one method, we carried out three complete analyses: one based on thrust identity (subscripts T), one on torque identity (subscripts Q), and one based on a mean (subscripts M) advance coefficient J_M defined as

$$J_M = (J_T + J_Q)/2 \tag{17}$$

where J_T and J_Q are the points of thrust and torque identity (between the behind hull condition and an equivalent open water condition of the propeller) respectively.

Our procedure for evaluating the propulsion factors can be briefly outlined as follows. Fig. 23 shows the typical result of a self-propulsion test at one Froude number, i.e. dimensionless coefficients of measured thrust T_H, torque Q_H, and residuary towing force F_D as functions of propeller advance coefficient J_H (based on hull speed). Obviously, this presentation is suitable for determining the self-propulsion points. Thus the model self-propulsion point lies at $C_{FD} = 0$ and the ship self-propulsion point at

$$\begin{aligned} C_{FD} &= C_{VM} - C_{VS} \\ &= (1 + k)(C_{FM} - C_{FS}) \end{aligned} \tag{18}$$

if viscous resistance is estimated by the form-factor method

and a surface roughness allowance is neglected for the sake of simplicity. Here C_{FM} and C_{FS} are the predetermined coefficients of friction at the model and ship Reynolds numbers respectively, see Equation (7). For instance, the self-propulsion point of a smooth geosim 80 times as long as the model (and running in fresh water at a temperature of 15°C) is found to lie at $J_H = 0.733$. Leaving aside the self-propulsion point for the moment, at <u>any</u> value of J_H (representing a certain propeller loading) the propulsion factors are found as follows. Take from the resistance test (Fig. 3) the coefficient of total resistance C_T at the given Froude number and obtain the propulsive efficiency*

$$\eta_D = (R_T - F_D)V/2\pi nQ_H$$
$$= (S/D^2)(C_T - C_{FD})/4\pi K_{QH}J_H^3 \qquad (19)$$

and the thrust deduction fraction

$$t = (T_H + F_D - R_T)/T_H$$
$$= 1 - (S/D^2)(C_T - C_{FD})/2K_{TH}J_H^2 \qquad (20)$$

Now read from the open water characteristics (Fig. 8) the advance coefficients J_T at thrust identity ($K_T = K_{TH}$) and J_Q at torque identity ($K_Q = K_{QH}$). Calculate J_M from Equation (17), and read the equivalent open water efficiencies η_{OT}, η_{OQ}, η_{OM} from Fig. 8 at J_T, J_Q, J_M respectively. Calculate

---

*For a truly self-propelled system the towing force $F_D = 0$, and then Equation (19) agrees with Equation (15).

effective wake fractions

$$w_T = 1 - J_T/J_H$$
$$w_Q = 1 - J_Q/J_H$$
$$w_M = 1 - J_M/J_H \qquad (21)$$

hull efficiencies

$$\eta_{HT} = (1-t)/(1-w_T)$$
$$\eta_{HQ} = (1-t)/(1-w_Q)$$
$$\eta_{HM} = (1-t)/(1-w_M) \qquad (22)$$

and relative rotative efficiencies

$$\eta_{RT} = \eta_D/\eta_{OT}\eta_{HT}$$
$$\eta_{RQ} = \eta_D/\eta_{OQ}\eta_{HQ}$$
$$\eta_{RM} = \eta_D/\eta_{OM}\eta_{HM} \qquad (23)$$

This completes the analysis.

The result of one such evaluation, out of fourteen actually carried out, is reproduced in Fig. 24. Since this is generally typical of all others, the following remarks are relevant. First, the thrust deduction fraction and relative rotative efficiency are relatively insensitive to changes in loading. Second, the equivalent open water efficiency decreases with increasing loading (decreasing J_H) as expected. Third, the effective wake fraction, and consequently the hull efficiency, decrease with increasing loading. This is in contradiction to the theoretical behavior in potential flow (see Appendix D). However, in a real flow the decrease in effective wake with increasing loading can

be explained qualitatively by a supposed contraction of the viscous wake due to propeller suction as first pointed out by Dickmann (1939), see also next section. Fourth, all propulsion factors vary slowly and almost monotonically with changes in loading, so that the arbitrary choice of one particular loading (e.g. that corresponding to the self-propulsion point of a ship of $\lambda = 80$) for further investigation is not liable to hide any important phenomena.

Fig. 25 shows the various propulsion factors as functions of Froude number over the range $3.5 \leq \nabla_o \leq 12.5$, all evaluated at the self-propulsion point of a smooth ship of $\lambda = 80$. (This choice of scale ratio is arbitrary, but not crucial as just pointed out.) The following features deserve special mention. First, all factors depicted exhibit a significant and oscillatory dependence on Froude number. Second, the self-propulsion point advance coefficient J_H, and consequently the equivalent open water efficiencies η_O, depend mainly on hull resistance, and hence reveal humps and hollows in inverse phase to the coefficient of wave resistance (compare Fig. 5) as expected. Third, contrary to common belief, the thrust deduction and effective wake fractions vary significantly with Froude number, the most remarkable feature being the sudden drop around $\nabla_o=5$. The hull efficiency η_H merely shows their combined effect. Fourth, the relative rotative efficiency η_R is exceptionally low, but approaches normal values at higher Froude numbers. Fifth, there is an unusually large discrepancy between thrust and torque identity points, but it tends to decrease with

increasing Froude numbers. The last two effects are presumably due to strong nonuniformities in the viscous wake of the hull, which would also explain why they are relatively weaker at higher Froude numbers.

3.6.2 - Wake

The next step in interaction analysis was an attempt to correlate by theory the measured wake and thrust deduction. This required first the generation of a mathematical model of the propeller in the behind hull condition. Again the computer program described in Appendix C was used. The inputs to the program were the advance coefficient J_M at the ship self-propulsion point, the corresponding thrust coefficient K_{TH}, the radial dustribution of measured nominal wake $w(R)$, and the two-dimensional foil characteristics already established on the basis of open water characteristics (see Propeller Analysis). In order to account for the difference between nominal and effective wake the program was allowed to determine by trial and error a wake corrector k_w, with which the nominal wake $w(R)$ was multiplied, such that the calculated thrust coefficient equalled the measured K_{TH}. The primary output of the program was the distribution of bound circulation along the radius. In addition, it also furnished a calculated torque coefficient K_{QH} and a mean effective wake $\tilde{w}_T$ (based on thrust average rather than volume average) from which followed the equivalent open water advance coefficient J_T. This elaborate analysis was done only for three selected

Froude numbers corresponding to γ_0 = 4.0, 7.0 and 12.5. The results are shown in Fig. 26 und 27. The effect of wake on circulation distribution is quite evident in Fig. 26 where the circulation maxima have been shifted toward smaller radii as compared to the open water condition of Fig. 11. Turning now to Fig. 27, the good agreement between calculated and measured advance coefficient J_T is a confirmation of the realistic simulation of thrust generation in the theoretical model, while the lack of agreement between calculated and measured torque coefficient K_{QH} points up the shortcomings of the theoretical model, specially the total neglect of all circumferential nonuniformities and the associated lack of any simulation of the relative rotative efficiency. However, we would not expect these defects to have any serious effect on the intended calculation of thrust deduction.

Before passing on to the evaluation of thrust deduction we pause to consider briefly the issue of nominal wake versus effective wake. Conceptually, the distinction is clear: Nominal wake is the flow peturbation created by the hull in the propeller plane with the propeller removed, while effective wake is the flow perturbation due to the hull in the propeller plane with the propeller in place and operating. In practice, however, the relative magnitudes of these two wakes have been a topic of considerable controversy and confusion in the literature on hull propeller interaction. It is generally agreed that there are two fundamentally different reasons why these two wakes need not be identical. First, there is a genuine

physical effect of the propeller on the flow perturbation caused by the hull. This has three partially counteracting components. a) The potential component, which may be understood as the additional flow induced by the image of the propeller in the hull, tends to increase the effective wake compared to the nominal wake, since this image consists predominantly of sinks in the afterbody. b) The viscous component, which results from a contraction of the viscous wake, is specially pronounced if the line of boundary layer separation is shifted rearward by propeller suction and generally tends to decrease the effective wake compared to the nominal wake by bringing more undisturbed flow into the propeller disk. c) The wave component, referred to as a pseudo-nonlinear effect of the propeller on the wavemaking properties of the hull in Section 3.5, can act in either direction depending upon Froude number. Second, there is a spurious computational effect due to different methods of averaging. The measured nominal wake is conventionally averaged over the disk on a volume flux basis, while the mean effective wake is measured by the propeller as a calibrated thrust (or torque) generating device which tends to put maximum weight near the radii where the circulation is a maximum. The following table, a by-product of our calculations, is likely to shed some light on the relative importance of these two effects (see next page).

First, note that the wake corrector k_w is a measure of the true physical difference between nominal and effective wake since, as explained earlier, it was determined by trial and

Speed-length parameter		Measured nominal wake		Wake correc-tor	Corrected nominal wake		Effective wake	
							Simu-lated	Meas-ured
γ_o	F_n	w	$w(.7R_p)$	k_w	$k_w w$	$k_w w(.7R_p)$	$\tilde{w}_T$	w_T
4.0	0.354	0.208	0.230	0.704	0.146	0.162	0.153	0.145
7.0	0.267	0.291	0.322	0.892	0.259	0.287	0.291	0.285
12.5	0.200	0.304	0.370	0.933	0.284	0.346	0.377	0.360

and error as the required multiplier of the measured nominal wake in the computer program to ensure that the simulated and measured thrusts were equal. This difference is here seen to vary from -7 % at the lowest Froude number to -30 % at the highest. That it is strongly negative, suggests that the viscous effect mentioned above was probably dominant in this case. Second, the residual difference (up to +33 %) between the corrected volume average wake $k_w w$ and the thrust average wake $\tilde{w}_T$ must be attributed to the difference in the methods of averaging. Note that this spurious effect is greatest at the lowest Froude number where the concentration of bound circulation over the inner radii was also the most pronounced. Third, the good agreement between the computer simulated and the experimentally measured mean effective wake is rather encouraging. Fourth, note that the effective wake is much better approximated by the corrected nominal wake at 0.7 radius, $k_w w(.7R_p)$, than by its disk average, $k_w w$. This observation has direct relevance to the design of wake-adapted propellers. Finally, as a word of caution,

it should be noted that the relative magnitudes of the nominal and effective wakes as well as the quantitative rankings of the different effects found here may be peculiar to this model and therefore should not necessarily be generalized.

To complete the discussion of wake, Fig. 28 shows the measured versus calculated wake as a function of Froude number. The following quantities are plotted: 1) The disk average of the measured nominal wake w. This was available at three speeds only (compare Fig. 7). 2) The disk average of the potential wake w_p calculated by thin ship theory, see Appendix B.5, especially Equation (B54). This is a zero Froude number approximation. 3) The disk average of the sum of potential and wave wakes (w_p+w_w) also calculated by thin ship theory, see Appendix B.5, especially Equation (B53). 4) The quantity $(w_T-w_p-w_w)$ as an approximate estimate of the viscous component w_v, see Equation (1). The striking correlation between the measured effective wakes and the calculated wave wake certainly suggests that the observed oscillations of wake with Froude number are indeed free-surface effects and that the thin ship wavemaking theory despite all its weaknesses does give a reasonable estimate of this phenomenon. Even the quantity $(w_T-w_p-w_w)$, which as the difference of a measured effective wake and calculated nominal wake components must be regarded with due caution, gives a credible impression of the magnitude of viscous wake w_v. However, one cannot put much faith in its observed oscillations.

3.6.3 - Thrust Deduction

We now turn to our final goal of calculating the thrust deduction fraction and its components. This was done to two different degrees of approximation. At the three selected Froude numbers, where the calculated circulation distribution was available (see Fig. 26), the Hough and Ordway relation, Equation (B16) in conjunction with the simulated effective wake $k_w w(R)$, was applied to generate the equivalent sink disks. At all other Froude numbers we had to be content with Dickmann's approximate relation between thrust coefficient and source strength, Equation (B15) in conjunction with the measured effective wake w_T. The numerical difference between these two approximations is illustrated in Fig. 29. Evidently, the Hough and Ordway approximation yields slightly higher mean values and, in accordance with the distribution of bound circulation, effects a concentration of sink strength toward the inner radii. It is believed to be more accurate than Dickmann's uniform sink disk since the vortex model yields a more realistic flow pattern than the simple momentum theory.

In either event, the sink disk was used to calculate first the wavemaking resistance of the propeller alone and of the system hull and propeller as explained in Appendix B. The wavemaking resistance (and free-wave spectrum) of the propeller in the behind hull condition calculated in this way were found to be in reasonable agreement with the corresponding results of measured wave profile analysis at two Froude numbers as already discussed in Section 3.5. Given the wavemaking resistances of

the hull R_{WH}, propeller R_{WP}, and total system R_{WT}, only one additional quantity $\delta_H R_{WP}$, see Equation (B64), was needed for calculating the combined potential and wave thrust deduction force $\delta_P R_{WH}$, see Equation (B65), from which followed the thrust deduction fraction (t_p+t_w) by Equation (B66). The potential component t_p alone was obtained from a simple degenerate case (zero Froude number wake) of this calculation, see remark following Equation (B67). The final results of this calculation are shown in Fig. 30 in comparison to the measured total thrust deduction t replotted from Fig. 25.

Let us try to interpret the salient features of Fig. 30. First, the wave component of thrust deduction t_w is small, but not negligible compared to the potential component t_p. Second, the oscillations in calculated thrust deduction are not due to t_w, but are already present in t_p. This can be understood by reference to Equation (B63) which defines thrust deduction as the Lagally force on the hull sources due to the axial flow induced by the propeller sources. Since our hull sources were assumed independent of Froude number and since the flow induced by a source upstream of itself is almost monotonic with Froude number, the observed oscillations of calculated thrust deduction can only be due to variations of propeller source strength with Froude number. This is indeed the case, for by Equation (B15) the source strength depends on loading and wake, which were both found to oscillate with Froude number. As a result the calculated thrust deduction t_p (as well as t_w) correlates strongly with advance coefficient J_H and effective

wake w_T (compare Fig. 25). Third, the oscillations in the measured thrust deduction t are much stronger than in the calculated (t_p+t_w). This means that either the residual viscous component of thrust deduction t_v, see Equation (2), oscillates appreciably with Froude number or that our assumption of the hull sources being independent of Froude number was invalid. This point cannot be decided at the moment. But in any case it points to a significant interaction of viscous and wave effects at the stern, presumably intensified by propeller suction. For instance, if the line of boundary layer separation is pulled rearward by the propeller, the result would be a negative viscous thrust deduction as well as a relative increase in the effective sink strength of the afterbody. Fourth, specifically the steep variation of measured thrust deduction around $\gamma_o = 5$ cannot presently be explained, except as a possible viscous effect, i.e. a reduction in the extent of boundary layer separation under the combined influence of a negative wave wake (Fig. 28) and a high propeller loading (Fig. 25). Fifth, the thrust deductions calculated from the Hough and Ordway sink disk are significantly higher than those calculated from the Dickmann sink disk and are in better agreement with measurements. This is a direct consequence of the significant difference between the two sink disks, both in average intensity and in its relative distribution over propeller radius, see Fig. 29.

4 - CONCLUDING REMARKS

It has been demonstrated by practical application to a specific example that our conceptual scheme for determining the potential, viscous and wave components of wake and thrust deduction is indeed workable. It has required the concerted application of miscellaneous analytical, computational and experimental techniques. The varying degrees of success achieved with the individual techniques have been discussed in detail in the appropriate sections and need not be repeated here. Several results were obtained by more than one method, for instance by independent calculation and measurement, and in most cases there was fair agreement, at least there were no striking contradictions except perhaps in the calculated and measured wavemaking resistance at low Froude numbers, which came as no surprise.

It would be rash to try to derive general conclusions concerning the quantitative role of wavemaking at the free surface in the phenomenon of hull propeller interaction on the basis of one single example. However, two salient results do seem to have a broader significance. First, it was found that contrary to common belief the wave component can be dominant in the wake and quite significant in the thrust deduction at Froude numbers around $F_n = 0.3$. Second, there seemed to be an appreciable viscous component in the thrust deduction at practically all Froude numbers. Moreover, the undulating variation of this

component with Froude number points to a complicated interaction of viscous boundary layer, hull wave pattern and propeller suction near the stern.

These two effects are of direct relevance to the hydrodynamic design of fast ships and also to the methods of extrapolating propulsive performance from model to full-scale.

It is recommended that further studies of this nature be undertaken to resolve the remaining issues and to collect systematic design data on the effect of wavemaking on the propulsive performance of ships.

5 - ACKNOWLEDGMENTS

We want to sincerely thank the following individuals and organizations for their valuable contributions to this project:

Mr. J. L. Beveridge and Dr. W. B. Morgan of the Naval Ship Research and Development Center for crucial consultations in the planning stage of this work,

Mr. W. S. Vorus, Ph. D. candidate at the University of Michigan, for a major share of the computer programming and test evaluation,

Dr. C. Östergaard, visiting scientist at the University of Michigan, for the computer program for propeller design originated at the Technical University of Berlin and extended at the University of Michigan to cover the off design performance,

Mr. A. M. Reed, graduate student at the University of Michigan, for the computer programs for wave profile analysis and theoretical wavemaking resistance,

Mr. B. Hutchison and Miss S. Pian, students at the University of Michigan, for their assistance in writing the computer program for hull wave flow calculations by thin ship theory,

Mr. E. Snyder of the Ship Hydrodynamics Laboratory, University of Michigan, for his expert execution of the model test program,

Messrs. T. Little, A. Toro, and B. L. Young, students at the University of Michigan, for their enthusiastic help in conducting the model tests,

The staff of the Ship Hydrodynamics Laboratory, University of Michigan, for their careful and patient handling of all jobs pertaining to the model tests,

The Hamburg Ship Model Basin (HSVA), Hamburg, Germany, for lending a model propeller for our experiments, and

The Naval Ship Research and Development Center, Carderock, Maryland, for providing copies of computer programs for propeller design (Lerbs induction factor program) and potential flow calculations (Hess and Smith program).

6 - BIBLIOGRAPHY

Note:- The following is a fairly complete list of recent publications, not necessarily cited in our text, directly dealing with the subject of hull propeller interaction. References to older literature can be found in Dickmann's (1939) monograph. We hope that this list will serve as a useful handy reference to future workers in this field.

Amtsberg, H.: Investigations with axisymmetric bodies into the interaction between hull and propeller (in German). Jahrbuch STG 54, 117-152 (1960).

Amtsberg, H., and Arlt, W.: Thrust deduction studies of bodies with bluff ends (in German). Schiff und Hafen 17, 786-790 (1965).

Bassin, A.M.: Theory of interaction between the propeller and hull of a vessel in an infinite fluid (in Russian). Bulletin of USSR Academy of Science, Division of Technical Sciences 12, 1723- (1946).

Beveridge, J.L.: Thrust deduction due to a propeller behind a hydrofoil. DTMB Report No. 1603 (1962).

Beveridge, J.L.: Effect of axial position of propeller on the propulsion characteristics of a submerged body of revolution. DTMB Report No. 1456 (1963).

Beveridge, J.L.: Pressure distribution on towed and propelled streamline bodies of revolution. DTMB Report No. 1665 (1966).

Beveridge, J.L.: Analytical prediction of thrust deduction for submersibles and surface ships. Journal of Ship Research 13, 258-271 (1969) = NSRDC Report No. 2713 (1968).

Chertock, G.: Forces on a submarine hull induced by the propeller. Journal of Ship Research 9, 122-130 (1965).

Dickmann, H.E.: Thrust deduction, wave resistance of a propeller, and interaction with ship waves (in German). Ingenieur Archiv 9, 452-486 (1938).

Dickmann, H.E.: Propeller and surface waves (in German). Schiffbau 40, 434-437 (1938).

Dickmann, H.E.: Wave resistance of a propeller and its interaction with ship waves. Proc. International Congress for Applied Mechanics 5, - (1938).

Dickmann, H.E.: Interaction between hull and propeller with special consideration to the influence of waves (in German). Jahrbuch STG 40, 234-291 (1939).

Dreger, W.: A procedure for computing the potential thrust deduction (in German). Schiffstechnik 6, 175-187 (1959).

Froude, R.E.: A description of a method of investigation of screw propeller efficiency. Transactions INA 24, 231-255 (1883).

Horn, F.: Study on the subject of interaction between hull and propeller (in German). Schiff und Hafen 7, 601-604 (1955).

Horn, F.: Relation between thrust deduction and wake in pure displacement flow (in German). Schiff und Hafen 8, 472-475 (1956).

Hucho, W.H.: On the influence of a stern propeller upon the pressure distribution and boundary layer of a body of revolution (in German). Institute of Fluid Mechanics, Braunschweig, Germany, Report No. 64/65 (1965).

Hucho, W.H.: On the relation between pressure thrust deduction, frictional thrust deduction and wake in flow about bodies of revolution (in German). Schiff und Hafen 20, 689-693 (1968).

Hunziker, R.R.: Hydrodynamic influence of the propeller on a deeply submerged submarine. International Shipbuilding Progress 5, 166-177 (1958).

Isay, W.H.: Propeller Theory - Hydrodynamic Problems (in German). Springer Verlag, Berlin/Heidelberg/New York (1964).

Isay, W.H.: Modern Problems of Propeller Theory (in German). Springer Verlag, Berlin/Heidelberg/New York (1970).

Korvin-Kroukovsky, B.V.: Stern propeller interaction with streamline body of revolution. International Shipbuilding Progress 3, 3-24 (1956).

Lefol, J.: The interaction between ship and propeller (in French). Bulletin ATMA 46, 221-252 (1947).

Martinek, J., and Yeh, G.C.K.: On potential wake and thrust deduction. International Shipbuilding Progress 1, 79-82 (1954).

Nakatake, K.: On the interaction between the ship hull and the screw propeller (in Japanese). Journal of Seibu Zosen Kai 34, 25-36 (1967).

Nakatake, K.: On the interaction between the ship hull and the screw propeller (in Japanese). Journal of Seibu Zosen Kai 36, 23-48 (1968).

Niemann, U.: Survey of investigations on the interaction between hull and propeller for partially submerged propellers (in German). Forschungszentrum des Deutschen Schiffbaus, Hamburg, Germany, Report No. 5 (1968).

Nowacki, H.: Potential wake and thrust deduction calculations for shiplike bodies (in German). Jahrbuch STG 57, 330-373 (1963).

Pohl, K.H.: On the interaction between hull and propeller (in German). Jahrbuch STG 55, 255-305 (1961).

Pohl, K.H.: Investigation of nominal and effective wake in the propeller plane of single-screw ships (in German). Schiffstechnik 10, 23-28 (1963).

St. Denis, M., and Craven, J.P.: Recent contributions under the Bureau of Ships Fundamental Hydromechanics Research Program. Journal of Ship Research 2, 1-36 (1958).

Tsakonas, S.: Analytical expressions for the thrust deduction and wake fraction for potential flows. Journal of Ship Research 2, 50-59 (1958).

Tsakonas, S., and Jacobs, W.R.: Potential and viscous parts of the thrust deduction and wake fraction for an ellipsoid of revolution. Journal of Ship Research 4, 1-16 (1960).

Tsakonas, S., and Jacobs, W.: Analytical study of the thrust deduction of a single-screw thin ship. International Shipbuilding Progress 9, 65-80 (1962).

Wald, Q.: Performance of a propeller in a wake and the interaction of propeller and hull. Journal of Ship Research 9, 1-8 (1965).

Weinblum, G.P.: The thrust deduction. Journal ASNE 63, 363-380 (1951).

Yamazaki, R.: Introduction to propulsion of ships in calm seas (in Japanese). Journal of Seibu Zosen Kai 33, 177-196 (1967).

7 - ADDITIONAL REFERENCES

Note:- References not belonging by virtue of their subject matter into the foregoing Bibliography but cited in our text for some specific reason are listed below.

Burrill, L.C.: Propeller Cavitation Committee Report. Proceedings ITTC 13, 353-355 (1960).

Eggers, K.W.H., Sharma, S.D., and Ward, L.W.: An assessment of some experimental methods for determining the wavemaking characteristics of a ship form. Transactions SNAME 75, 112-144 (1967).

Gradshteyn, I.S., and Ryzhik, I.M.: Table of Integrals, Series and Products. Academic Press, New York and London (1965).

Haskins, E.W.: Calculation of design data for moderately loaded marine propellers by means of induction factors. NSRDC Report No. 2380 (1967).

Havelock, T.H.: The theory of wave resistance. Proceedings of Royal Society (A) 138, 339-348 (1932).

Hess, J.L., and Smith, A.M.O.: Calculation of non-lifting potential flow about arbitrary three-dimensional bodies. Douglas Aircraft Co. Report E.S. 40622 (1962).

Hough, G.R., and Ordway, D.E.: The generalized actuator disk. Developments in Theoretical and Applied Mechanics 2, 317-336 (1965).

Küchemann, D., and Weber, J.: Aerodynamics of Propulsion. McGraw-Hill Book Company, New York/Toronto/London (1953).

Lerbs, H.: Moderately loaded propellers with a finite number of blades and an arbitrary distribution of circulation. Transactions SNAME 60, 73-123 (1952).

Luft, H.: Wave probes for model tanks. Hamburg Ship Model Basin Report No. F 46/67, translated from German by W.H. Roth and S.D. Sharma, University of Michigan, Department of Naval Architecture and Marine Engineering (1968).

Lunde, J.K.: On the linearized theory of wave resistance for displacement ships in steady and accelerated motion. Transactions SNAME 59, 25-85 (1951).

Meyne, K.: Experimental and theoretical considerations on scale effect in propeller model tests (in German). Hamburg Ship Model Basin Report No. 1361 (1967).

Michell, J.H.: The wave resistance of a ship. Philosophical Magazine 45, 106-123 (1898).

Östergaard, C.: On computer-aided propeller design. The University of Michigan, Department of Naval Architecture and Marine Engineering Report No. 88 (1970).

Östergaard, C., Kruppa, C., and Lessenich, J.: Contribution to problems of propeller design (in German). Schiff und Hafen 23, 531-538 (1971).

Prohaska, C.W.: A simple method for the evaluation of the form factor and the low speed wave resistance. Proceedings ITTC 11, 65-66 (1960).

Sharma, S.D.: An attempted application of wave analysis techniques to achieve bow-wave reduction. Proceedings of Symposium on Naval Hydrodynamics 6, 731-773 (1966).

Sharma, S.D.: Some results concerning the wavemaking of a thin ship. Journal of Ship Research 13, 72-81 (1969).

Shiba, H.: Air-drawing of marine propellers. Transportation Technical Research Institute of Japan, Report No. 9 (1953). English translation published by Unyu-Gijutsu Kenyujo, Tokyo, Japan.

Wehausen, J.V., and Laitone, E.V.: Surface Waves. Encyclopedia of Physics 9, 446-814 (1960). Springer Verlag, Berlin/Göttingen/Heidelberg.

APPENDIX A - EXPERIMENTAL PROCEDURES

All hull and propeller model experiments were conducted in the towing tank of the Ship Hydrodynamics Laboratory of the University of Michigan following essentially standard test procedures. Some of the more interesting, but less obvious details are documented here for the sake of record.

A.1 - Hull Resistance Test

The University of Michigan ship model No. UM 1201, built out of wood to the shape and size determined by Equations (3) through (5), without appendages was used for the hull resistance test. An unusually high freeboard (equal to full draft) was provided to enable testing at high Froude numbers up to $F_n = 0.5$. Circular cylindrical studs of 1/8 inch diameter and 1/8 inch height were fitted at 5/8 inch spacing center-to-center along the entire girth of station No. 1 (that is, 0.05 L abaft of the vertical stem) to stimulate turbulence.

Departing from standard practice, the model was almost rigidly attached to the towing carriage by means of a three-point system of vertical supporting rods in addition to the usual grasshopper type anti-yaw guides at the two ends. This constraint was necessitated by the marginal transverse stability of the model and by the desire to preclude dynamic trim and sinkage for the ease of comparison with theory. The model was correctly weighted before making the connections, and static

draft, heel and trim were verified before and after each test.

The resistance was measured by means of tare weights and a horizontal load call built into a floating beam arrangement between the model and the carriage. Carriage speed was measured from wheel contacts and displayed on a calibrated digital counter. The speed range was extended up to V_m = 9.75 ft/sec (about F_n = 0.45), which was the highest attainable within the limitations imposed by tank length, model freeboard, and instrumentation.

A.2 - Propeller Performance Test

The Hamburg Ship Model Basin model propeller No. HSVA 1222 with a standard nose fairing piece as shown in Fig. 2 was used for the propeller performance tests in open water. The propeller material is bronze.

The test procedure was to keep a constant rate of revolution and measure thrust and torque at various speeds of advance so as to cover the entire range of advance coefficient from the bollard condition ($J = 0$) up to the zero thrust condition ($J \approx P/D$). A standard Kempf & Remmers propeller dynamometer was used. The measured torque was corrected for bearing friction determined under identical test conditions with the propeller replaced by a dummy hub. No "dummy hub correction" was applied to the measured thrust.

The Reynolds number for open water propeller test is conventionally defined as

$$(R_n)_{0.7R_P} = \frac{nD^2}{\nu} \left(\frac{c}{D}\right)_{0.7R_P} \sqrt{J_D^2 + (0.7\pi)^2}$$

with the design advance coefficient J_D usually approximated by 0.75 P/D. Given the propeller geometry

$$D = 0.2 \text{ m} \quad (c/D)_{0.7R_P} = 0.328 \quad P/D = 1$$

and our test conditions

$$n = 11 \text{ rps}^* \quad t = 69^\circ F \quad \nu = 0.9904 \cdot 10^{-6} \text{ m}^2/\text{s}$$

it is seen that the Reynolds number was about $3.4 \cdot 10^5$. This might appear to be barely sufficient to avoid scale effects due to laminar flow. However, we obtained satisfactory agreement with previous tests run at the Hamburg Ship Model Basin at a Reynolds number of $3.6 \cdot 10^5$. By contrast, a test series run at the Institut für Schiffbau in Hamburg with the same propeller at a Reynolds number of $6.0 \cdot 10^4$ showed systematic scale effect at advance coefficients $J \leq 0.6$, cf. report by Meyne (1967).

A.3 - Self-Propulsion Test

Special care was taken in the self-propulsion tests to ensure that test conditions were identical to those of hull resistance and propeller performance tests. The model was constrained in the same fashion as in the resistance test and the

---

*This was the highest rate of revolutions possible without overloading the propeller dynamometer in the bollard condition.

towing force was measured by the same instrumentation used for resistance measurements. The model propeller was driven by an electric motor at predetermined rate of revolutions and thrust and torque were measured by the same dynamometer used for the open water tests. A streamlined tail fairing piece (see Fig.2) was fitted to the propeller hub. The measured torque was corrected for bearing friction determined by replacing the propeller temporarily by a dummy hub. No "dummy hub correction" was applied to the measured thrust.

The self-propulsion points were determined by the so-called British method, i.e. for each test run the towing speed and propeller rate of revolutions were preset while thrust, torque and residual towing force were the quantities to be measured when the steady state condition had been reached. For each Froude number investigated, five to eight test runs at the same towing speed but varying rates of revolution were conducted to cover a wide range of propeller loading around the ship self-propulsion point (and usually extending up to and beyond the model self-propulsion point).

There was some indication (a characteristic knocking sound familiar from the previous open water tests) of mild ventilation at the highest propeller loadings encountered in the self-propulsion tests. However, there was no visible effect on the measured thrust and torque values.

A.4 - Wake measurement

A set of standard Kempf & Remmers four-bladed wake wheels

was used to measure the nominal wake in the propeller plane behind the hull in both forward and reverse motion. The diameters of the wheels available ranged from 40 to 220 mm in steps of 20 mm. The wheels were designed to yield directly the circeumferential average of the axial flow velocity at the wheel radius. There was provision for turning the wheels around by 180 deg on their axis to ensure that the direction of flow relative to the blades was the same for both forward and reverse motions of the model (thus requiring only one set of calibrations).

The wheels were first calibrated in open water at a submergence of 150 mm (identical to that used for the model wake measurements) by means of a special towing device also supplied by the manufacturer. In principle, the calibration curves (i.e. wheel rate of revolution as a function of towing speed) should have been linear. In practice, a few wheels showed pronounced nonlinearities and even mild discontinuities at some speeds, presumably due to flow instabilities. However, all calibrations were highly repeatable.

For the actual wake measurements, the wheel towing device was mounted rigidly to the inside of the model with only its axis projecting out of the stern tube on to which each respective wake wheel was mounted at the appropriate propeller clearance (45 mm from wheel center to the vertical stem profile). Every measurement was repeated at least once.

It has been noted elsewhere that the measured wake in both forward and reverse motion showed somewhat erratic undulations

at the outer radii (see Fig. 6 and 7). This could possibly be blamed on the method of measurement. We had no way of establishing just how accurately the uniform flow calibrations could be relied upon for determining the circumferential averages of a varying axial velocity in a complex nonuniform flow involving significant circemferential and radial components.

A.5 - Wave Measurement

A stationary wave probe was mounted at a point about midway along the length of the towing tank and at a fixed transverse distance y_o = 605 mm from the center plane of the model (which coincided nearly with the center plane of the tank itself). Hence, a time record of local wave height at the probe, while the model passed by, was obviously equivalent to a longitudinal cut $z = \zeta(x,y_o)$ through the steady wave pattern of the model in a coordinate system Oxyz moving with the model.

A thin light beam was set up across the tank at a known fixed distance (x_1 = 336 mm) upstream of the probe. During the run a shutter affixed to the model at a known fixed distance (x_s = 2933 mm) forward of the midship section interrupted the light beam and generated an event signal marking the point $x = x_s - x_1$ on the wave record, thus defining the coordinate origin.

The wave probe itself was of the conductance wire type adapted from the HSVA design of Luft (1968) to match the available Sanborn carrier frequency preamplifiers. The circuit output was fed into one channel of a Sanborn strip chart recorder.

The overall sensitivity was set at 6 to 9 mm deflection per inch of wave height so as to produce full scale deflection at the measured wave peaks. Wave height records were manually read off at about 350 points at equal time intervals $\Delta t = 0.03$ sec, that is at a step size $\Delta x = -V \Delta t$, and key-punched on IBM cards. All further analysis was done by computer programs.

It should be noted that at the highest Froude number investigated the length of useful record (taken before running into tank wall reflection) was not really adequate to establish with confidence the asymptotic character of the wave profile behind the model which is needed for the application of a truncation correction (see Fig. 16). However, this was due to a purely geometrical constraint resulting from the given ratio of model length to tank width, so there was little we could do about it.

APPENDIX B - WAVEMAKING CALCULATIONS

All calculations concerning the wavemaking of the hull and the propeller were based on the strictly linearized theory and therefore involved the usual assumptions of irrotational flow, infinitesimal wave heights etc., see e.g. Lunde (1951) or Wehausen and Laitone (1960). The following is essentially a compilation of the important formulas used in the present study without attempting to give complete proofs or derivations.

B.1 - Nondimensional Notation

Throughout this Appendix a special nomenclature particularly adapted to the analysis of steady-state gravity-wave problems will be used. This differs from the nomenclature in the rest of the report only in that all* dimensional variables have been consistently rendered dimensionless by reference to a set of three fundamental quantities, namely the acceleration due to gravity $\underline{g}$, water density $\underline{\rho}$, and ship speed $\underline{V}$. Thus if $\underline{Q}$ is any dimensional quantity involving only the units of mass, length and time, its nondimensional counterpart Q is defined simply as

$$Q = \underline{Q} \; / \; \underline{g}^{\alpha} \; \underline{\rho}^{\beta} \; \underline{V}^{\gamma} \qquad \text{(B1)}$$

---

*Where dimensional variables are nevertheless required, e.g. for purposes of definition, they are identified by underlining to avoid any possible ambiguity.

where the choice of α, β and γ is obviously unique. For instance,

$$x = \underline{x} \,/\, \underline{g}^{-1}\, \underline{V}^2, \qquad l = \underline{l} \,/\, \underline{g}^{-1}\, \underline{V}^2$$
$$\sigma = \underline{\sigma} \,/\, \underline{V}$$
$$R_W = \underline{R}_W / \underline{g}^{-2}\, \underline{\rho}\, \underline{V}^6 \qquad \text{(B2)}$$

where x is the longitudinal coordinate, l the half-length of hull (now identical to the dimensionless speed-length parameter γ_o used elsewhere in the report), σ the density of a surface distribution of sources, R_W the wavemaking resistance etc. With this notation the quantities ρ, V and g can be formally eliminated from the analysis, thus leading to a considerable simplification of many formulas without any essential loss of generality.

B.2 - Source Representations

All wavemaking calculations were based on the Havelock (1932) theory of sources moving under a free surface. It was therefore necessary to first define mathematical representations of the hull and propeller by means of source distributions.

The standard first order (linearized) approximation in thin ship theory is to represent the hull by a center-plane source distribution of density

$$\sigma(x,z) = -\,(\partial f/\partial x)/2\pi \qquad \text{(B3)}$$

where

$$|y| = f(x,z) \geq 0 \qquad \text{(B4)}$$

defines the hull surface (see Fig. 1). The results obtained by

Havelock's theory are then identical to those of Michell (1898).

The family of hull forms considered in the present study is defined by

$$y = \pm b\{1 - (x/l)^{2m}\}\{1 - \epsilon(-z/T)^{n}\} \qquad (B5)$$

where b, l and T are half-beam, half-length and draft respectively, while ϵ is a flat-bottom parameter that can vary from $\epsilon = 0$ (wall sided hull with completely flat bottom) to $\epsilon = 1$ (sharp keeled hull with completely curved bottom). By virtue of Equations (B3, B4) this form is represented by the polynomial source distribution

$$\sigma(x,z) = (m/\pi)(b/l)(x/l)^{2m-1}\{1-\epsilon(-z/T)^{n}\} \qquad (B6)$$

over the rectangular plane

$$-l \le x \le l, \qquad y = 0, \qquad -T \le z \le 0 \qquad (B7)$$

Following Dickmann (1938), the propeller can be represented by a continuous distribution of sources of (negative) density $\sigma(R,\theta)$ over the propeller disk

$$x = x_p, \qquad R_H \le R \le R_p, \qquad -\pi \le \theta \le \pi \qquad (B8)$$

where R,θ are polar coordinates

$$y = R\cos\theta, \qquad z = z_p + R\sin\theta \qquad (B9)$$

the point $(x_p,0,z_p)$ is the geometrical center of the propeller and R_H, R_p are the hub and tip radius of the propeller respectively. There is no simple way of relating the source strength directly to propeller geometry, speed and rate of revolutions. However, using momentum theory, Dickmann derived two useful

approximations connecting propeller source strength to thrust loading, one of which yields a uniform sink disk of source density

$$\sigma(R,\theta) = -(\sqrt{1+C_{Th}} - 1)/4\pi$$

$$\text{over} \qquad x = x_P, \qquad R_H \le R \le R_P, \qquad -\pi \le \theta \le \pi \tag{B10}$$

and the other a discrete point sink of source strength

$$-(\sqrt{1+C_{Th}} - 1)(R_P^2 - R_H^2)/4 \quad \text{at} \quad (x_P, 0, z_P) \tag{B11}$$

where

$$C_{Th} = 2\,\underline{T} \,/\, \underline{\rho}\,\underline{V}^2\,\pi\,(\underline{R}_P^2 - \underline{R}_H^2) \tag{B12}$$

is the thrust loading coefficient based on disk area (excluding the hub).

In addition to the above we have also used the following alternative relation due to Hough and Ordway (1965):

$$\sigma(R,\theta) = -\,Z\,G \,/\, 4\,J \tag{B13}$$

where

$$G(R) = \underline{\Gamma}(\underline{R}) / \,2\,\pi\,\underline{V}\,\underline{R}_P \tag{B14}$$

is a nondimensional function representing the radial distribution of bound circulation $\underline{\Gamma}$ along each blade of a Z bladed propeller at advance coefficient $J = \underline{V} \,/\, 2\,\underline{n}\,\underline{R}_P$. Here the source density is a function of radius R, but still independent of angle θ. Since the circulation is obtained numerically from a computer program at discrete radii, σ will generally be defined merely as a tabulated function. Unless analytical interpolation is used for further processing, it is tantamount

to a radially stepped sink disk.

A certain ambiguity arises in interpreting the speed $\underline{V}$ in the above relations when the propeller is operating in a wake behind the hull. We believe that the physical sink strength of the propeller should be determined by the local speed of advance $\underline{V}_A$ while its wave pattern must be charaterized by the speed $\underline{V}$ relative to the fluid at infinity. Hence the corresponding relations in the presence of an effective axial wake w_E become

$$\sigma(R,\theta) = -(\sqrt{1+C_{Th}} - 1)(1 - w_E)/4\pi$$
$$C_{Th} = 2\,\underline{T} \;/\; \underline{\rho}\,\underline{V}_A^{\,2}\,\pi\,(\underline{R}_P^{\,2}-\underline{R}_H^{\,2}) \qquad \text{(B15)}$$

in the Dickmann approximation, and

$$\sigma(R,\theta) = -\,Z\,\underline{n}\,\underline{\Gamma}(\underline{R}) \;/\; \underline{V}^2\,\{1 - w_E(R)\} \qquad \text{(B16)}$$

in the Hough and Ordway approximation. In either case, the left hand side is the appropriate dimensionless source density σ to be used in the subsequent calculations of wavemaking and thrust deduction.

It may be noted that source disk representations of the propeller are only useful for calculating the induced flow field (outside the slipstream). For calculating propeller performance (thrust and torque) resort must be taken to the correct vortex model. In principle, it is possible to calculate also flow field and wavemaking directly from the vortex model, cf. e.g. Nakatake (1968). However, the increased computational effort is hardly justified in view of the other approximations in the analysis.

B.3 - Free-Wave Spectrum

A useful description of the wavemaking characteristics of a ship is provided by its free-wave spectrum as defined for example in Eggers, Sharma and Ward (1967). Given an arbitrary source distribution $\sigma(x,y,z)$ over a domain D, its complex-valued free-wave spectrum (as a function of transverse wave number u) becomes

$$G(u)+iF(u) = 8\pi \left\{\frac{1+v}{v}\right\} \int_D \sigma(x,y,z) \exp\left\{s^2 z+i(sx+uy)\right\} dD \qquad (B17)$$

where $v = \sqrt{1+4u^2}$ and $s = \sqrt{(1+v)/2}$ (B18)

The significance of the free-wave spectrum lies in its ability to yield a simple description of the asymptotic wave pattern behind the ship.

$x \to -\infty$:

$$\zeta(x,y) = \frac{1}{4\pi} \int_{-\infty}^{\infty} \left\{F(u)\sin(sx+uy) + G(u)\cos(sx+uy)\right\} du \qquad (B19)$$

Here s and u can be interpreted as the circular wave numbers induced by a free plane wave (moving with the ship) in the x and y direction respectively. Hence $F(u)$ and $G(u)$ are called the sine and cosine components of the spectrum and its amplitude is given by

$$E(u) = \sqrt{F^2(u)+G^2(u)} \qquad (B20)$$

The phase of the free-wave spectrum depends on the choice of the coordinate origin but its amplitude does not. The associated

wavemaking resistance

$$R_W = \frac{1}{16\pi} \int_{-\infty}^{\infty} E^2(u) \frac{v}{1+v} du \qquad (B21)$$

is determined solely by the amplitude spectrum.

By virtue of formulas (B6) and (B17) the free-wave spectrum of the hull becomes

$$G_H(u)+iF_H(u) = 8\pi\left\{\frac{1+v}{v}\right\} \int_{-l}^{l} dx \int_{-T}^{0} dz \left[\frac{m}{\pi}\left\{\frac{b}{l}\right\}\left\{\frac{x}{l}\right\}^{2m-1}\left\{1-\epsilon(-z/T)^n\right\}\times \exp(s^2z+isx)\right] \qquad (B22)$$

or after some simplification

$$G_H(u) = 0$$
$$F_H(u) = 16 \frac{b}{v} F^{(1)}(m,sl)\, F^{(2)}(n,\epsilon,Ts^2) \qquad (B23)$$

with

$$F^{(1)}(m,p) = m \int_{-1}^{1} \xi^{2m-1} \sin(\xi p)\, d\xi$$
$$F^{(2)}(n,\epsilon,q) = F^{(3)}(0,q) - \epsilon F^{(3)}(n,q)$$
$$F^{(3)}(n,q) = q \int_{0}^{1} \zeta^n \exp(-\zeta q)\, d\zeta \qquad (B24)$$

The integrals $F^{(1)}$ and $F^{(3)}$ can be solved in closed form [see formulas 2.6334 and 2.3212 in Gradshteyn and Ryzhik (1965)] or evaluated by recurrence formulas:

$$F^{(1)}(0,p) = 0,$$
$$F^{(1)}(m,p) = 2m\left\{(2m-1)[\sin(p)-F^{(1)}(m-1,p)]/p-\cos(p)\right\}/p$$
$$F^{(3)}(0,q) = 1-\exp(-q),$$
$$F^{(3)}(n,q) = -\exp(-q) + nF^{(3)}(n-1,q)/q \qquad (B25)$$

Similarly, the free-wave spectrum of the propeller can be

written as

$$G_P(u)+iF_P(u) = 8\pi\left\{\frac{1+\nu}{\nu}\right\}\int_{R_H}^{R_P} dR \int_{-\pi}^{\pi} Rd\theta \left[\sigma(R,\theta)\exp\left\{s^2(z_P+R\sin\theta) + i(sx_P+uR\cos\theta)\right\}\right] \quad (B26)$$

If the propeller source distribution σ is a function of radius only, then this simplifies by virtue of transverse symmetry to

$$G_P(u)+iF_P(u) = 8\pi\left\{\frac{1+\nu}{\nu}\right\}\exp(s^2z_P+isx_P)\int_{R_H}^{R_P} R\sigma(R)dR \int_{-\pi}^{\pi} \exp(s^2R\sin\theta)\times \cos(uR\cos\theta)d\theta$$

$$= 16\pi^2\left\{\frac{1+\nu}{\nu}\right\}\exp(s^2z_P+isx_P)\int_{R_H}^{R_P} R\sigma(R)I_o(sR)dR \quad (B27)$$

where I_o is the modified Bessel function of zero order [see Gradshteyn and Ryzhik (1965), formula 3.9372]. This last integral can be easily evaluated for any numerically defined function $\sigma(R)$.

B.4 - Wavemaking Resistance

The individual wavemaking resistances of the bare hull R_{WH} and the free running propeller R_{WP} are found directly by substituting the appropriate free-wave spectra (B23) and (B27) into the general formula (B21).

$$R_{WH} = \frac{1}{8\pi}\int_0^{\infty}\left\{\frac{16b}{\nu}F^{(1)}(m,sl)F^{(2)}(n,\varepsilon,Ts^2)\right\}^2\frac{\nu}{1+\nu}\,du \quad (B28)$$

$$R_{WP} = \frac{1}{8\pi}\int_0^{\infty}\left[16\pi^2\left\{\frac{1+\nu}{\nu}\right\}\exp(s^2z_P)\int_{R_H}^{R_P}R\sigma(R)I_o(sR)dR\right]^2\frac{\nu}{1+\nu}\,du \quad (B29)$$

To calculate the wavemaking resistance R_{WT} of the total system hull with propeller one can use the principle of linear

superposition of free-wave spectra, that is

$$G_T(u) = G_H(u) + G_P(u)$$
$$F_T(u) = F_H(u) + F_P(u) \qquad \text{(B30)}$$

provided both spectra are expressed in the same coordinate system. The general formula (B21) can then be applied to the total spectrum

$$E_T(u) = \sqrt{\{G_T{}^2(u) + F_T{}^2(u)\}}$$

Evidently, in general

$$R_{WT} \neq R_{WH} + R_{WP} \qquad \text{(B31)}$$

and the difference

$$R_{WT}-R_{WH}-R_{WP} = \frac{1}{8\pi}\int_0^\infty 2\{G_H(u)G_P(u)+F_H(u)F_P(u)\}\frac{v}{1+v}\,du \qquad \text{(B32)}$$

is a measure of the interference between the wave patterns of the hull and the propeller. The interaction term can be positive or negative.

B.5 - Wave Flow due to Hull

The perturbation flow induced at the propeller plane by the motion of the hull under the free surface can also be calculated by thin ship theory. We start with the Green's function of the problem as defined by Equation (63) of Eggers, Sharma and Ward (1967): (see next page)

$$G(x,y,z,x',y',z') = -\frac{1}{r_1} + \frac{1}{r_2}$$

$$-\mathrm{Re}\,\frac{2}{\pi}\int_{-\infty}^{\infty} du \int_{|u|}^{\infty} \frac{\exp[-w|x-x'|+iu(y-y')+i\sqrt{w^2-u^2}(z+z')]}{\sqrt{w^2-u^2}-iw^2}\,dw$$

$$+\mathrm{Im}\,\frac{1}{2}\left\{1-\mathrm{sgn}(x-x')\right\}\int_{-\infty}^{\infty}\frac{4s}{\nu}\exp\left\{is(x-x')+iu(y-y')+s^2(z+z')\right\}du \qquad \text{(B33)}$$

with

$$r_1^2 = (x-x')^2+(y-y')^2+(z-z')^2$$

$$r_2^2 = (x-x')^2+(y-y')^2+(z+z')^2$$

This is the velocity potential due to a point source of unit strength at (x',y',z'). Integration over the hull source distribution (B6) yields the velocity potential of the hull $\varphi(x,y,z)$, and subsequent differentiation with respect to x,y,z yields the components of perturbation velocity φ_x, φ_y, φ_z. It is convenient to break up each expression into four parts corresponding to the four terms of the Green's function (B33). For instance,

$$\varphi_x(x,y,z) = \varphi_x^{(1)} + \varphi_x^{(2)} + \varphi_x^{(3)} + \varphi_x^{(4)} \qquad \text{(B34)}$$

with

$$\varphi_x^{(1)}(x,y,z) = \int_{-l}^{l} dx' \int_{-T}^{0} \frac{bm}{\pi l}\left\{\frac{x'}{l}\right\}^{2m-1}\left\{1-\varepsilon(-z'/T)^n\right\} \times \frac{(x-x')}{\left\{(x-x')^2+(y-y')^2+(z-z')^2\right\}^{3/2}}\,dz' \qquad \text{(B35)}$$

etc. It turns out that in the resulting integrals the x',z' integrations can be carried out in closed form, while the u,w integrations must be performed by numerical quadrature.

It takes some algebra to reduce the expressions to a form

suitable for computer programming. We will show this for one example. Substitute in (B35)

$$\xi = x/l,\ \xi' = x'/l,\ \eta = y/l,\ \zeta = z/l,\ \zeta' = z'/l,\ \tau = T/l \qquad \text{(B36)}$$

Then

$$\varphi_x^{(1)} = \frac{b}{l}\frac{m}{\pi}\int_{-1}^{1} d\xi' \int_{-\tau}^{0} \frac{(\xi')^{2m-1}[1-\epsilon(-\zeta'/\tau)^n](\xi-\xi')}{\left\{(\xi-\xi')^2+\eta^2+(\zeta-\zeta')^2\right\}^{3/2}}\, d\zeta' \qquad \text{(B37)}$$

Now put

$$\bar{\xi} = \xi-\xi' , \qquad \bar{\zeta} = \zeta-\zeta' \qquad \text{(B38)}$$

Then

$$\varphi_x^{(1)} = \frac{b}{l}\frac{m}{\pi}\int_{\xi+1}^{\xi-1} d\bar{\xi} \int_{\zeta+\tau}^{\zeta} \frac{(\xi-\bar{\xi})^{2m-1}\,\bar{\xi}[1-\epsilon(-1/\tau)^n(\zeta-\bar{\zeta})^n]}{\left\{\bar{\xi}^2+\eta^2+\bar{\zeta}^2\right\}^{3/2}}\, d\bar{\zeta}$$

Now factor out the constants and apply the binomial theorem to get

$$\varphi_x^{(1)} = \frac{b}{l}\frac{m}{\pi}\Bigg[\left\{\sum_{i=0}^{2m-1}(-)^i\binom{2m-1}{i}\xi^{2m-1}E_{i+1,0}\right\}$$

$$-\epsilon\left\{-\frac{1}{\tau}\right\}^n\sum_{i=0}^{2m-1}\sum_{j=0}^{n}(-)^{i+j}\binom{2m-1}{i}\binom{n}{j}\xi^{2m-1}\zeta^{n-j}E_{i+1,j}\Bigg]$$

where

$$E_{i,j}(\xi,\eta,\zeta,\tau) = \int_{\xi+1}^{\xi-1} d\bar{\xi} \int_{\zeta+\tau}^{\zeta} d\bar{\zeta}\, \frac{\bar{\xi}^i\,\bar{\zeta}^j}{\left\{\bar{\xi}^2+\eta^2+\bar{\zeta}^2\right\}^{3/2}} \qquad \text{(B39)}$$

This double integral $E_{i,j}$ has a closed form solution (for constant limits of integration) amenable to numerical evaluation by a recurrence formula. (The authors are indebted to Drs. K. Eggers and H. Kajitani for this suggestion.) Consider the indefinite

integral

$$E_{i,j}(x,y,z) = \iint \frac{x^i z^j}{r^3}\, dx\, dz, \qquad r = \sqrt{x^2+y^2+z^2} \tag{B40}$$

By repeated use of formula 2.2631 from Gradshteyn and Ryzhik (1965) it can be shown that

$$E_{i,j} = \frac{1}{i+j-1}\left\{jx^{i-1}E_{1,j} - (i-1)(z^{j+1}E_{i-2,1} + y^2 E_{i-2,j})\right\}$$

$$= \frac{1}{i+j-1}\left\{iz^{j-1}E_{i,1} - (j-1)(x^{i+1}E_{1,j-2} + y^2 E_{i,j-2})\right\} \tag{B41}$$

Hence, starting from the four fundamental solutions

$$E_{0,0} = -\frac{1}{y}\arctan(yr/xz)$$

$$E_{0,1} = -\ln(x+r)$$

$$E_{1,0} = -\ln(z+r)$$

$$E_{1,1} = -r \tag{B42}$$

any element $E_{i,j}$ can be constructed by recurrence, for example

$$E_{2,2} = -\frac{xzr}{3} + \frac{x^3}{3}\ln(z+r) + \frac{z^3}{3}\ln(x+r) + \frac{y^3}{3}\arctan(xz/yr)$$

$$E_{3,3} = \frac{r}{5}\left\{\frac{2}{3}y^2(x^2+z^2-2y^2) + 2(x^4+z^4) - x^2z^2\right\} \tag{B43}$$

For a computer algorithm, however, it is not necessary to develop the analytical expressions explicitly since the recurrence formula (B41) can be applied numerically to each of the four summands (corner values) of the definite integral (B39).

A similar analysis can be applied to the second term of (B34), but the final result is obtained more easily by

considerations of symmetry:

$$\varphi_x^{(2)}(x,y,z) = -\varphi_x^{(1)}(x,y,-z) \tag{B44}$$

Restricting our attention to field points <u>behind the hull</u> ($x < -1$), the third and fourth terms of (B34) can be simplified as follows.

$$\varphi_x^{(3)} = -\mathrm{Re}\,\frac{2}{\pi}\int_{-\infty}^{\infty}du\int_{|u|}^{\infty}dw\int_{-1}^{1}dx'\int_{-T}^{0}dz'\left[\frac{b}{l}\frac{m}{\pi}\left\{\frac{x'}{l}\right\}^{2m-1}\left\{1-\epsilon(-z'/T)^n\right\}\times\right.$$

$$\left.\frac{w\,\exp[w(x-x')+iuy+i\sqrt{w^2-u^2}(z+z')]}{\sqrt{w^2-u^2}\,-iw^2}\right]$$

$$= -\frac{b}{l}\frac{4}{\pi}\int_0^{\infty} I(u,x,z,l,m,n,\epsilon,T)\cos(uy)\,du \tag{B45}$$

where

$$I = -\frac{\exp[u(x+l)]}{x+l}\int_0^{\infty}\frac{G^{(1)}(m,wl)}{\sqrt{w^2-u^2}}\mathrm{Re}\left\{\frac{\exp(iz\sqrt{w^2-u^2})\,G^{(2)}(n,\epsilon,T\sqrt{w^2-u^2})}{\sqrt{w^2-u^2}\,-iw^2}\right\}\times$$

$$\exp(-t)\,dt \tag{B46}$$

with $t = -(w-u)(x+l)$ and

$$G^{(1)}(m,p) = \frac{m}{\pi}\,p\,\exp(-p)\int_{-1}^{1}\xi^{2m-1}\exp(-p\xi)\,d\xi$$

$$G^{(2)}(n,\epsilon,q) = G^{(3)}(0,q) - \epsilon\,G^{(3)}(n,q)$$

$$G^{(3)}(n,q) = p\int_0^{1}\zeta^n\exp(-iq\zeta)\,d\zeta \tag{B47}$$

The integrals $G^{(1)}$ and $G^{(3)}$ can be solved in closed form or

evaluated by recurrence formulas:

$$G^{(1)}(0,p) = 0,$$

$$G^{(1)}(m,p) = m\left\{(2m-1)[(1-e^{-2p})/\pi+2G^{(1)}(m-1,p)/p]/p-(1+e^{-2p})/\pi\right\}$$

$$G^{(3)}(0,q) = (1-e^{-iq})/i$$

$$G^{(3)}(n,q) = \left\{nG^{(3)}(n-1,q)/q - e^{-iq}\right\}/i \qquad \text{(B48)}$$

The integral I has an exponentially decaying factor in the integrand and is therefore suited to Gauss-Laguerre numerical quadrature. The real part in (B46) need not be evaluated analytically, if complex arithmetic may be used in the program.

Similarly, for $x < -1$:

$$\varphi_x^{(4)} = \mathrm{Im}\int_{-\infty}^{\infty}du\int_{-1}^{1}dx'\int_{-T}^{0}dz'\left[\frac{b}{1}\frac{m}{\pi}\left\{\frac{x'}{1}\right\}^{2m-1}\left\{1-\epsilon(-z'/T)^n\right\}4i\,\frac{s^2}{v}\times \exp\left\{is(x-x')+iuy+s^2(z+z')\right\}\right]$$

$$= \frac{8b}{\pi}\int_0^{\infty}\left\{\frac{\exp(s^2z)}{v}\sin(sx)F^{(1)}(m,sl)F^{(2)}(n,\epsilon,s^2T)\right\}\cos(uy)\,du \qquad \text{(B49)}$$

where $F^{(1)}$ and $F^{(2)}$ are the functions already defined in (B24). The integrals (B45) and (B49) can be truncated at a sufficiently large value of u and approximated by the known recurrence formulas for Fourier series. Suppose

$$C + iS = \int_0^{\infty} I(u)\left\{\cos(uy) + i\,\sin(uy)\right\}du$$

$$\approx \Delta u\sum_{\nu=0}^{N} I(u_\nu)\left\{\cos(u_\nu y) + i\,\sin(u_\nu y)\right\}\epsilon_\nu \qquad \text{(B50)}$$

with

$$u_\nu = \nu\,\Delta u, \quad \varepsilon_\nu = \frac{1}{2} \text{ for } \nu = 0, \quad \varepsilon_\nu = 1 \text{ for } \nu \neq 0$$

where Δu is a suitable step size and N is sufficiently large. Then

$$C = \frac{1}{2}\,(U_0 - U_2)\,\Delta u$$

and

$$S = U_1 \sin(y\,\Delta u)\,\Delta u \tag{B51}$$

where the U_ν are defined by the sequence

$$U_{N+1} = U_{N+2} = 0$$

$$\nu = N, N-1, \ldots, 0:$$

$$U_\nu = I(u_\nu) + 2\cos(y\,\Delta u)U_{\nu+1} - U_{\nu+2} \tag{B52}$$

This completes the wanted algorithm for all four terms of (B34).

By our definition, φ_x evaluated in the propeller plane is identical to the total potential wake fraction, i.e. the sum of the so-called potential wake (zero Froude number effect) and the wave wake (finite Froude number effect). Thus

$$w_p(R,\theta) + w_w(R,\theta) = \varphi_x(x,y,z) \tag{B53}$$

if $x = x_p, \quad y = R\cos\theta, \quad z = z_p + R\sin\theta$

By evaluating φ_x at a sufficiently large number of field points the circumferential and disk averages of the theoretical wake can be estimated. Moreover, it can be shown that the zero Froude number wake, the infinite Froude number wake and the bow wake $(x > 1)$ can also be derived from the four components

of expression (B34).

$$F_n = 0: \quad w_w = 0, \quad w_p = \varphi_x^{(1)} - \varphi_x^{(2)} \tag{B54}$$

$$F_n = \infty: \quad w_p + w_w = \varphi_x^{(1)} + \varphi_x^{(2)} \tag{B55}$$

$$x > 1: \quad \varphi_x(x,y,z) = \varphi_x^{(1)}(-x,y,z) + \varphi_x^{(2)}(-x,y,z) + \varphi_x^{(3)}(-x,y,z) \tag{B56}$$

This last quantity evaluated at $x = -x_p$ yields by virtue of longitudinal symmetry the desired theoretical wake in the propeller plane "behind" the hull in reverse motion.

B.6 - Wave Flow due to Propeller

In order to calculate the perturbation flow induced by the motion of the propeller under the free surface, we start with an alternative expression for the Green's function (B33), see formula (56) in Eggers, Sharma and Ward (1967):

$$G = -\frac{1}{r_1} + \frac{1}{r_2} + \mathrm{Re}\,\frac{2}{\pi}\int_{-\pi/2}^{\pi/2} \sec^2\theta \; d\theta \int_0^{\infty} \frac{\exp[k(z+z'+i\bar{w})]}{k-\sec^2\theta}\, dk + \mathrm{Im}\; 2\int_{-\pi/2}^{\pi/2} \sec^2\theta \, \exp[\sec^2\theta \; (z+z'+i\bar{w})]\, d\theta \tag{B57}$$

with $\bar{w} = (x-x')\cos\theta + (y-y')\sin\theta$ and r_1, r_2 as before. Differentiating with respect to x, and taking advantage of the symmetry in θ, we obtain (see next page):

$$G_x(x-x',y-y',z,z') = \frac{x-x'}{r_1^3} - \frac{x-x'}{r_2^3} - \frac{4}{\pi}\int_0^{\pi/2} \sec\theta\, d\theta \times$$

$$\int_0^{\infty} \exp[k(z+z')]\sin[k(x-x')\cos\theta]\cos[k(y-y')\sin\theta]\frac{k\, dk}{k-\sec^2\theta}$$

$$+ 4\int_0^{\pi/2} \sec^3\theta\, \exp[(z+z')\sec^2\theta]\cos[(x-x')\sec\theta]\cos[(y-y')\tan\theta\sec\theta]d\theta \qquad \text{(B58)}$$

Since we are interested only in the flow induced by the propeller in its own plane (the so-called self-induced wake), we confine further analysis to the case $x = x' = x_p$. The first three terms of (B58) then vanish and in the last we substitute

$$u = \sec\theta\tan\theta, \quad v = \sqrt{1+4u^2}, \quad s = \sqrt{(1+v)/2}, \quad du/d\theta = sv \qquad \text{(B59)}$$

to get

$$G_x(0,y-y',z,z') = 2\int_0^{\infty} \exp[(z+z')s^2]\cos[(y-y')u]\frac{1+v}{v}\, du \qquad \text{(B60)}$$

Now integrating over the propeller source distribution $\sigma(R)$ and taking advantage of its transverse symmetry, we get for the self-induced wake the following expression:

$$w_f(R,\theta) = \int_{R_H}^{R_P} dR' \int_{-\pi/2}^{\pi/2} G_x(0,y-y',z,z')\, \sigma(R')\, R'd\theta'$$

$$= 4\pi\int_0^{\infty} \left\{\frac{1+v}{v}\right\}\exp[(z+z_p)s^2]\left\{\int_{R_H}^{R_P} R'\sigma(R')I_0(sR')dR'\right\}\cos(uy)du \qquad \text{(B61)}$$

where the integral formula quoted after (B27) has been applied again. Since the function $\sigma(R')$ is in general not analytic, the R' integral must be evaluated by numerical quadrature

(e.g. Simpson's rule) for suitable values $s(u_\nu)$ such that the u integral can be approximated by the recurrence formulas for Fourier series, see Equations (B50-B52).

By proper choice of the field points $y = R\cos\theta$, $z = z_P + R\sin\theta$ the self-induced free-surface wake $w_f(R,\theta)$ can be calculated at suitable points (R_j,θ_k) on the disk, from which the circumferential average $w_f(R)$ and the disk average w_f can be obtained by numerical integration.

A useful check on the numerical accuracy of the calculated values of $w_f(R,\theta)$ is obtained by using them to determine the wavemaking resistance of the propeller by virtue of Lagally's theorem [see equation (11) of Eggers, Sharma and Ward (1967)]:

$$R_{WP} = 8\pi \int_{R_H}^{R_P} R\,\sigma(R) \int_{-\pi/2}^{\pi/2} w_f(R,\theta)\, d\theta\, dR \qquad \text{(B62)}$$

Analytically, of course, this is identical to the more direct formula (B29) based on the free-wave spectrum. Numerically, we found that the differences were negligibly small for a reasonable step size $\Delta\theta \leq \pi/6$.

B.7 - Thrust Deduction

We wish to calculate the force of thrust deduction, i.e. the augmentation of hull resistance due to propeller action. Let us call it $\delta_P R_{WH}$. Conceptually, the most direct approach would be to use Lagally's theorem, i. e.

$$\delta_P R_{WH} = 4\pi \int_{-1}^{1} dx \int_{-T}^{0} dz \left\{\sigma(x,z)\, \varphi_x^P(x,0,z)\right\} \qquad \text{(B63)}$$

This would seem to necessitate the explicit calculation of the longitudinal perturbation flow w_x^P induced by the propeller on the center-plane of the hull $y = 0$, which is not quite easy due to the singular double integral in formula (B58). However, we will circumvent this difficulty by an indirect approach. Let us denote by $\delta_H R_{WP}$ the augmentation of propeller resistance due to hull action. Then again by Lagally's theorem

$$\delta_H R_{WP} = 8\pi \int_{R_H}^{R_P} dR \int_{-\pi/2}^{\pi/2} R \, d\theta \left\{ \sigma(R,\theta) \; w_x^H(x_P,R,\theta) \right\} \tag{B64}$$

where w_x^H now is the axial perturbation flow induced by the hull in the propeller plane, i.e. the wake as already defined by (B53). On the other hand, by virtue of previous definitions we have

$$R_{WT} = R_{WH} + R_{WP} + \delta_P R_{WH} + \delta_H R_{WP}$$

Hence,

$$\delta_P R_{WH} = R_{WT} - R_{WH} - R_{WP} - \delta_H R_{WP} \tag{B65}$$

where the sum of the first three terms as defined by (B32) is relatively easy to calculate. Thus we see that the calculation of thrust deduction requires no further effort beyond that already expended for the calculation of hull wake and the wave-making resistances of hull alone, propeller alone and the total system hull with propeller. In particular, it is needless to calculate the flow induced by the propeller on the hull.

Note that $\delta_P R_{WH}$ is the total potential thrust deduction, i.e. the sum of the so-called "potential" component (zero Froude

number effect) and the "wave" component (finite Froude number effect). The thrust deduction fraction becomes

$$t_p + t_w = \delta_P R_{WH}/T_H$$

$$= (\delta_P R_{WH}/K_{TH})(V^2/gD)^2(V/nD)^2$$

$$= (\delta_P R_{WH}/K_{TH})(L/D)^2(F_n)^4(J_H)^2 \qquad \text{(B66)}$$

At zero Froude number, of course,

$$R_{WT} = R_{WH} = R_{WP} = 0$$

and therefore

$$\delta_P R_{WH} = - \delta_H R_{WP} \qquad \text{(B67)}$$

Thus if we use the zero Froude number wake (B54) in (B64) to calculate $\delta_H R_{WP}$, we can determine the "potential" component of thrust deduction t_p from the simple principle of reciprocity (B67) already exploited by Dickmann (1939).

It must be emphasized that the force $\delta_H R_{WP}$ apparently exerted on the propeller by the hull does not necessarily have a physical meaning since the source disk is an inappropriate model for calculating propeller forces. However, it is a perfectly valid mathematical artifice for a simple, although indirect, determination of the quantity $\delta_P R_{WH}$ which is a real force exerted on the hull due to propeller action, viz. the force of thrust deduction.

Incidentally, if the source strength is uniform over the disk, as in Equation (B15), the integral (B64) simplifies to

$$\delta_H R_{WP} = 4\pi^2(R_P^2 - R_H^2)\ \sigma(R)\ (w_p + w_w) \tag{B68}$$

where w_p and w_w are the disk averages of the potential and wave wake respectively. Moreover, if only the potential component of thrust deduction is wanted, substituting from (B15) in (B68) and taking advantage of (B67) one obtains

$$\begin{aligned} t_p &= -\delta_H \underline{R}_{WP}/\underline{T}_H \\ &= \frac{2}{1+\sqrt{1+C_{Th}}} \left\{ \frac{w_p}{1-w_T} \right\} \end{aligned} \tag{B69}$$

This is slightly different from the classical result of Dickmann (1939), cf. his equation (15). However, it agrees with Tsakonas' (1958) equation (12), except that he does not distinguish between the potential component w_p and the total wake w_T.

B.8 - Wave Profile Analysis

The purpose of wave profile analysis was to establish the true or experimental free-wave spectrum (and associated wave-making resistance) of the hull and propeller as opposed to the theoretical spectrum based on linearized source representations discussed in the previous sections. The longitudinal cut method of Sharma (1966) as described in Eggers, Sharma and Ward (1967) was used. The essential steps of the analysis are given below.

Let $z = \zeta(x,y_o)$ be a longitudinal cut through the wave pattern of the model as measured at a fixed transverse location

$y = y_o$ in the coordinate system of Fig. 1. Define modified* Fourier transforms

$$C^*(s,y_o) + iS^*(s,y_o) = \int_{-\infty}^{\infty} \sqrt{s^2-1}\, \zeta(x,y_o)\, \exp(isx)\, dx \qquad (B70)$$

Then the free-wave spectrum of the model is given by

$$G(u) = \frac{4}{2s^2-1} \left\{C^*(s,y_o)\cos(uy_o) - S^*(s,y_o)\sin(uy_o)\right\}$$
$$F(u) = \frac{4}{2s^2-1} \left\{C^*(s,y_o)\sin(uy_o) + S^*(s,y_o)\cos(uy_o)\right\} \qquad (B71)$$

where $u = s\sqrt{s^2-1}$ in accordance with (B18). By applying this procedure separately to the model hull with and without propeller one can obtain the spectrum $G_T(u)$, $F_T(u)$ of the total system hull and propeller and the spectrum $G_H(u)$, $F_H(u)$ of the bare hull respectively. The spectrum of the propeller alone $G_P(u)$, $F_P(u)$ then follows from the principle of linear superposition.

$$G_P(u) = G_T(u) - G_H(u)$$
$$F_P(u) = F_T(u) - F_H(u) \qquad (B72)$$

For the ease of comparison with theory the propeller spectrum

---

*The asymptotic nature of the wave pattern behind a ship is such

$$x/|y| \to -\infty : \qquad \zeta(x,y) \simeq \exp(ix)/\sqrt{c-x}$$

that the modified Fourier transform remains finite for any s, while the ordinary Fourier transform becomes infinite at $s = 1$.

may be transformed to a new coordinate system $O\tilde{x}\tilde{y}\tilde{z}$ which has its origin in the propeller plane. If $\tilde{x} = x-x_p$, $\tilde{y} = y$, $\tilde{z} = z$, then

$$\tilde{G}_p(u) = G_p(u)\cos(sx_p) + F_p(u)\sin(sx_p)$$

$$\tilde{F}_p(u) = F_p(u)\cos(sx_p) - G_p(u)\sin(sx_p) \qquad \text{(B73)}$$

The associated wavemaking resistances of bare hull (R_{WH}), bare propeller (R_{WP}) and total system hull-propeller (R_{WT}) are obtained from the respective spectra by use of the general formula:

$$R_W = \frac{1}{8\pi} \int_0^\infty \left\{F^2(u)+G^2(u)\right\} \frac{\sqrt{1+4u^2}}{1+\sqrt{1+4u^2}}\, du \qquad \text{(B74)}$$

It is assumed here that the wave pattern has transverse symmetry.

APPENDIX C - LIFTING LINE CALCULATIONS

C.1 - Problem Formulation

The principal method for calculating thrust deduction and free-surface effects due to a propeller as described in Appendix B presupposes that a lifting line representation of the propeller, i.e. the distribution of bound circulation along the radius, is known. In order to be able to apply this method to a given propeller we need a scheme for determining the circulation distribution for any given operating condition of a propeller of predetermined geometry. This is essentially the classical "performance" problem in propeller theory (as opposed to the design problem , in which a certain performance criterion is prescribed and the optimum propeller geometry is sought for).

Physically, the problem can be formulated as a set of relations which must be satisfied at every propeller radius between the hub and the tip. Using standard symbols, these relations are:

$$C_L = C_L(\alpha) \tag{C1}$$

$$\alpha = \Phi - \beta_i \tag{C2}$$

$$\tan \Phi = P/2\pi R \tag{C3}$$

$$\tan \beta_i = \left\{(1-w)V + u_A\right\}/\left\{\omega R - u_T\right\} \tag{C4}$$

$$u_A = \frac{1}{4\pi} \int_{R_H}^{R_P} i_A(R/R_P, \beta_i, Z) \left\{\frac{d\Gamma(R')}{dR'}\right\} \frac{dR'}{R-R'} \tag{C5}$$

$$u_T = \frac{1}{4\pi} \int_{R_H}^{R_P} i_T(R/R_P, \beta_i, Z) \left\{\frac{d\Gamma(R')}{dR'}\right\} \frac{dR'}{R-R'} \qquad (C6)$$

$$\Gamma = C_L c \left\{(1-w)V + u_A\right\}/(2\sin \beta_i) \qquad (C7)$$

Here, Equation (C1) represents the predetermined two-dimensional foil characteristics, i.e. the lift coefficient C_L as a function of angle of attack α. Equations (C2) to (C4) establish the local angle of attack α as the difference between the predetermined geometric pitch angle Φ and the unknown hydrodynamic pitch angle β_i. The velocities u_A and u_T induced by the free vortex trail of the propeller may be obtained from Biot-Savart's Law and are expressed in Equations (C5) and (C6) as integrals involving the slope of the bound circulation $\Gamma(R)$ and two special functions i_A and i_T (of three variables), the so-called induction factors, see Lerbs (1952). Equation (C7), finally, is the relation between lift and circulation in accordance with Kutta-Joukowsky's theorem. Mathematically, the problem is an integral equation for the unknown function $\beta_i(R/R_P)$, which can be solved by iteration if efficient algorithms are available for computing the induced velocities u_A and u_T.

The solution of the above problem yields the distribution of circulation, and hence lift, over the radius:

$$dL = \rho \left\{(1-w)V+u_A\right\} \Gamma \, dR/(\sin \beta_i) \qquad (C8)$$

Now the drag can also be estimated from the known foil characteristics:

$$C_D = C_D(\alpha) \tag{C9}$$

$$dD = \frac{c}{2} \rho \left\{(1-w)V+u_A\right\}^2 C_D dR/(\sin \beta_i)^2 \tag{C10}$$

Hence, by resolving lift and drag along the axial and circumferential directions and integrating over the radius, one can calculate the thrust and torque produced by the propeller.

C.2 - Method of Solution

Our method of solution was dictated by the computational tools and the information on propeller characteristics available to us. The principal computational tools at our disposal were two computer programs for propeller design, both based on the lifting line theory and incorporating efficient algorithms for numerical evaluation of induced velocities. One was obtained from the Naval Ship Research and Development Center and the other from the Technical University of Berlin by courtesy of Dr. Östergaard. They are well documented in the literature, cf. Haskins (1967) and Östergaard (1970), and therefore need not be described here in detail. After several test runs had revealed that the two programs yielded practically identical solutions of the design problem, we chose the Berlin program for further use and adapted it to a solution of the performance problem. The principal modification necessary was the following. In the design problem the hydrodynamic pitch angle $\beta_i(R/R_p)$ is generally prescribed to fulfil the optimum (minimum energy loss) condition thus eliminating the need to solve an integral equation. In the performance problem, however, the integral

equation must be solved. This was done by the method of successive approximations to the unknown function $\beta_i(R/R_P)$. Starting with an initial guess $(\beta_i)_o$, say corresponding to the optimum condition, a better approximation was found by cycling through Equations (C1) to (C7). In order to prevent the iteration from diverging it was found necessary to weight the successive approximations as follows:

$$(\beta_i)_{n+2} = w_1(\beta_i)_n + w_2(\beta_i)_{n+1} \tag{C11}$$

With $w_1 = 0.9$ and $w_2 = 0.1$ the final error in $\beta_i(R/R_P)$ after ten iterations was found to be generally less than 1 %.

A major handicap in this algorithm was that the two-dimensional foil characteristics of our propeller (see Fig. 2) were not explicitly known to us. We therefore back-calculated the foil characteristics from the known measured performance (thrust and torque) of the propeller (in the deeply submerged open water condition). This was done by treating any given operating condition as a small perturbation from an assumed design (optimum) condition, i.e.

$$C_L(\alpha) = C_{LD} + 2\pi(\alpha-\alpha_D)k \tag{C12}$$

$$C_D(\alpha) = a_1|C_L(\alpha)-C_{LD}|^{a_2} + C_{DD} \tag{C13}$$

The design angles of attack α_D and the corresponding lift coefficients C_{LD} were specified indirectly by the choice of a design advance coefficient J_D. Let β_{iD} be the optimum hydrodynamic pitch angle at any radius at the design point J_D. Then

for calculating the performance at any other advance coefficient J (and assumed pitch angle β_i), it is only necessary to evaluate the differences

$$(\alpha-\alpha_D) = \beta_{iD}-\beta_i \tag{C14}$$

$$C_L(\alpha)-C_{LD} = 2\pi(\alpha-\alpha_D)k \tag{C15}$$

$$C_D(\alpha)-C_{DD} = a_1|C_L(\alpha)-C_{LD}|^{a_2} \tag{C16}$$

It is thus seen that in all five arbitrary constants (J_D, C_{DD}, k, a_1, a_2) were used to match the calculated propeller performance to the actual measured performance. By trial and error the following best fit values were determined for our propeller:

$$J_D = 0.8, \qquad C_{DD} = 0.01$$

$$k = 0.67$$

$$a_1 = 0.17, \qquad a_2 = 6 \tag{C17}$$

Note that the only critical parameter here is the factor k, which may be interpreted as an empirical catch-all to account for viscous losses and miscellaneous three-dimensional effects.

The degree of agreement finally achieved between the measured and calculated (more precisely, simulated) performance of the propeller is obvious from the following table (see next page) and from Fig. 10.

Further details of this method of calculating off-design performance and results obtained with other propellers are reported in a recent paper by Östergaard,Kruppa and Lessenich(1971).

J	Measured		Simulated	
	K_T	$10K_Q$	K_T	$10K_Q$
0.6	0.223	0.355	0.223	0.353
0.7	0.179	0.300	0.178	0.296
0.8	0.135	0.242	0.135	0.242
0.9	0.087	0.182	0.088	0.179

C.3 - Applications

It should be obvious from the foregoing that as far as the deeply submerged open water condition is concerned, our computer program as described above did not really predict propeller performance analytically but rather simulated the known measured performance by means of a lifting line model. This was perfectly acceptable because our primary aim here was not to predict propeller performance, but to determine the equivalent lifting line for use in calculating thrust deduction and free-surface effects. However, in two subsequent applications this program was indeed used to obtain certain genuine predictions of propeller performance.

First, for estimating the effect of free surface on propeller performance at shallow submergence the program was run with the calculated self-induced wake $w_f(R)$ of the propeller as an additional input (see Section B.6) without any attempt to manipulate the foil characteristics fixed once for all on the basis of the deeply submerged condition, see Equation (C17). Hence, the thrust and torque calculated for shallow submergence as

plotted in Fig. 13 and reproduced in the following table are, in a certain sense, true predictions of the free-surface effect.

J	$h/R_P = 3.47 \approx \infty$ Measured		$h/R_P = 1.00$ Measured		$h/R_P = 1.00$ Calculated	
	K_T	$10K_Q$	K_T	$10K_Q$	K_T	$10K_Q$
0.6	0.223	0.355	0.194	0.313	0.198	0.324
0.7	0.179	0.300	0.163	0.275	0.165	0.280
0.8	0.135	0.242	0.124	0.226	0.126	0.229
0.9	0.087	0.182	0.079	0.170	0.084	0.170

It may be noted that the wake $w_f(R)$ input to the program was here calculated for the lifting line corresponding to the deeply submerged propeller. In principle, it would be possible to run a second iteration with the wake $w_f(R)$ recomputed for the new lifting line determined by the program for the shallow submergence. However, this refinement is considered unnecessary.

Second, for evaluating the propeller performance in the behind hull condition again the same procedure was used, with the measured nominal wake $w(R)$ substituted in Equations (C4) and (C7). However, the calculated thrust and torque were found to deviate substantially from the measured values. Since the primary purpose of this calculation was to obtain a realistic simulation of actual propeller performance by a mathematical lifting line, it was decided to enforce a thrust identity.

However, this was accomplished not by further manipulating the assumed foil charecteristics but by multiplying the input wake $w(R)$ with a constant wake corrector k_w whose final value was determined by iteration. Thus the program was here used not only to determine the equivalent circulation distribution but also to simulate the physical difference between the nominal and effective wake through the factor k_w. Moreover, the program also calculated a mean effective wake $\tilde{w}_T$ which was based on a thrust average rather than a volume flux average. This was defined as

$$\tilde{w}_T = \frac{k_w \int_{R_H}^{R_P} w(R)\{\omega R - u_T\}\{1 - \epsilon \tan \beta_i\}\Gamma(R)dR}{\int_{R_H}^{R_P} \{\omega R - u_T\}\{1 - \epsilon \tan \beta_i\}\Gamma(R)dR} \qquad (C18)$$

where not only the nominal wake w and the circulation Γ but also the quantities u_T, β_i, and $\epsilon = C_D/C_L$ vary with radius, even though this has not been explicitly indicated in the formula. The numerical values obtained for k_w and $\tilde{w}_T$ and their practical significance have been discussed in Section 3.6.2.

APPENDIX D - DOUBLE BODY CALCULATIONS

D.1 - Motivation

All calculations described in Appendix B are based on the first-order thin ship theory in which the hull is represented by a linearized (with respect to the beam) source distribution on the center plane, see Equation (B6). This has the great advantage that "potential" (i.e. zero Froude number) effects and wave (i.e. finite Froude number) effects can be calculated consistently using the same source distribution. However, the accuracy of the results depends in an uncontrolled manner on the "thinness" of the ship. In order to obtain a quantitative estimate of the error involved in the application of thin ship theory to our hull, a few wake calculations were also performed by the method of Hess and Smith (1962), which does not impose any restrictions on hull geometry. As is well known, the Hess and Smith algorithm provides a general solution of the Neumann problem of nonlifting potential flow about arbitrary bodies by means of a surface distribution of sources. Due to the enormous amount of numerical computation involved, however, the application of this method to the calculation of flow about ships is still limited to the so-called zero Froude number approximation, in which the ship (including the propeller) is conceptually replaced by a deeply submerged double body generated by reflecting the under water form about the static water plane. In our terminology, therefore, only the pure potential effects (as distinguished

from the viscous and wave effects) can be evaluated by this method. An improved version of the original Hess and Smith computer program was made available to us by the Naval Ship Research and Development Center.

D.2 - Results

Without going into the intricate details of the Hess and Smith method we report here only a few relevant results obtained by this program. First, a series of nominal wake calculations was performed with the propeller disk assumed in its proper transverse and vertical position ($y_p = 0$, $z_p = -0.5$ T) but at five different longitudinal positions as shown in the following table. Since the accuracy and computing effort in this method

Potential wake w_p averaged over the propeller disk

$2x_p/L$	Hess and Smith Program				Thin Ship Theory
	N =100	N =125	N =145	N =150	
-1.01	0.1785	0.1769	0.1756	0.1769	0.1758
-1.02	0.1520	0.1502	0.1496	0.1506	0.1492
-1.03	0.1307	0.1295	0.1287	0.1296	0.1278
-1.04	0.1136	0.1127	0.1120	0.1127	0.1107
-1.05	0.0998	0.0990	0.0985	0.0991	0.0969

depend critically on the number and size of the body surface elements, we tried four different arrangements involving N = 100, 125, 145 and 150 elements. As our double body had three

planes of symmetry, the elements are understood to cover only one eighth of the total body surface. To ensure finer detail near the stern the element size was not uniform over the entire length of the hull but made increasingly smaller toward the ends. The results showed that the arrangement with 125 elements yielded adequate accuracy for our purposes. Moreover, the average wake was practically identical to that calculated by thin ship theory. (This gave us, of course, more confidence in applying the thin ship theory also to the finite Froude number case where no such accuracy control was possible.)

Next, a series of effective wake calculations was conducted with the propeller located in its proper position (x_p = -0.51 L) and assumed operating at the advance coefficients J_H = 0.733, 0.889 and 1.131 corresponding to the ship self-propulsion points at γ_o = 4.0, 7.0 and 12.5 respectively, see Section 3.6. This involved two extra complications compared to the previous nominal wake calculations. One, the presence of the propeller destroyed the longitudinal symmetry of the flow so the number of significant hull surface elements had to be doubled from 125 to 250. Two, the flow induced by the propeller (and its mirror image about the plane $z = 0$) on the hull surface had to be given as an additional input to the Hess and Smith program. For this the Hough and Ordway source disk representation of the propeller (see Fig. 29) was used. The algorithm for computing the flow induced by source rings at arbitrary field points was taken from Küchemann and Weber (1953), pp. 310-316. The results showed that the calculated effective

wake was slightly higher than the nominal wake as would be expected from theoretical considerations. However, the numerical difference (less than 2 %) seemed to be of no practical consequence.

We hope to be able to report this investigation in more detail at a later date.

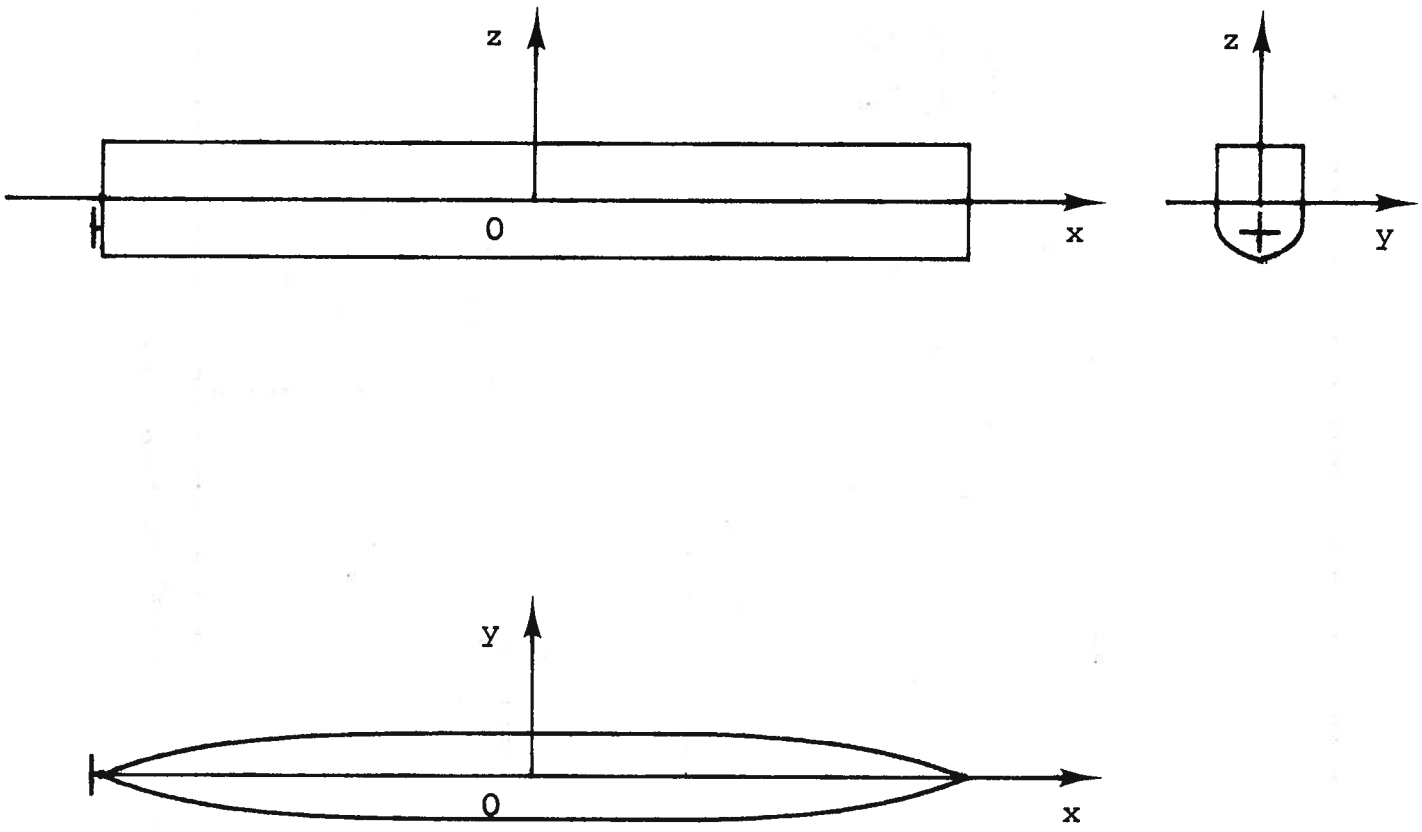

Fig. 1 Hull propeller configuration and coordinate system.

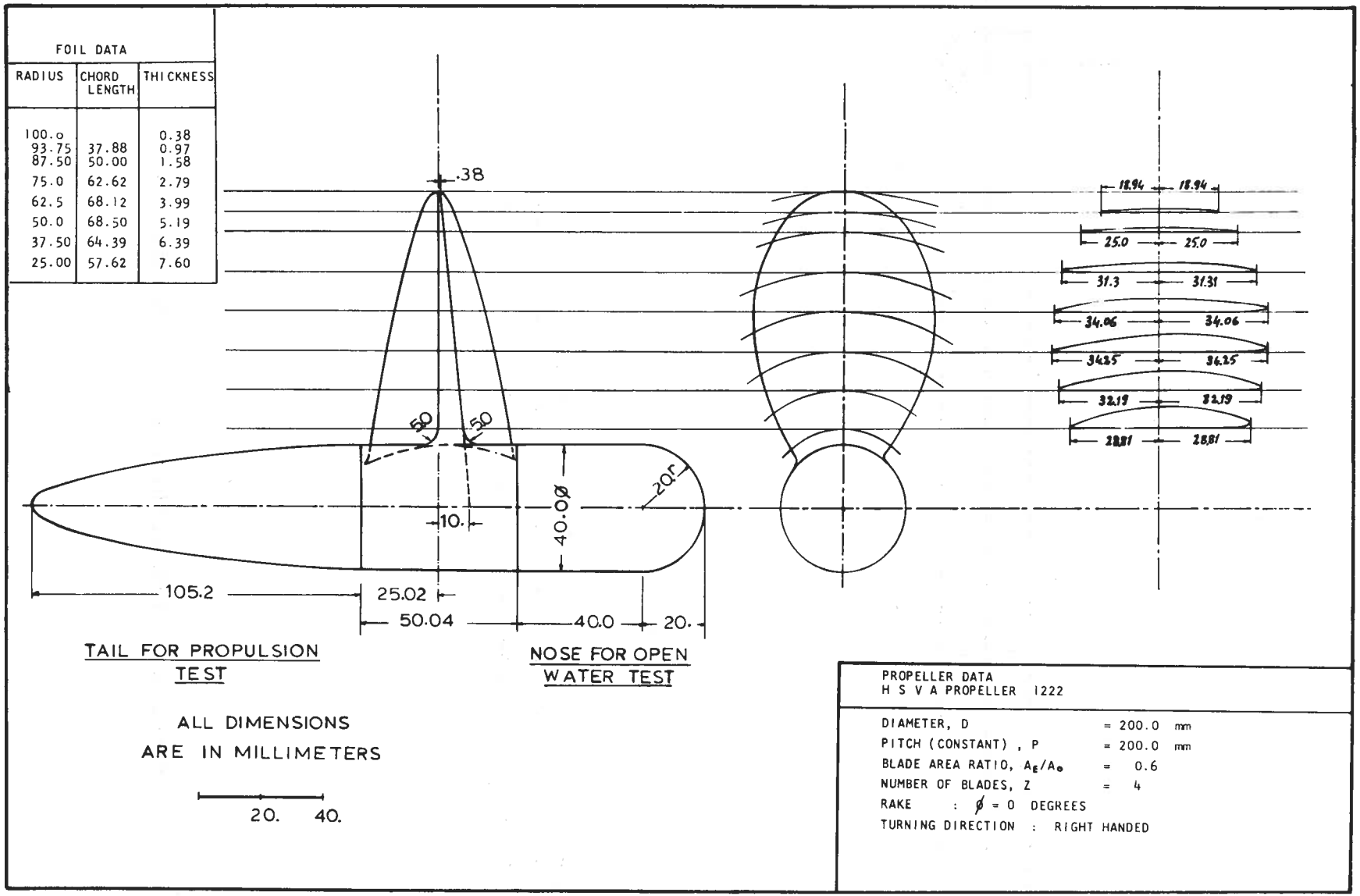

Fig. 2 Propeller geometry.

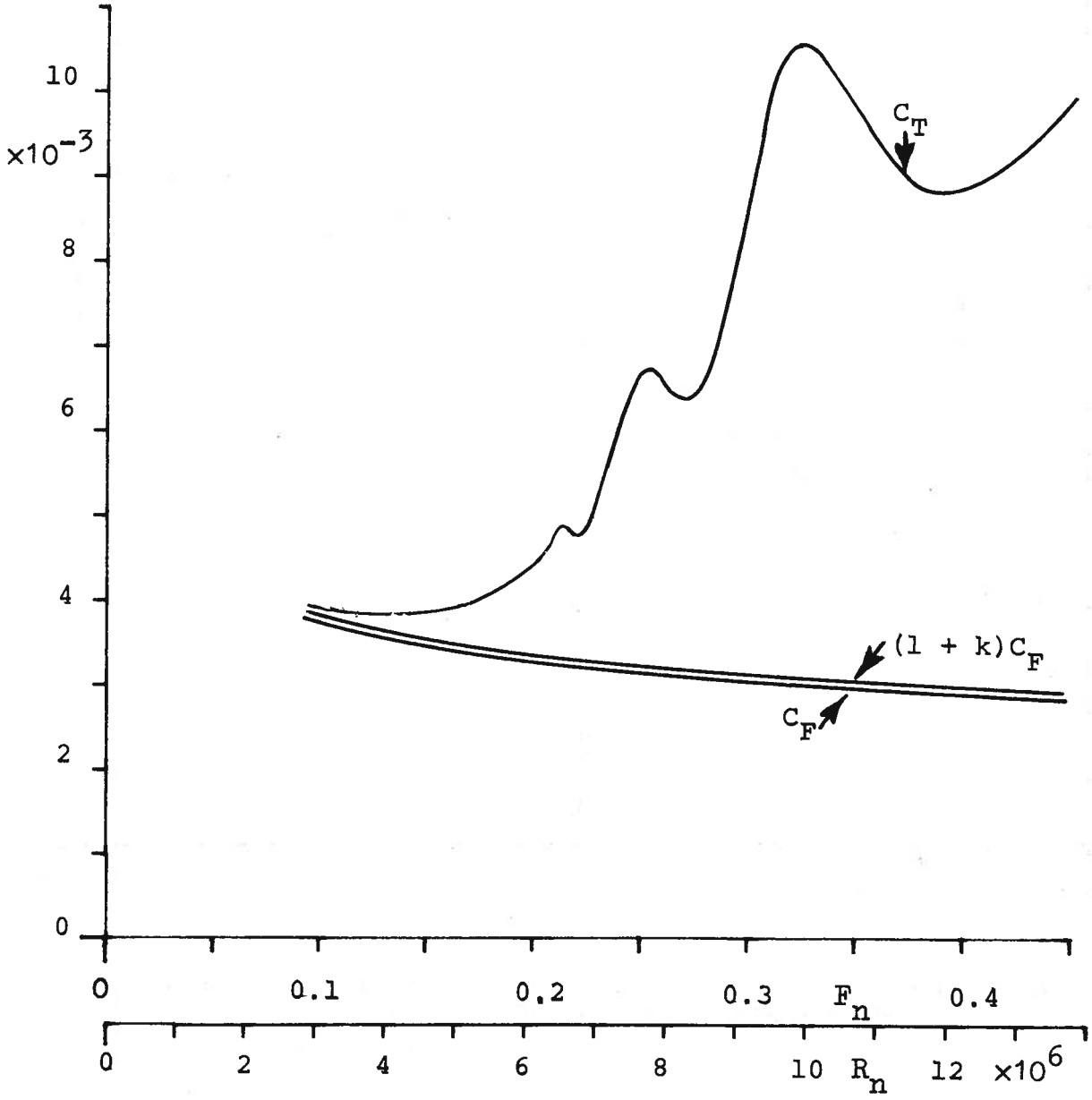

Fig. 3 Measured total resistance.

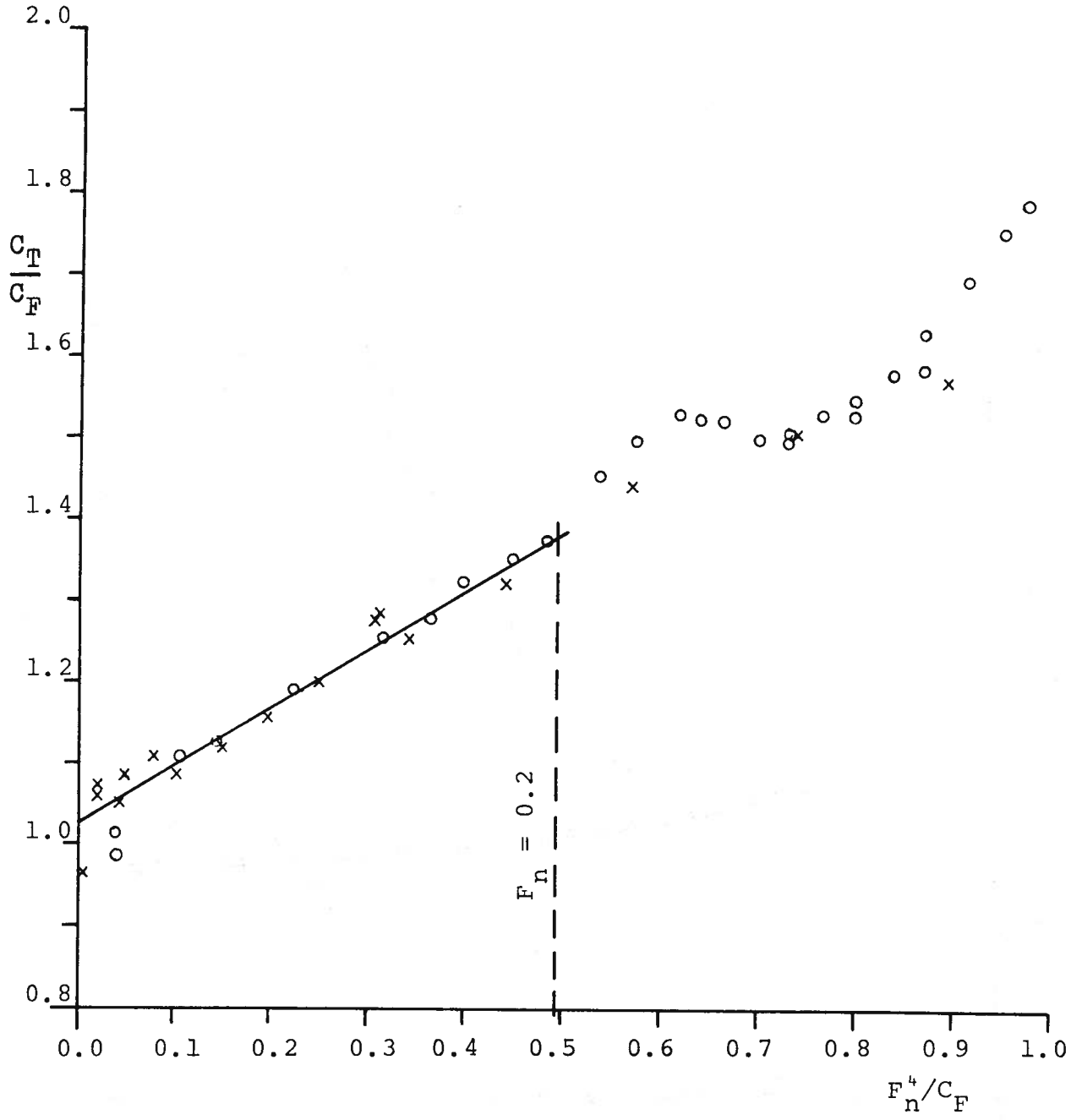

Fig. 4 Measured total resistance at low Froude numbers. Determination of viscous form factor.

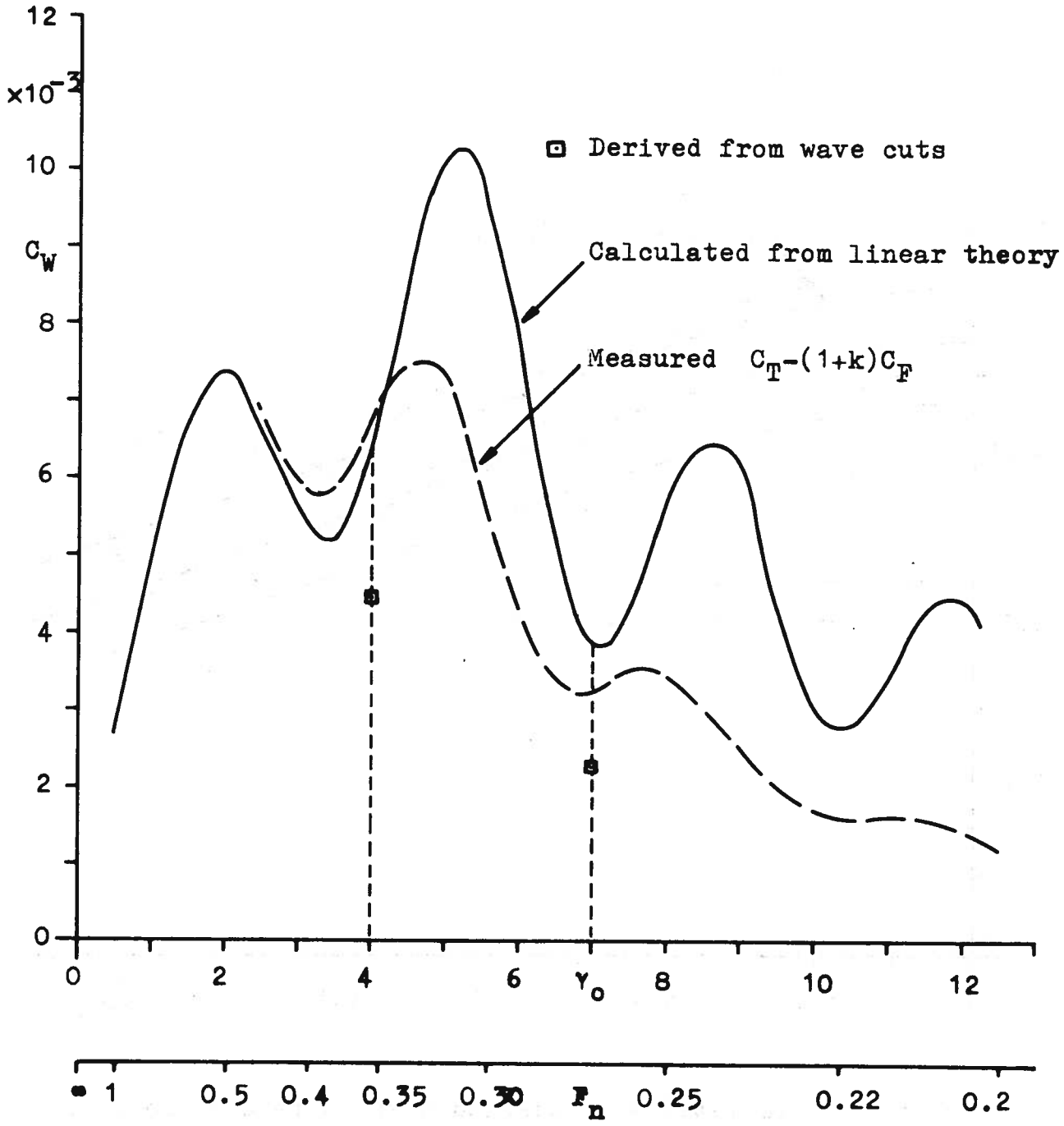

Fig. 5 Calculated and measured wave resistance.

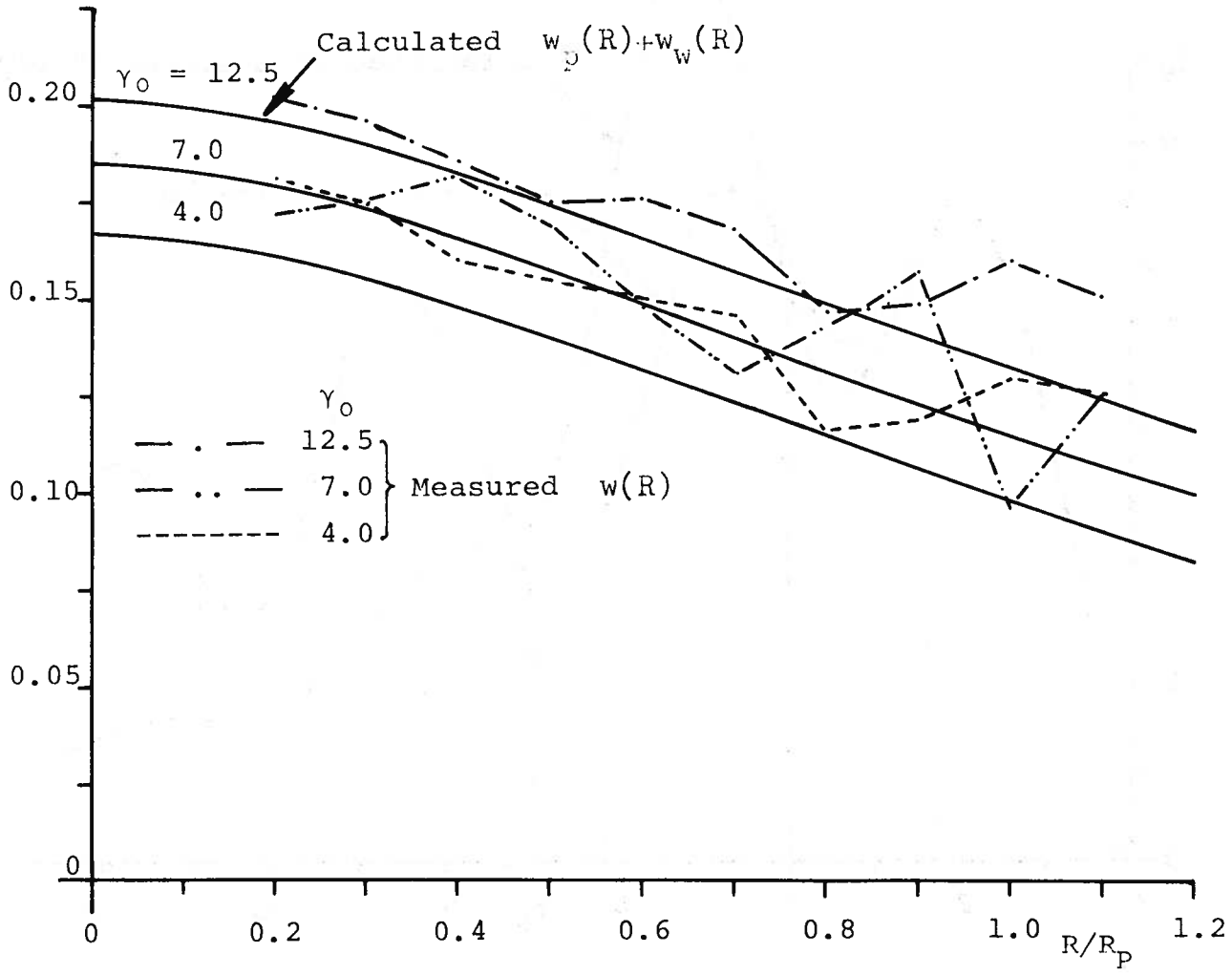

Fig. 6 Calculated and measured wake in reverse motion.

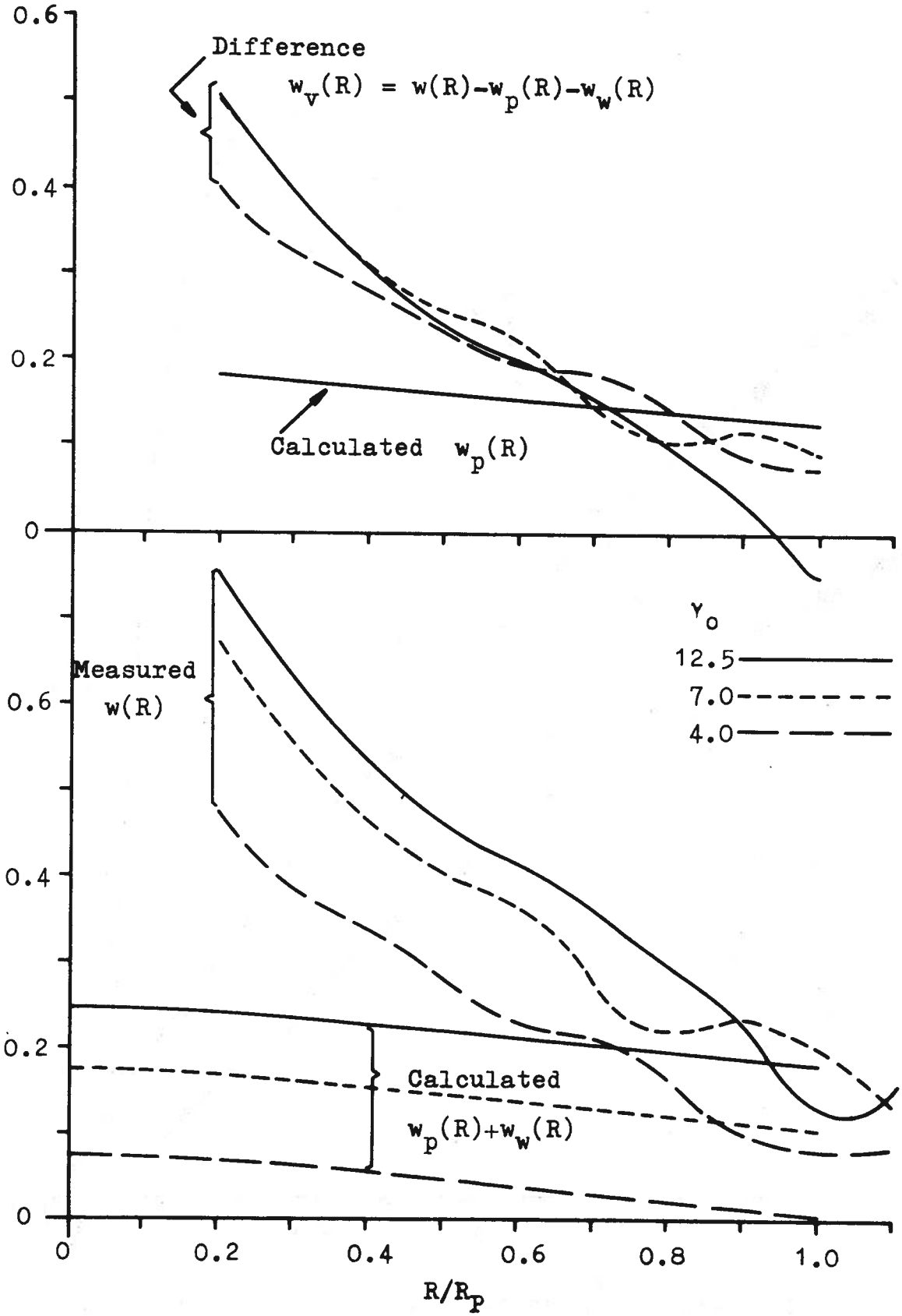

Fig. 7 Calculated and measured wake components.

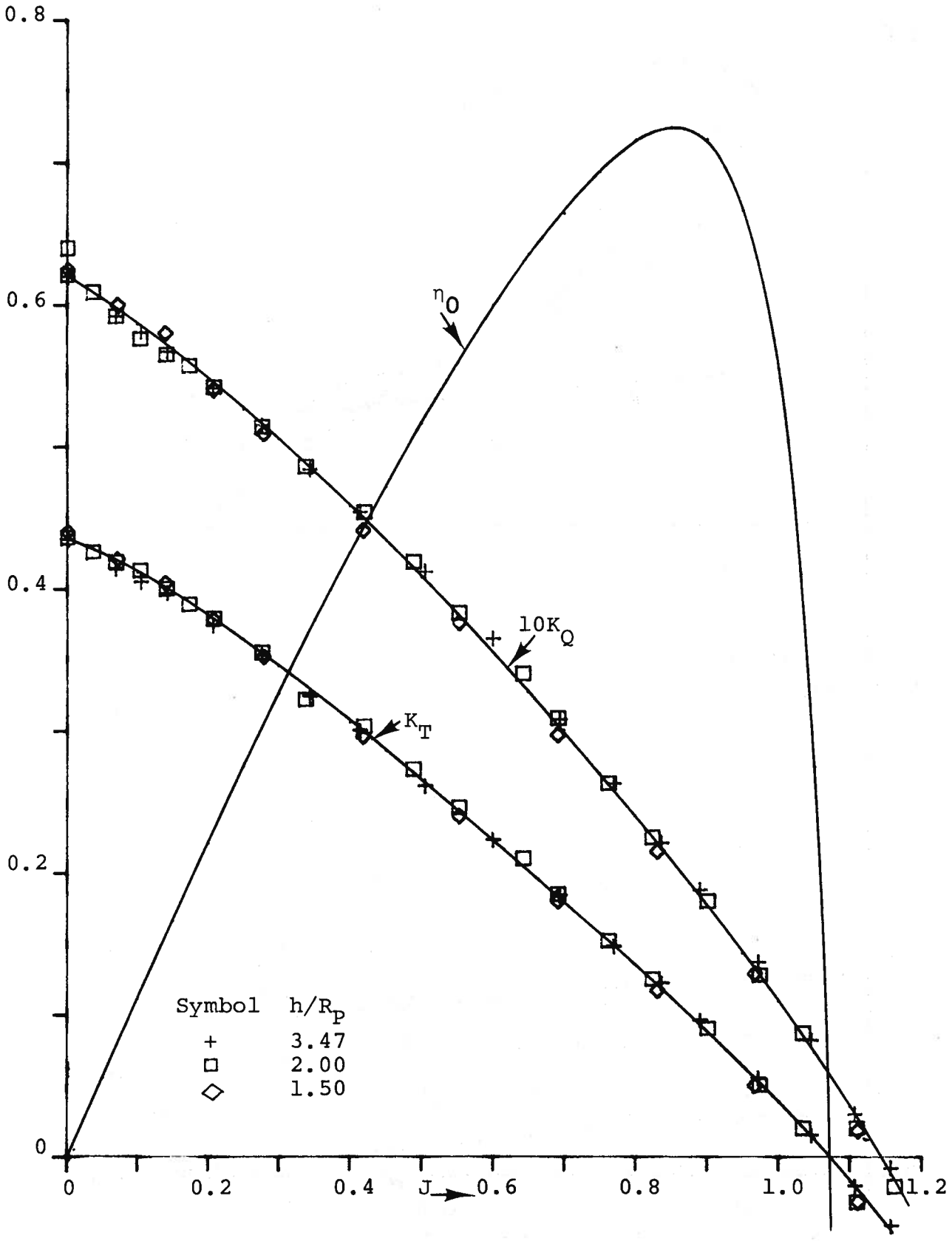

Fig. 8 Propeller characteristics at deep submergence.

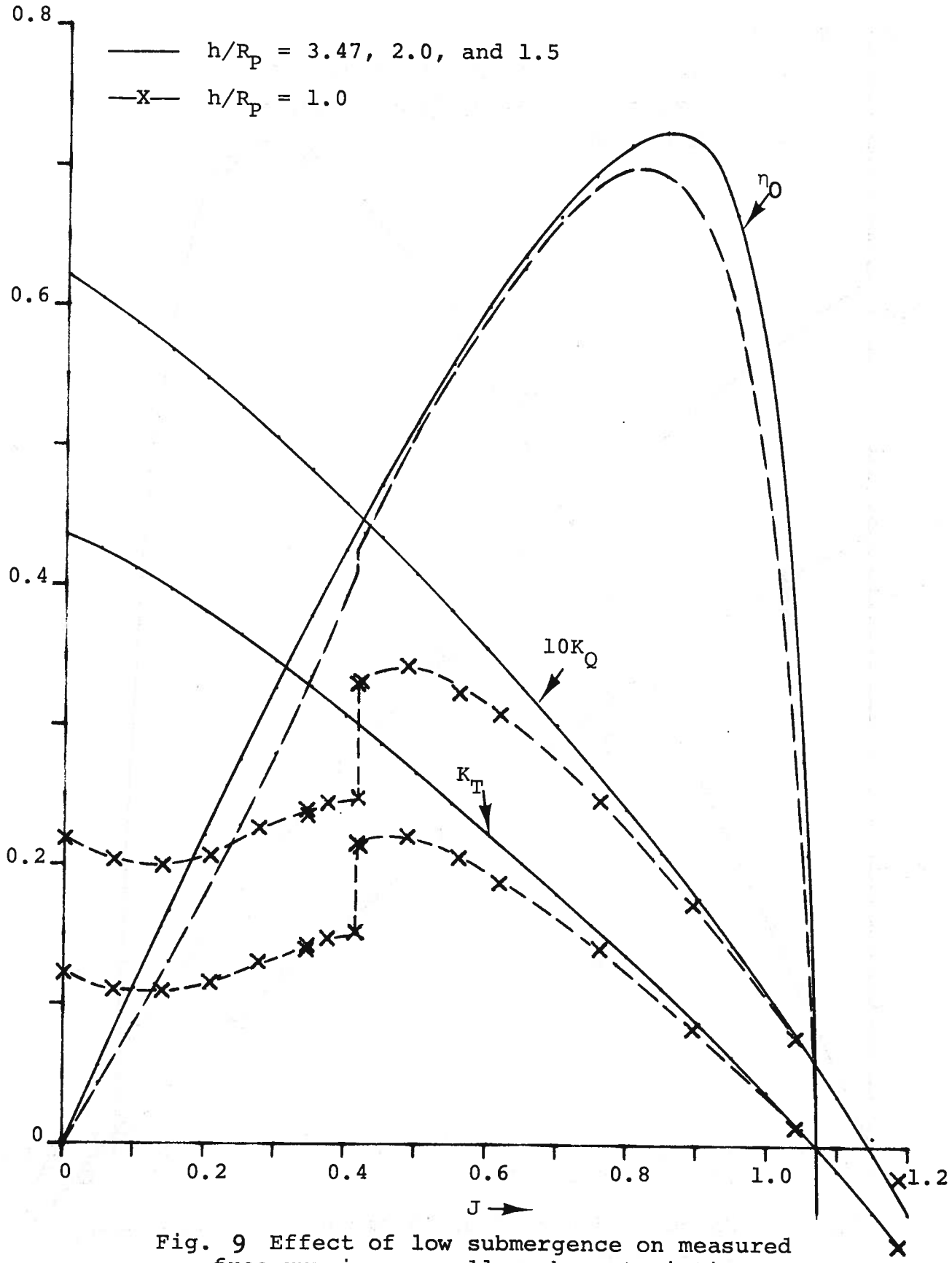

Fig. 9 Effect of low submergence on measured free-running propeller characteristics.

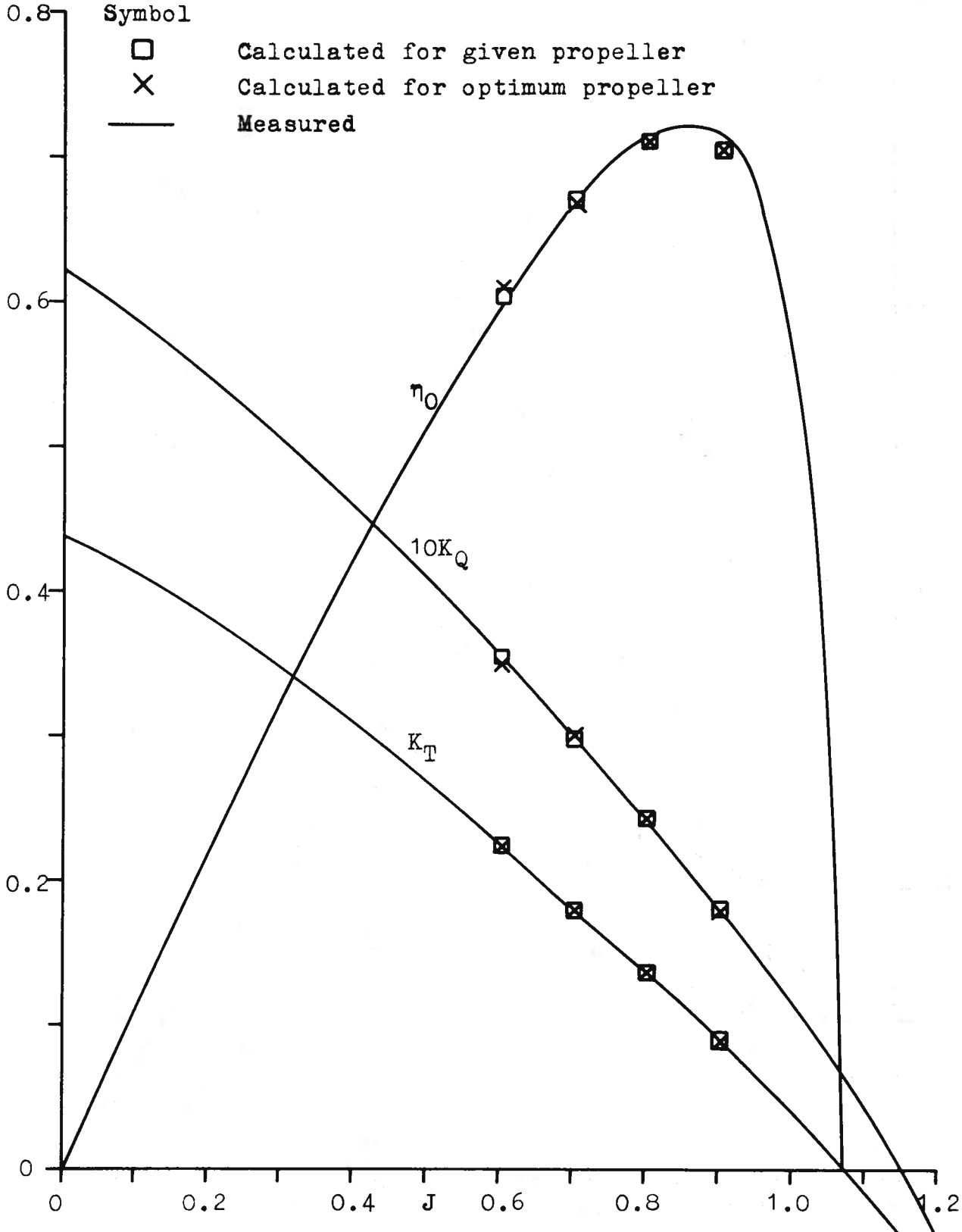

Fig. 10 Calculated and measured propeller characteristics at deep submergence.

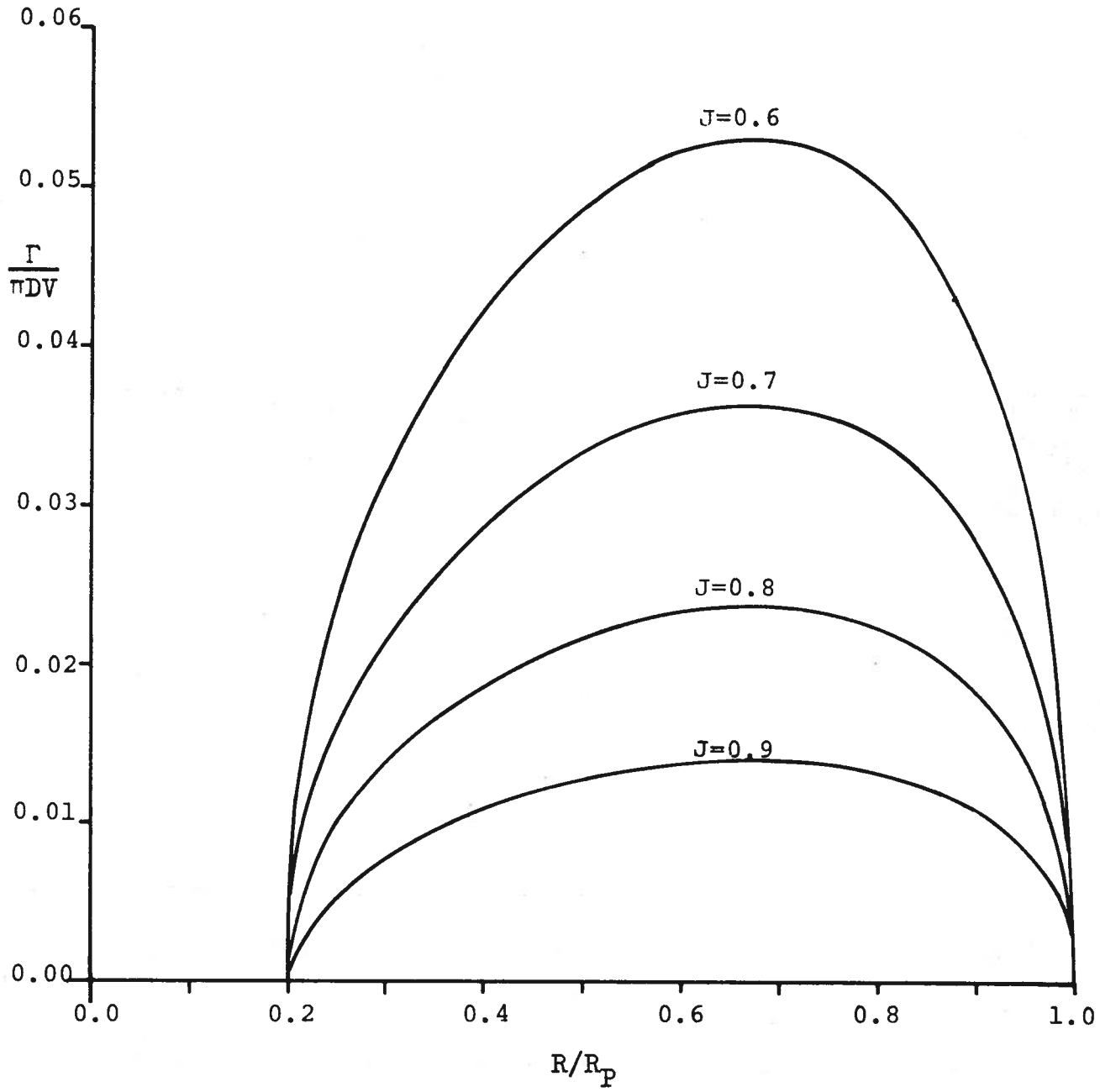

Fig. 11 Calculated distribution of bound circulation for free-running propeller at deep submergence.

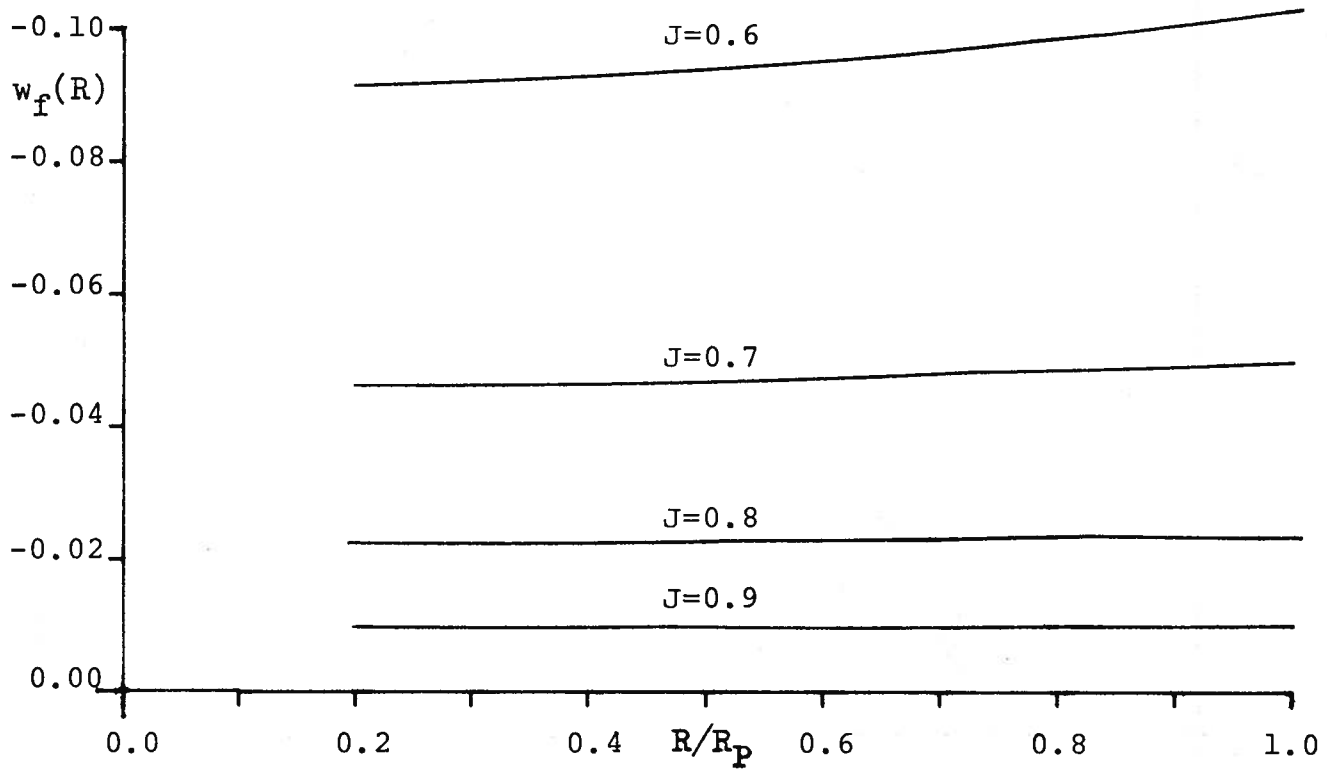

Fig. 12 Calculated self-induced free-surface wake of free-running propeller at submergence h = R_p.

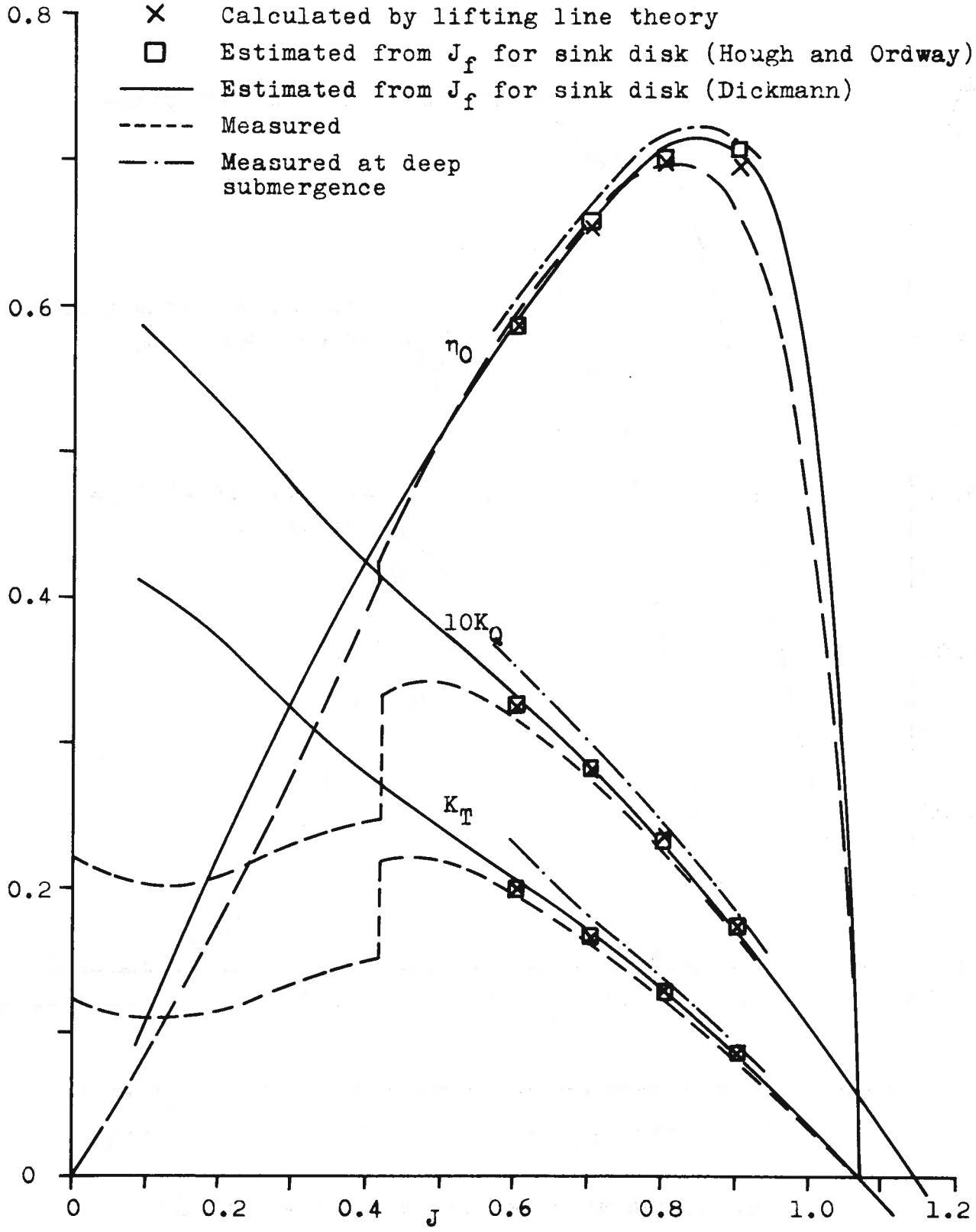

Fig. 13 Calculated and measured propeller characteristics at shallow submergence.

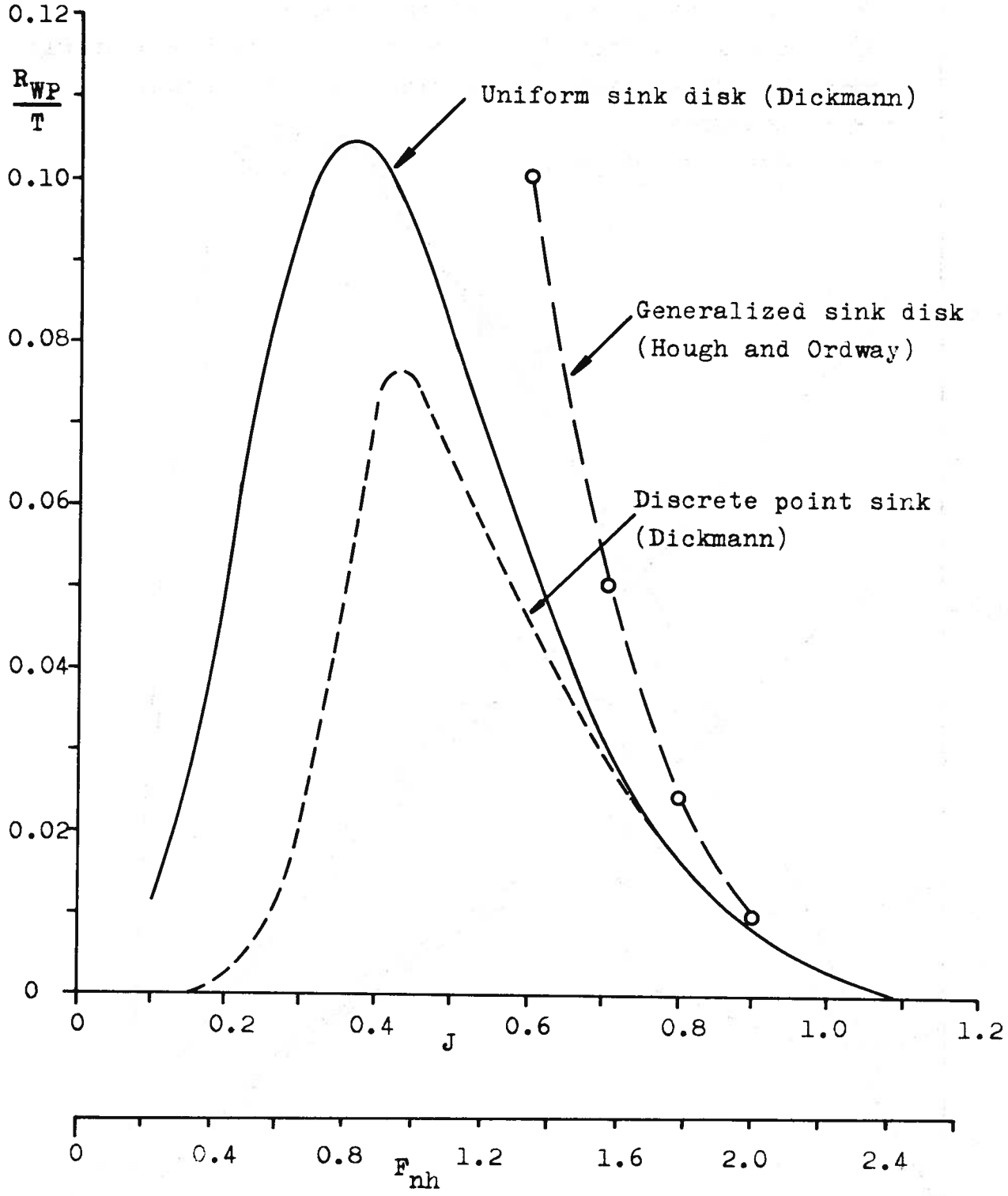

Fig. 14 Calculated wave resistance of free-running propeller at shallow submergence $h = R_P$.

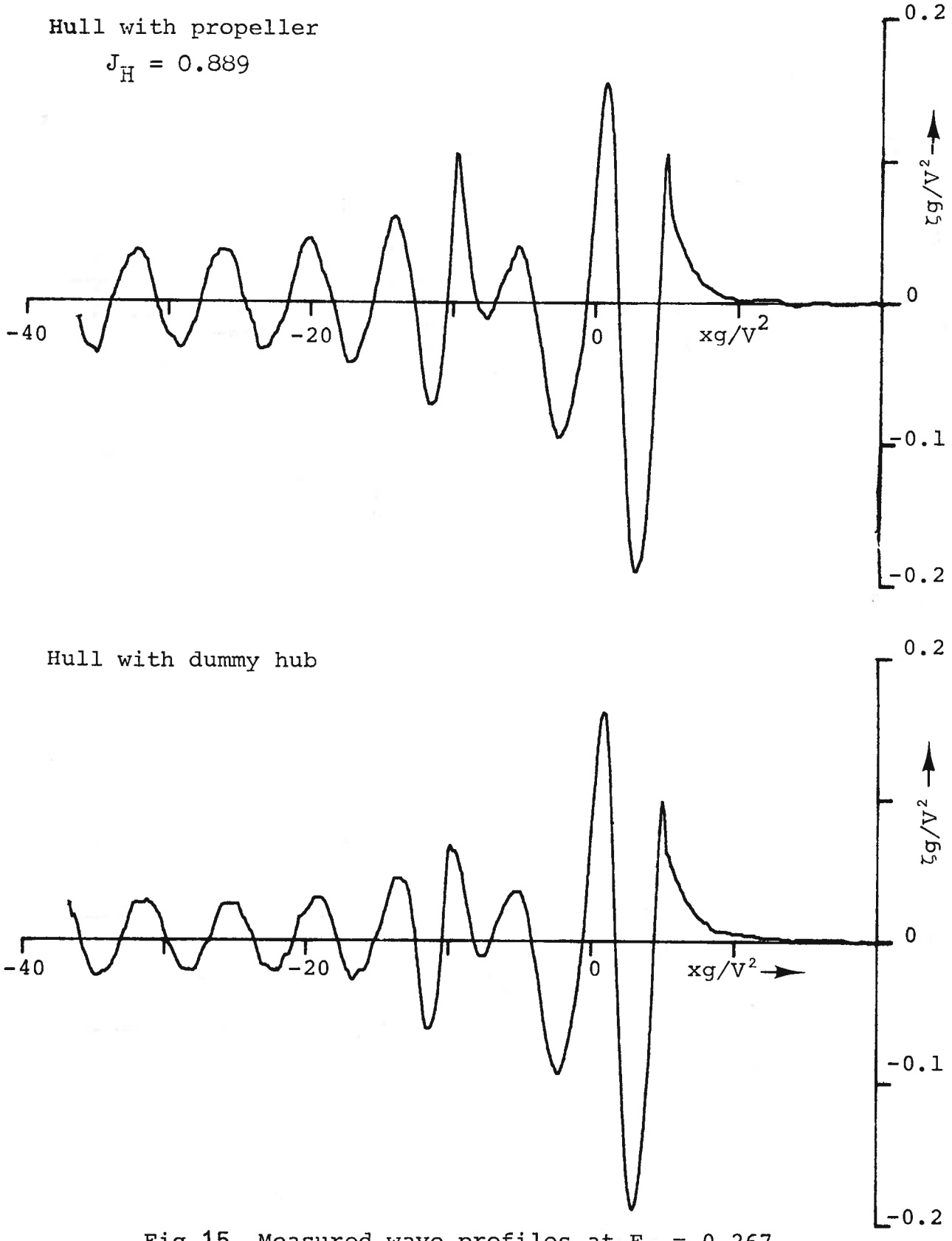

Fig.15 Measured wave profiles at F_n = 0.267.

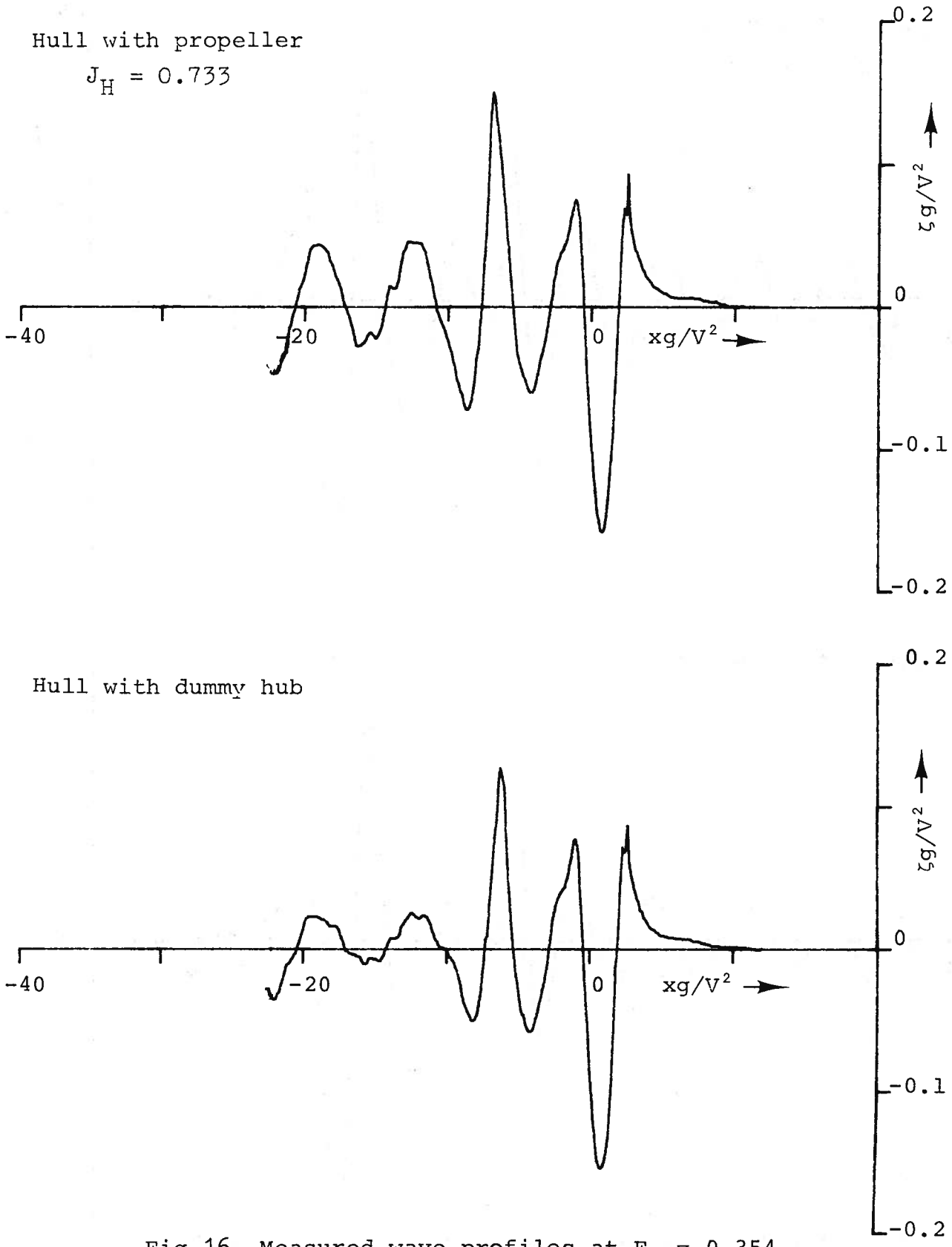

Fig.16 Measured wave profiles at F_n = 0.354.

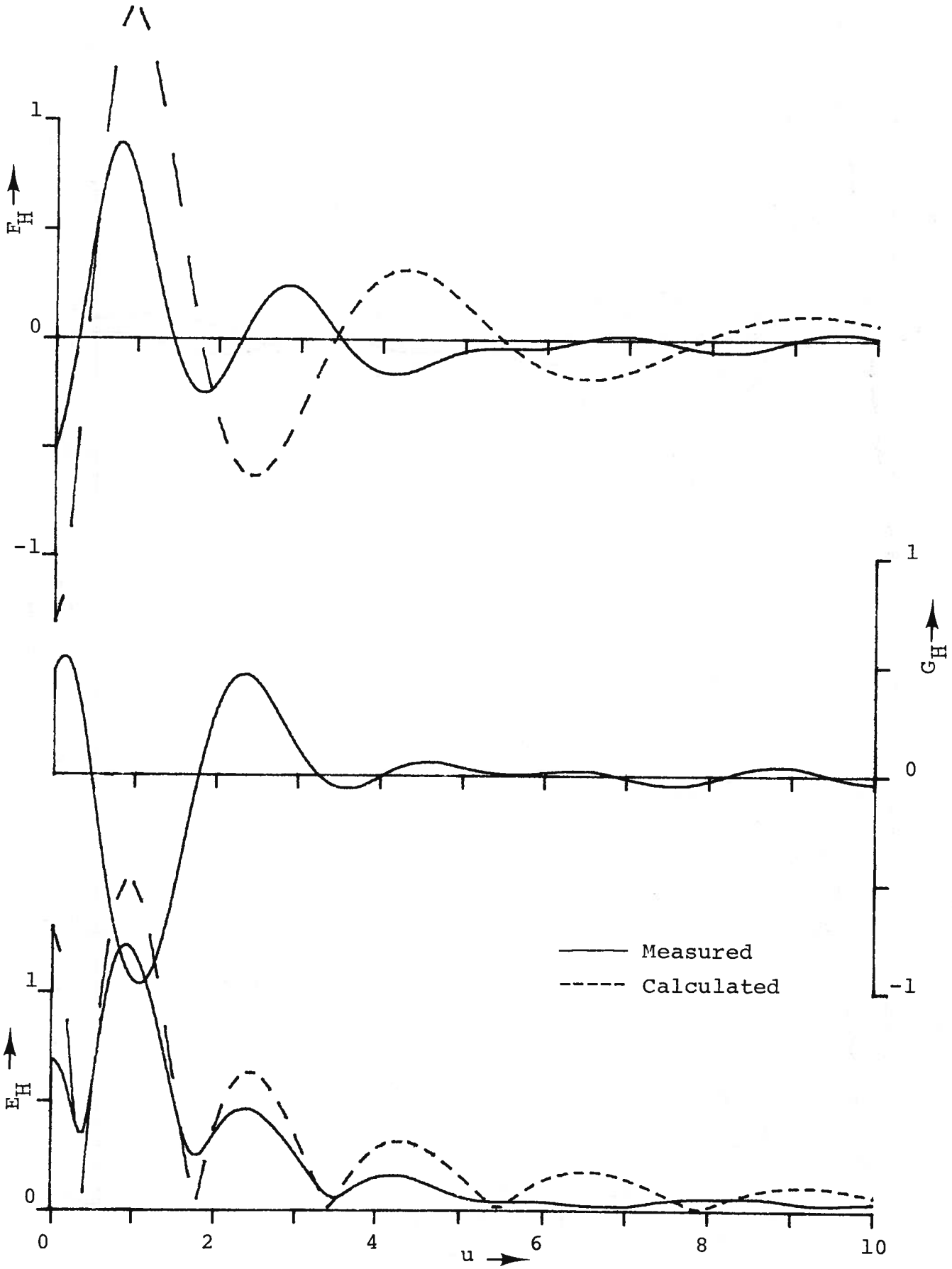

Fig.17 Free-wave spectrum of bare hull at F_n = 0.267.

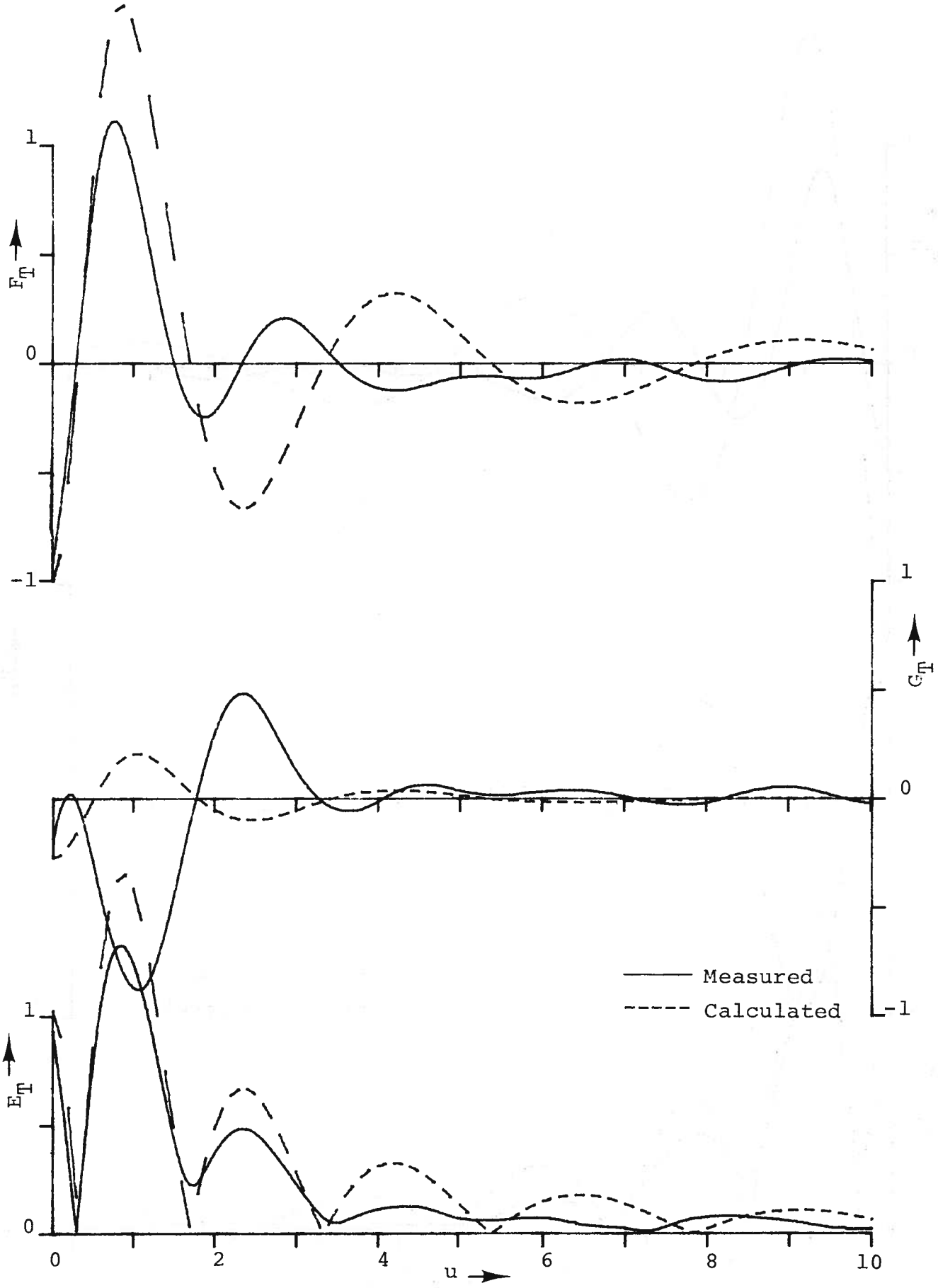

Fig.18 Free-wave spectrum of hull with propeller at F_n = 0.267.

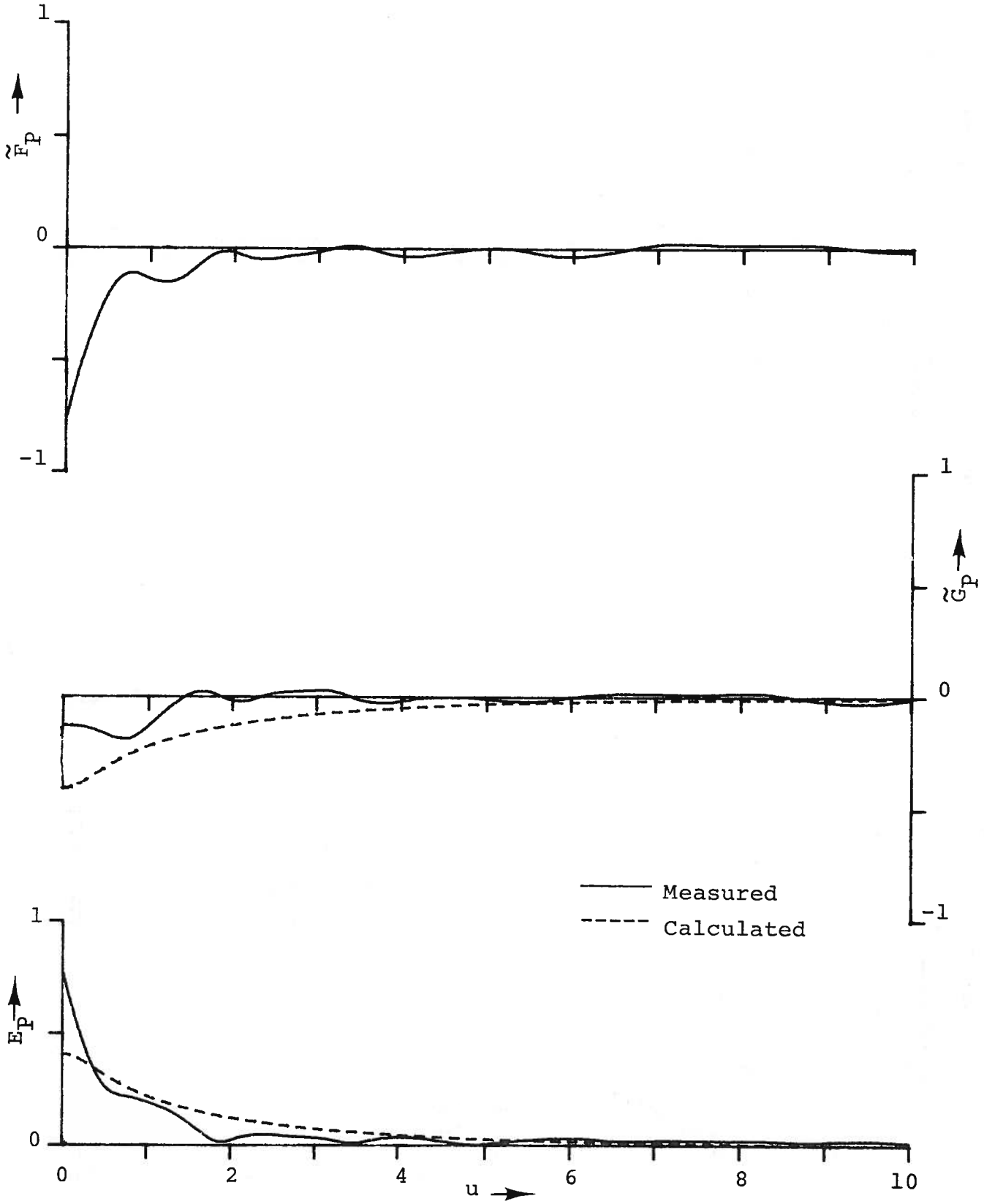

Fig.19 Free-wave spectrum of propeller at F_n = 0.267.

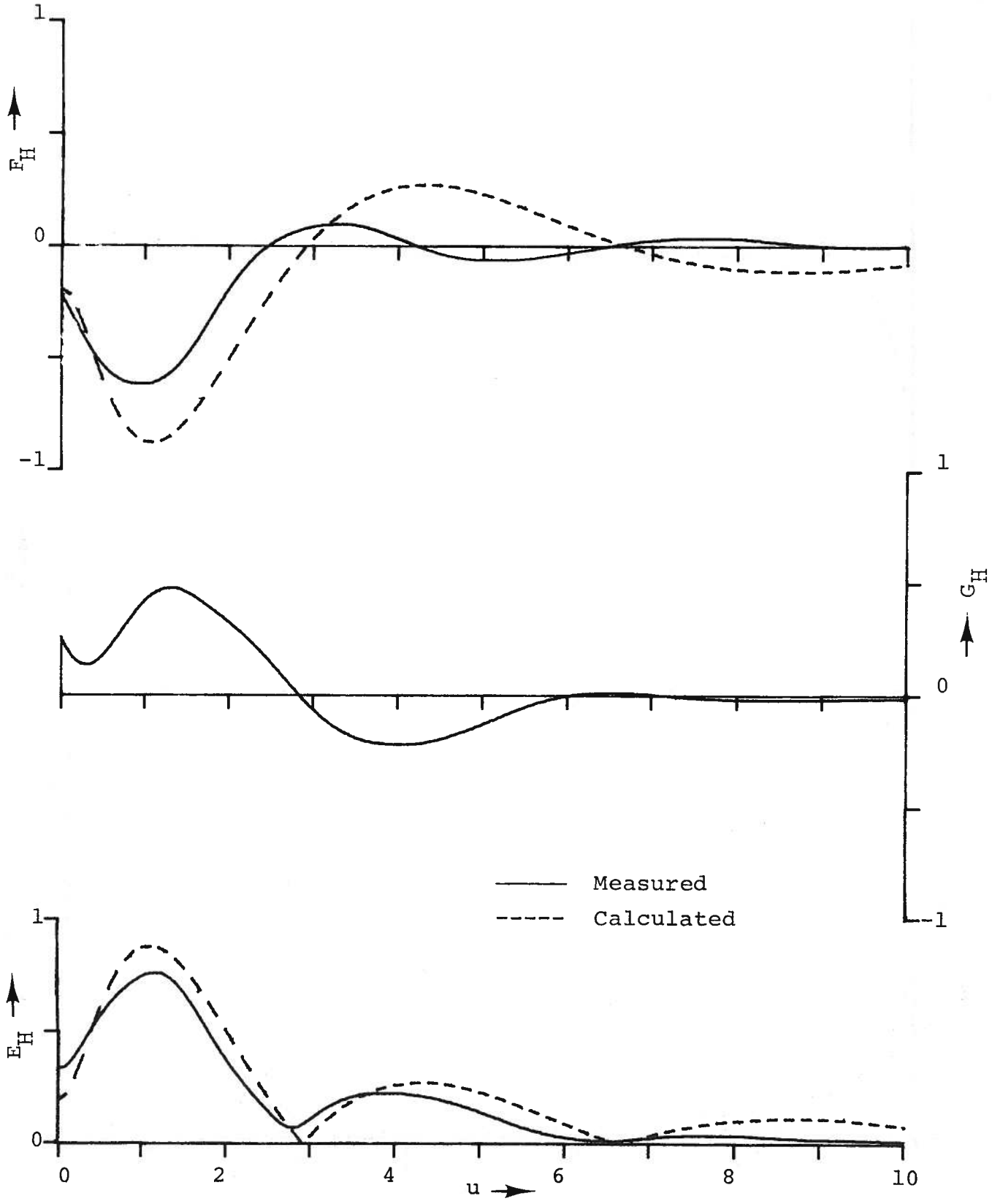

Fig.20 Free-wave spectrum of bare hull at F_n = 0.354.

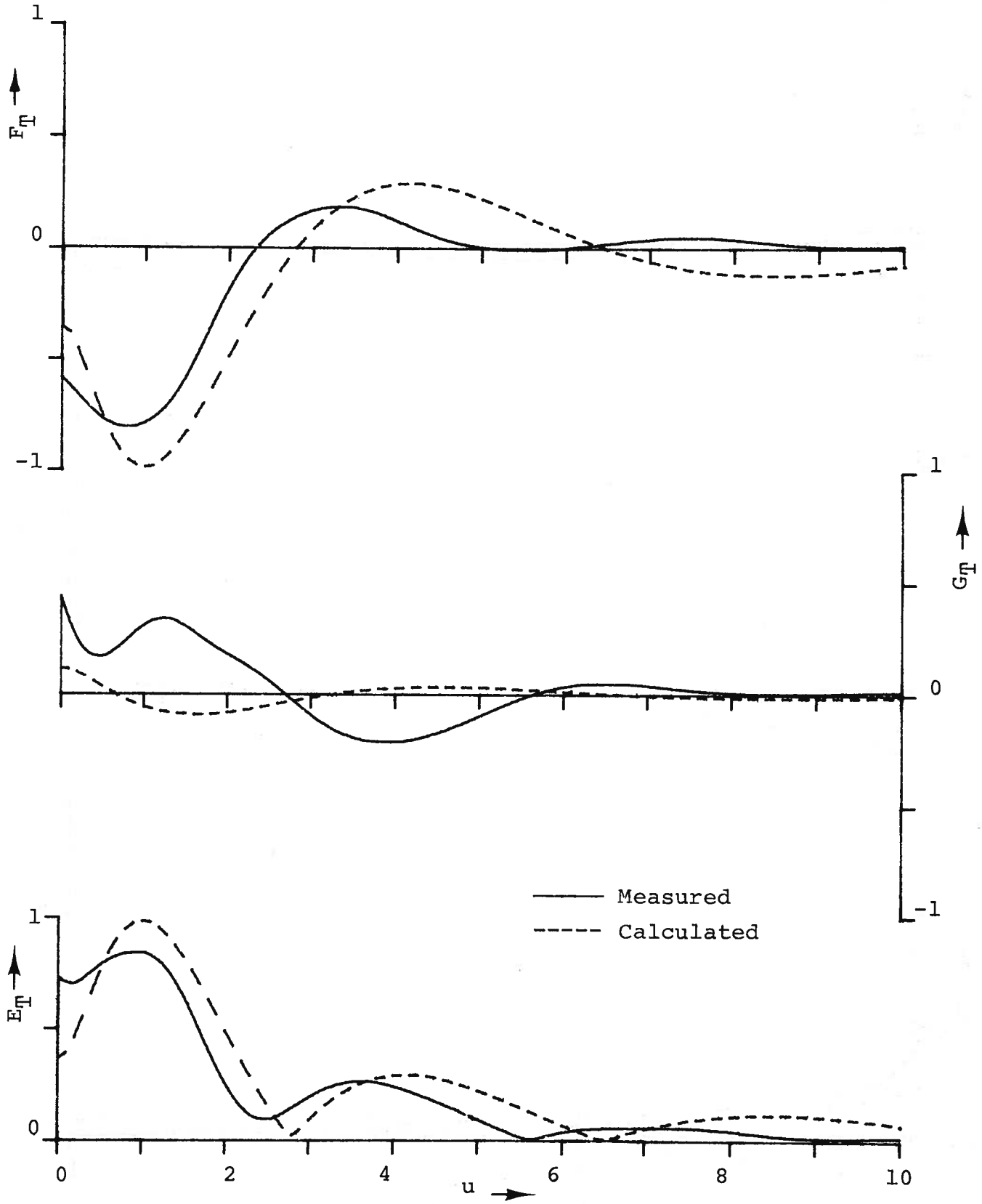

Fig.21 Free-wave spectrum of hull with propeller at F_n = 0.354.

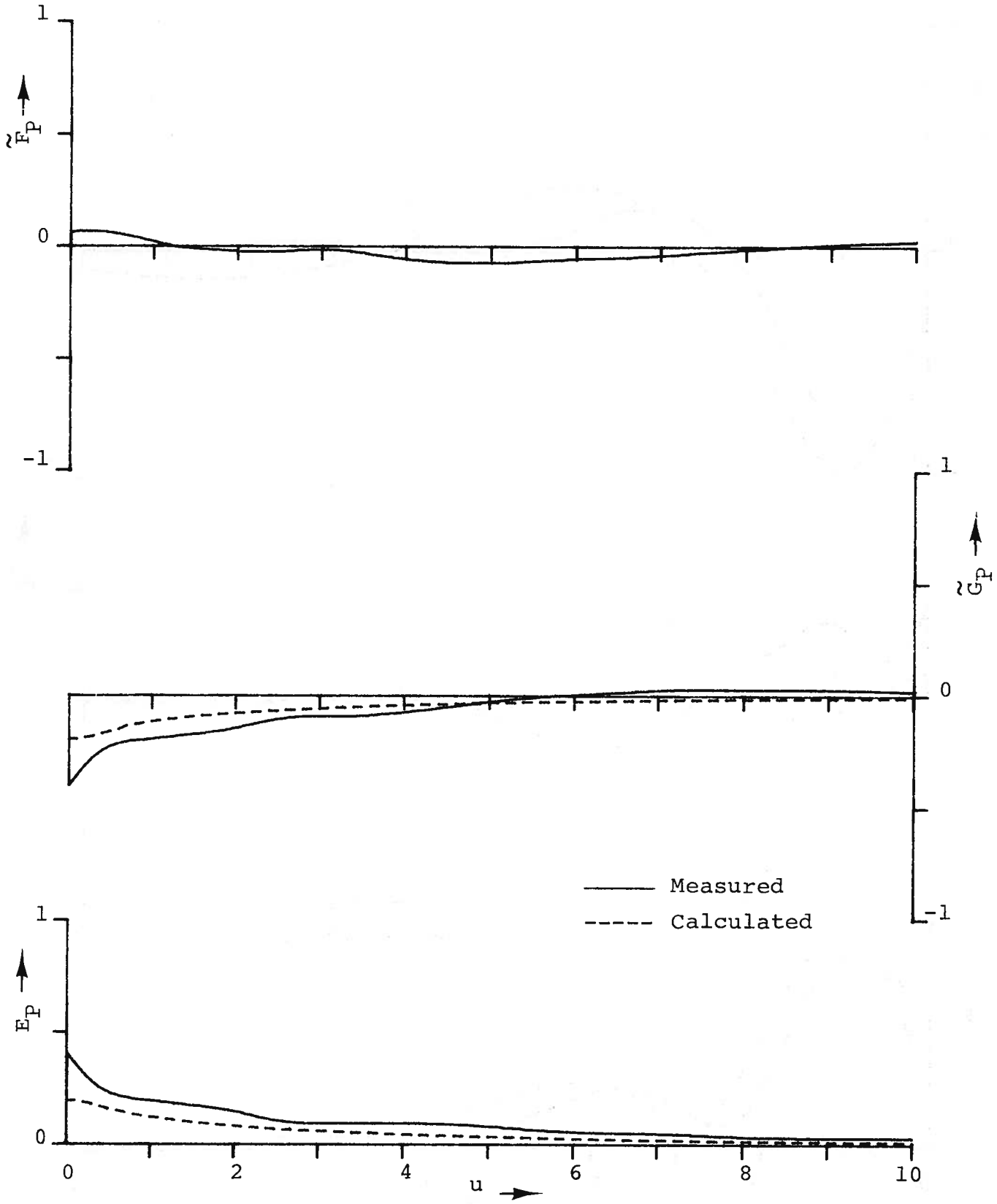

Fig. 22 Free-wave spectrum of propeller at F_n = 0.354.

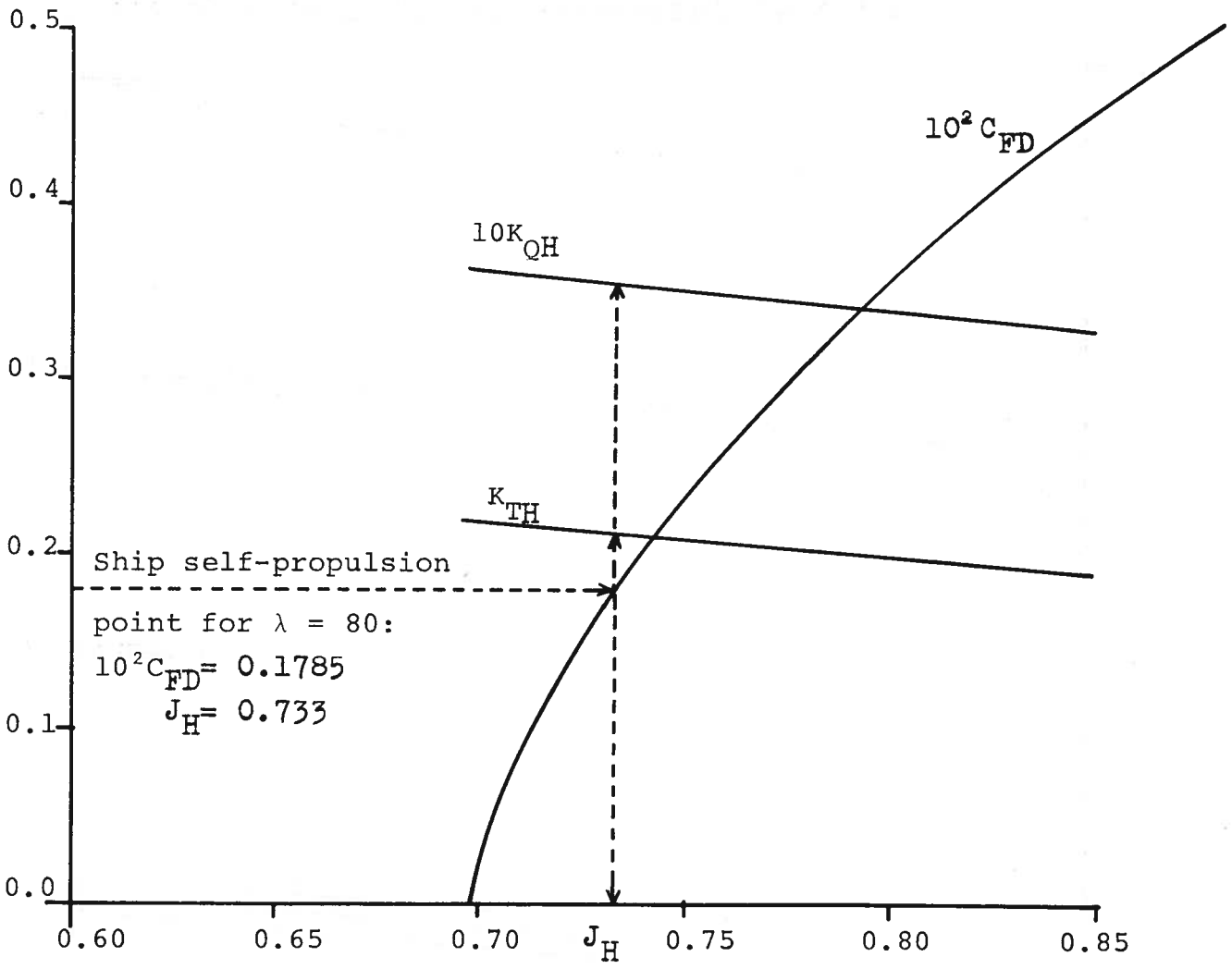

Fig. 23 Typical result of a propulsion test and the determination of self-propulsion points, $\gamma_o = 4.0$.

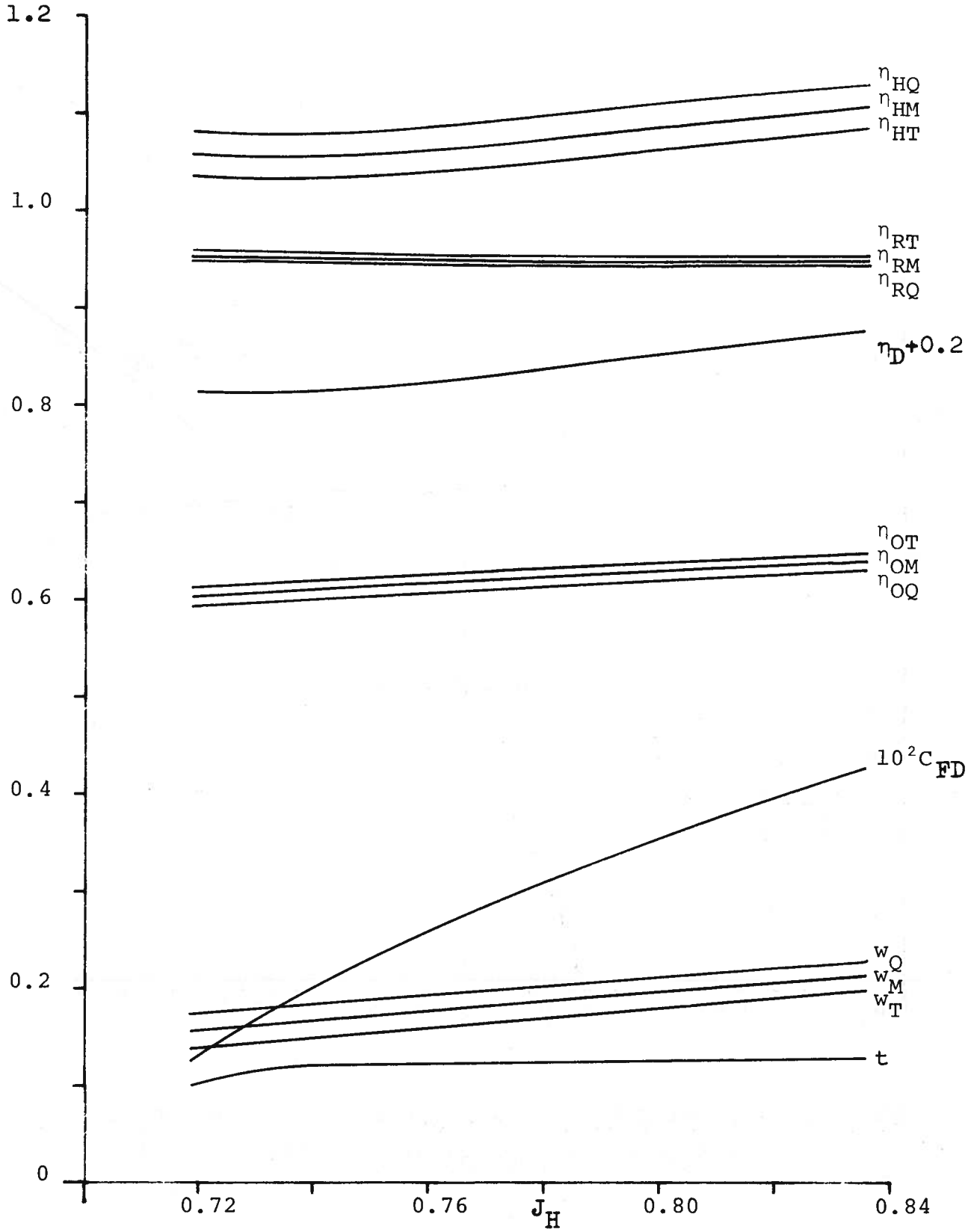

Fig. 24 Variation of propulsion factors with loading for $\gamma_o = 4$.

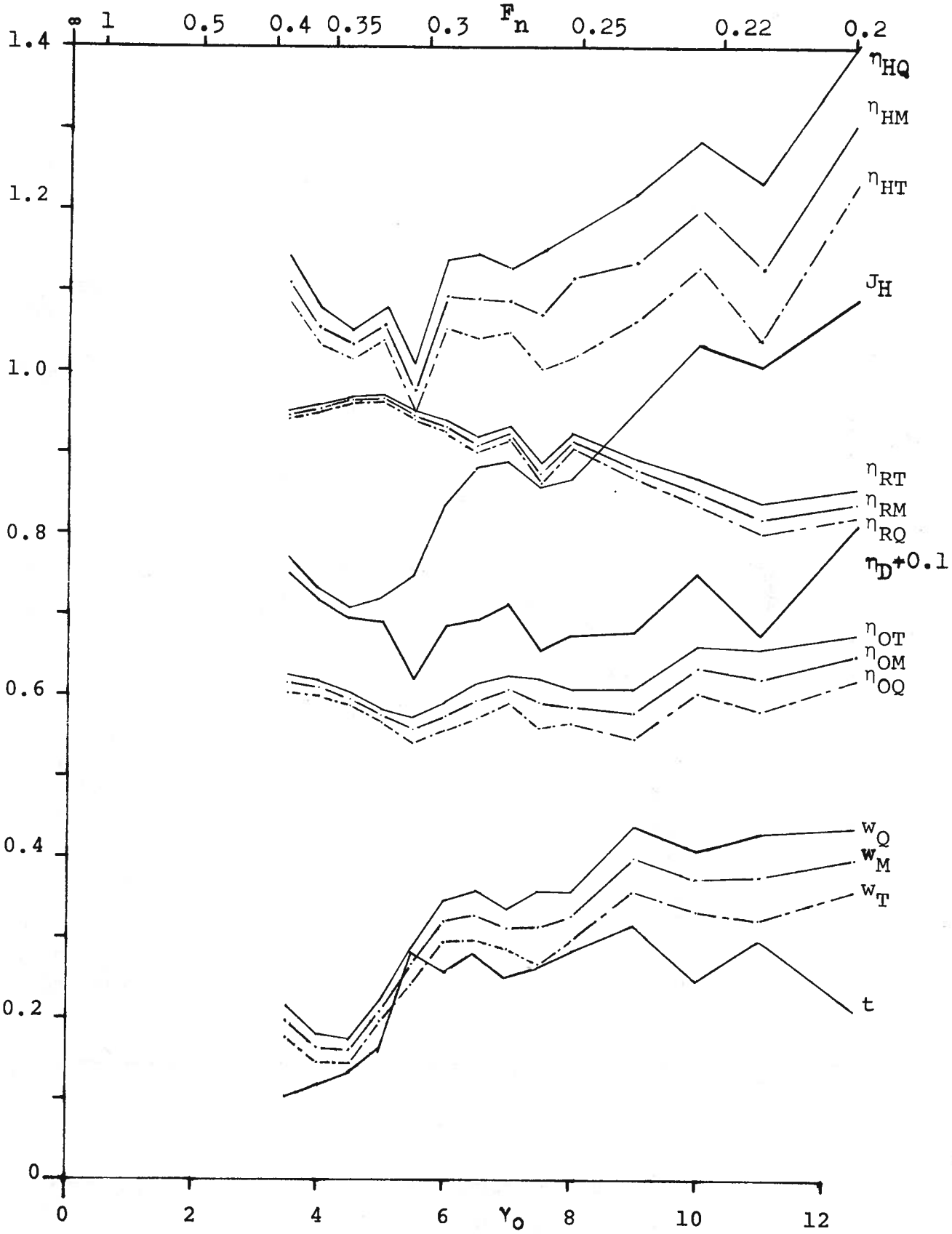

Fig. 25 Variation of propulsive factors with Froude number at the ship self-propulsion point.

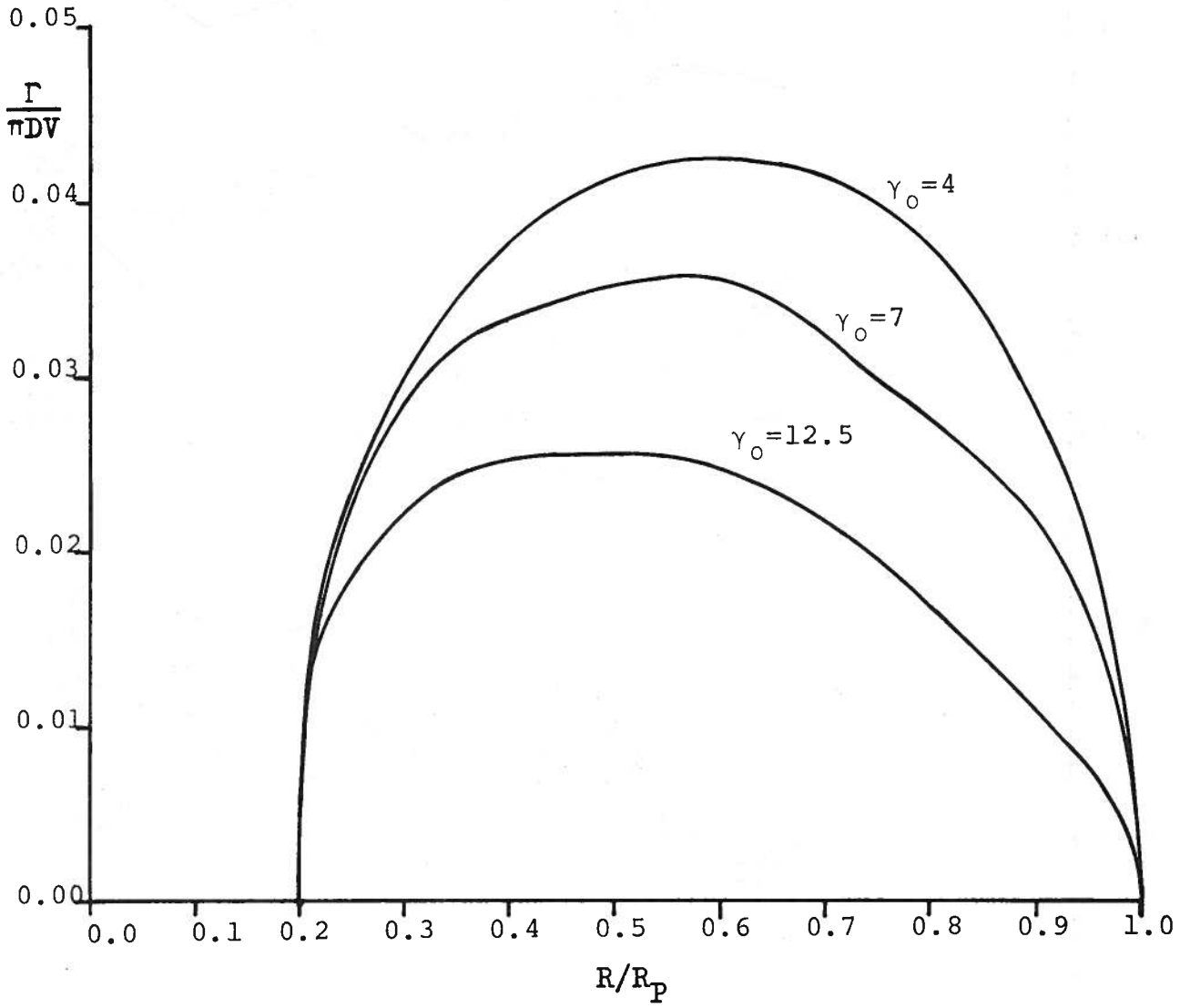

Fig. 26 Calculated distribution of bound circulation for propeller behind hull at self-propulsion point.

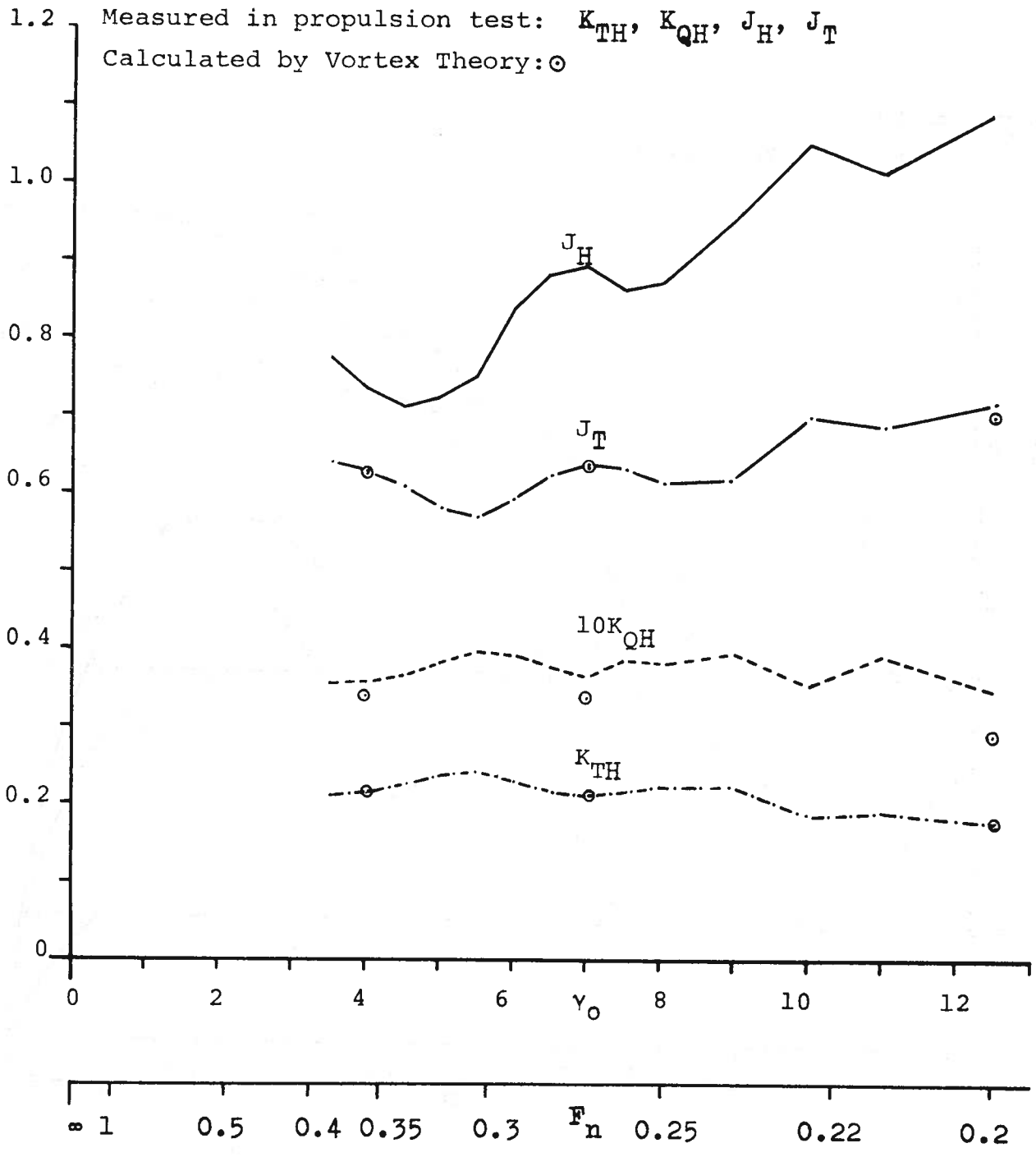

Fig. 27 Calculated and measured characteristics of propeller operating behind hull at self-propulsion point.

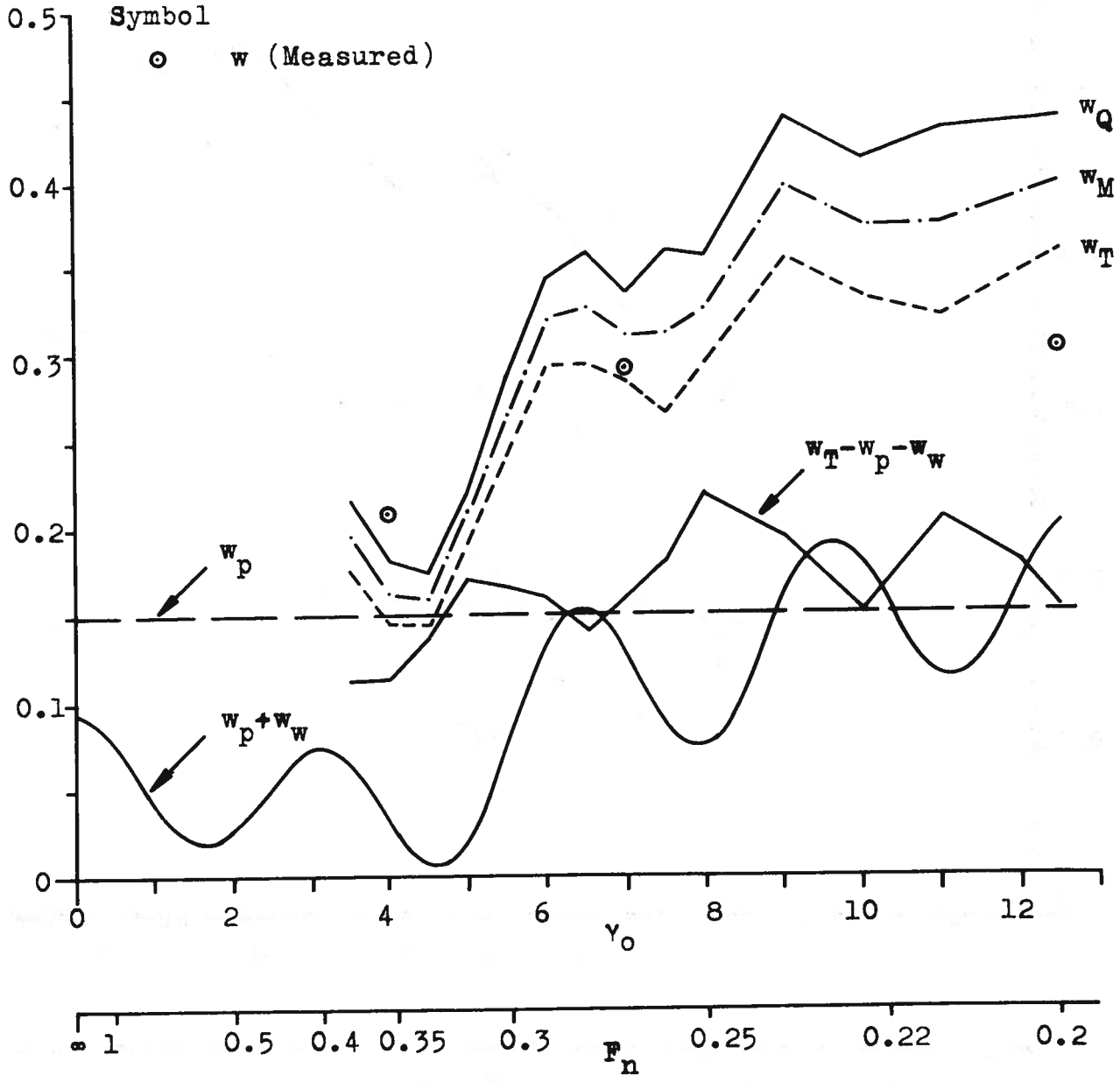

Fig. 28 Calculated and measured wake fractions as functions of Froude number.

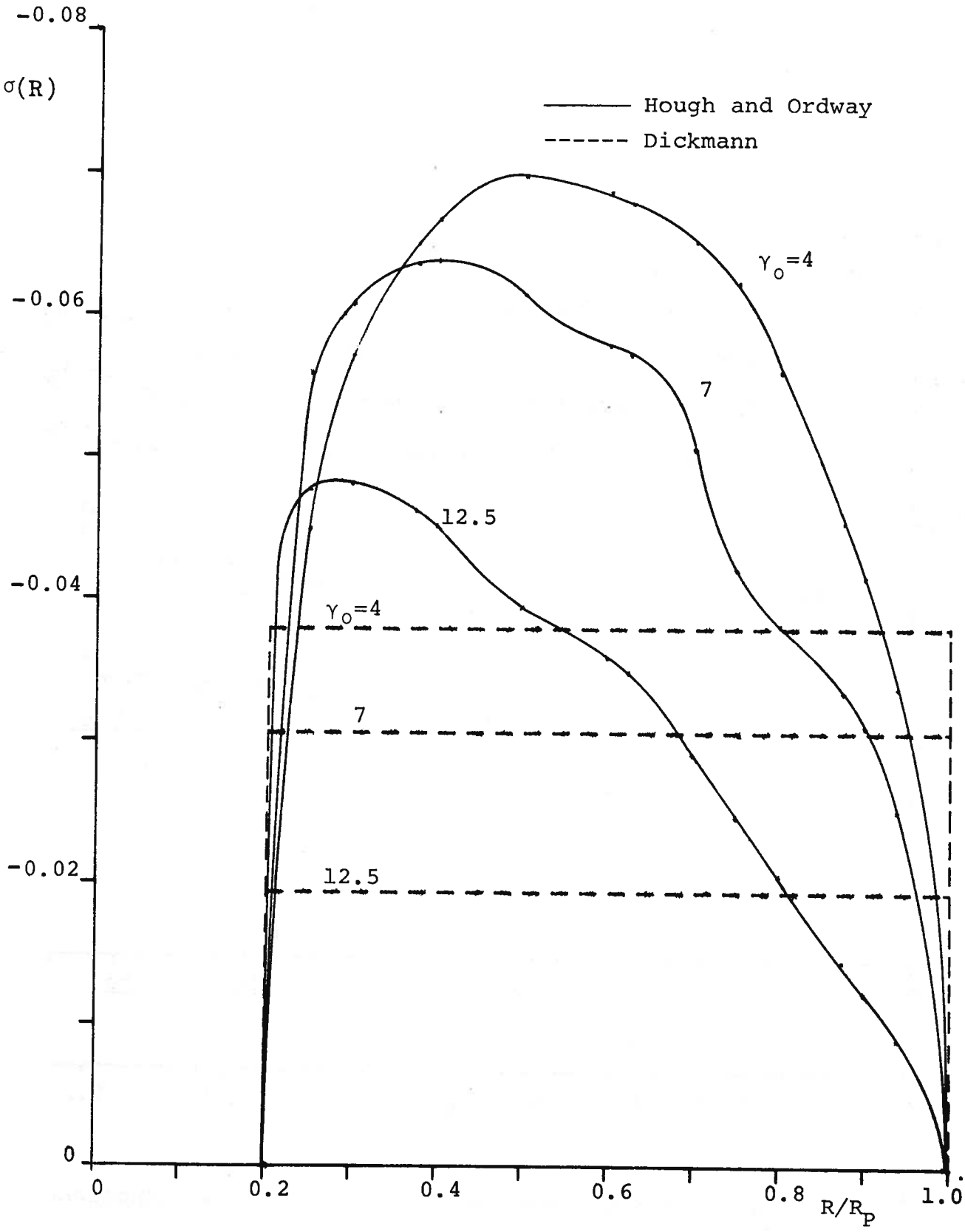

Fig. 29 Calculated distribution of source strength for propeller behind hull at self-propulsion point.

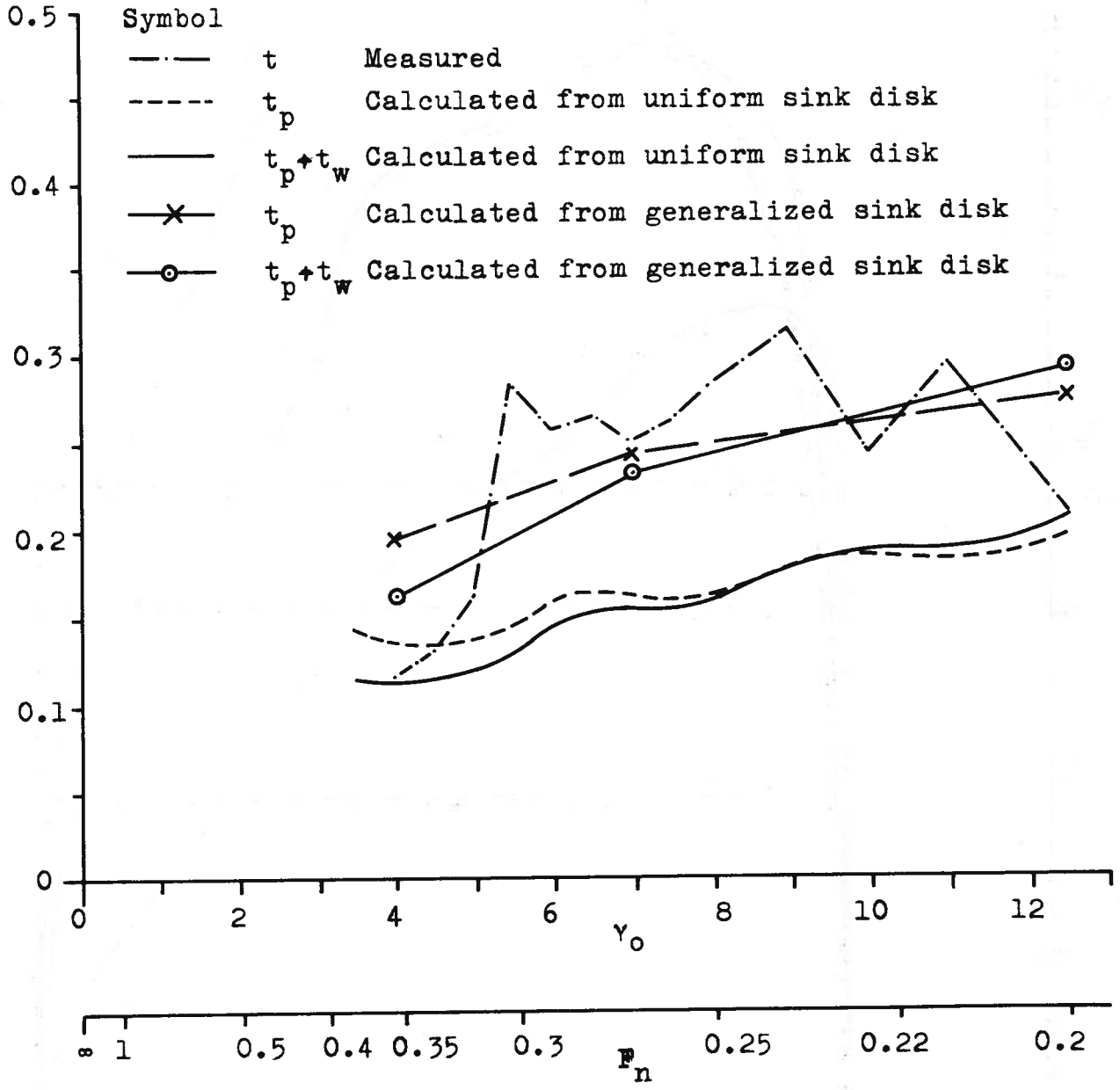

Fig. 30 Calculated and measured thrust deduction fractions as functions of Froude number.

UNCLASSIFIED

Security Classification

DOCUMENT CONTROL DATA - R & D

(Security classification of title, body of abstract and indexing annotation must be entered when the overall report is classified)

1. ORIGINATING ACTIVITY (Corporate author)

UNIVERSITY OF MICHIGAN, Dept. of Naval Architecture & Marine Engineering, Ann Arbor, Michigan 48104

2a. REPORT SECURITY CLASSIFICATION

UNCLASSIFIED

2b. GROUP

3. REPORT TITLE

FREE-SURFACE EFFECTS IN HULL PROPELLER INTERACTION

4. DESCRIPTIVE NOTES (Type of report and inclusive dates)

Final Report

5. AUTHOR(S) (First name, middle initial, last name)

Horst NOWACKI

Som D. SHARMA

6. REPORT DATE

September 1971

7a. TOTAL NO. OF PAGES

xvi + 118

7b. NO. OF REFS

57

8a. CONTRACT OR GRANT NO.

N00014-67-A-0181-0028

b. PROJECT NO.

SR 009 01 01

c.

d.

9a. ORIGINATOR'S REPORT NUMBER(S)

No. 112

9b. OTHER REPORT NO(S) (Any other numbers that may be assigned this report)

none

10. DISTRIBUTION STATEMENT

Approved for public release; distribution unlimited

11. SUPPLEMENTARY NOTES

12. SPONSORING MILITARY ACTIVITY

Naval Ship Research and Development Center

13. ABSTRACT

The quantitative role of wavemaking at the free surface in the phenomenon of hull propeller interaction is investigated by means of a general scheme devised to determine the potential, viscous and wave components of wake and thrust deduction. It requires the concerted application of various analytical tools such as the lifting line theory of propellers, the method of singularities for representing the hull and propeller by source distributions and the linearized free-surface theory of wavemaking, as well as model experiment techniques such as the conventional Froude analysis of propulsion factors, nominal wake measurements and wave profile measurements. The procedure is actually applied to the specific case of a thin mathematical hull form driven by a four-bladed propeller of simple geometry. It is found that the wave component is dominant in the wake and quite significant in the thrust deduction at Froude numbers around 0.3. Surprisingly, there seems to be an appreciable viscous component in the thrust deduction at practically all Froude numbers.

DD FORM 1 NOV 68 1473

UNCLASSIFIED

Security Classification

14. KEY WORDS	LINK A		LINK B		LINK C	
	ROLE	WT	ROLE	WT	ROLE	WT
Interaction, Hull Propeller						
Hull Propeller Interaction						
Propeller Hull Interaction						
Thrust Deduction						
Free-Surface Effects						